A KINETIC THEORY DESCRIPTION OF RAREFIED GAS FLOWS WITH THE EFFECT OF ROTATIONAL RELAXATION

A THESIS

Presented to

The Faculty of the Graduate Division

by

Pang Feng Hwang

In Partial Fulfillment

of the Requirements for the Degree

Doctor of Philosophy

in the School of Aerospace Engineering

Georgia Institute of Technology

August, 1971

A KINETIC THEORY DESCRIPTION OF RAREFIED GAS FLOWS

WITH THE EFFECT OF ROTATIONAL RELAXATION

Approved: _____

Chairman

_____

_____

Date approved by Chairman: 8/27/71

ACKNOWLEDGEMENTS

I would like to express my appreciation to Dr. A. B. Huang who suggested this thesis topic and provided guidance, advice, and cooperation during this research and a great portion of my graduate academic career. I would also like to thank Dr. D. P. Giddens for his invaluable suggestions during the research endeavor. Dr. D. P. Giddens and Dr. Howard M. McMahon, who served on the reading committee, are gratefully thanked for their encouragement and for their patient examination of the manuscript.

The assistance of Mr. R. Srinivasan in helping carry out the computation of the leading edge problem and in helping plot some of the graphs is very much appreciated. I thank Mr. C. S. Lu for his contributing comments on the research. I am grateful to several of my fellow graduate students for their advice and cooperation. Also, I received invaluable advice from Dr. Y. J. Lin on the various numerical and computational aspects of the problems during the early stage of my research; his contribution must not go unnoticed. I am especially grateful for the generosity of Mrs. Mattie Jo Sims for typing the rough draft and the final copy of this thesis.

I am also grateful for the financial aid provided by NASA Research Grant NGL 11-002-062. Especially I would like to thank the staff of the Rich Electronic Computer Center for many hours of valuable service.

Finally, I thank my wife Ellen for her patience, understanding, and encouragement during my years of graduate work.

TABLE OF CONTENTS

Page

ACKNOWLEDGEMENTS ii

LIST OF ILLUSTRATIONS v

LIST OF SYMBOLS viii

SUMMARY xii

Chapter

I. INTRODUCTION. 1

Background and Review of Recent Literature
Discussion of the Method
Purpose of Research

II. THE MODEL EQUATIONS FOR A GAS WITH INTERNAL STRUCTURE . . . 8

III. NONLINEAR COUETTE FLOW FOR A DIATOMIC GAS 14

Background of the Problem
Formulation of the Problem
Computational Procedures
Results

IV. NONLINEAR RAYLEIGH'S FLOW FOR A DIATOMIC GAS. 62

Background of the Problem
Formulation of the Problem
Computational Procedures
Results

V. THE TWO DIMENSIONAL LEADING EDGE PROBLEM. 94

Background of the Problem
Formulation of the Problem
Computational Procedures
Results
Concluding Remarks

VI. DISCUSSION AND CONCLUSIONS. 128

Page

APPENDICES

A. THE NEW "ODD" EQUALLY SPACED QUADRATURE. 133

B. APPROXIMATE ENERGY LEVELS FOR ROTATIONAL RELAXATION. 135

BIBLIOGRAPHY 138

VITA 146

LIST OF ILLUSTRATIONS

Figure		Page
1.	Geometry and Coordinate System for the Couette Flow Problem.	16
2.	Comparisons of Density Profiles with Experimental Data ($1/K_n = 15.5$).	33
3.	Comparisons of Density Profiles with Experimental Data ($1/K_n = 11.25$)	34
4.	Comparisons of Density Profiles with Experimental Data ($1/K_n = 5.62$).	35
5.	Comparisons of Density Profiles with Experimental Data ($1/K_n = 2.58$).	36
6.	Comparisons of Heat Transfer with Experimental Data (Diatomic Gas)	37
7.	Comparisons of Heat Transfer with Experimental Data (Monatomic Gas).	38
8.	Comparisons of Density Profiles with Experimental Data ($K_{n_o} = 0.583$).	41
9.	Comparisons of Density Profiles with Experimental Data ($K_{n_o} = 0.288$).	42
10.	Comparisons of Density Profiles with Experimental Data ($K_{n_o} = 0.191$).	43
11.	Comparisons of Density Profiles with Experimental Data ($K_{n_o} = 0.11$)	44
12.	Comparisons of Density Profiles with Experimental Data ($K_{n_o} = 0.053$).	45
13.	Couette Flow Density Profiles for $\hat{W}' = 1$, $\hat{T}_2 = 0.4$	47
14.	Couette Flow Velocity Profiles for $\hat{W}' = 1$, $\hat{T}_2 = 0.4$	48
15.	Couette Flow Temperature Profiles for $\hat{W}' = 1$. $\hat{T}_2 = 0.4$. . .	49
16.	Couette Flow Density Profiles for $\hat{W}' = 0$, $\hat{T}_2 = 0.4$.	50

Figure		Page
17.	Couette Flow Temperature Profiles for $\hat{W}' = 0$, $\hat{T}_2 = 0.4$. . .	51
18.	Couette Flow Density Profiles for $\hat{W}' = 5$, $\hat{T}_2 = 1$.	52
19.	Couette Flow Velocity Profiles for $\hat{W}' = 5$, $\hat{T}_2 = 1$	53
20.	Couette Flow Temperature Profiles for $\hat{W}' = 5$, $\hat{T}_2 = 1$. . . .	54
21.	Couette Flow Translational and Rotational Temperature Profiles for $\hat{W}' = 5$, $\hat{T}_2 = 1$	55
22.	Couette Flow Density Profiles for $\hat{W}' = 5$, $\hat{T}_2 = 0.4$.	56
23.	Couette Flow Velocity Profiles for $\hat{W}' = 5$, $\hat{T}_2 = 0.4$	57
24.	Couette Flow Temperature Profiles for $\hat{W}' = 5$, $\hat{T}_2 = 0.4$. . .	58
25.	Couette Flow Translational and Rotational Temperature Profiles for $W' = 5$, $\hat{T}_2 = 0.4$	59
26.	Geometry and Coordinate System for the Rayleigh Flow Problem	65
27.	Raleigh Flow Density Profiles for $\hat{W} = 2$, $\hat{T}_w = 1$, $Z_R = 3.2$.	78
28.	Rayleigh Flow Tangential Velocity Profiles for $\hat{W} = 2$, $\hat{T}_w = 1$, $Z_R = 3.2$.	79
29.	Rayleigh Flow Normal Velocity Profiles for $\hat{W} = 2$, $\hat{T}_w = 1$, $Z_R = 3.2$.	80
30.	Rayleigh Flow Total Temperature Profiles and Internal Temperature Profiles for $\hat{W} = 2$, $\hat{T}_w = 1$, $Z_R = 3.2$, ...	81
31.	Rayleigh Flow Pressure Profiles for $\hat{W} = 2$, $\hat{T}_w = 1$, $Z_R = 3.2$.	82
32.	Rayleigh Flow Density Profiles for $\hat{W} = 2$, $\hat{T}_w = 1.6$, $Z_R = 3.2$.	83
33.	Rayleigh Flow Normal Velocity Profiles for $\hat{W} = 2$, $\hat{T}_w = 1.6$, $Z_R = 3.2$.	84
34.	Rayleigh Flow Tangential Velocity Profiles for $\hat{W} = 2$, $\hat{T}_w = 1.6$, $Z_R = 3.2$.	85
35.	Rayleigh Flow Pressure Profiles for $\hat{W} = 2$, $\hat{T}_w = 1.6$, $Z_R = 3.2$.	86

Figure Page

36. Rayleigh Flow Pressure Profiles for $\hat{W} = 2$, $\hat{T}_w = 1.6$, $Z_R = 3.2$ 87

37. Rayleigh Flow Density Profiles for $\hat{W} = 2$, $\hat{T}_w = 1.6$, $Z_R = 25$ 88

38. Rayleigh Flow Tangential Velocity Profiles for $\hat{W} = 2$, $\hat{T}_w = 1.6$, $Z_R = 25$ 89

39. Rayleigh Flow Normal Velocity Profiles for $\hat{W} = 2$, $\hat{T}_w = 1.6$, $Z_R = 25$ 90

40. Rayleigh Flow Temperature Profiles for $\hat{W} = 2$, $\hat{T}_w = 1.6$, $Z_R = 25$ 91

41. Rayleigh Flow Pressure Profiles for $\hat{W} = 2$, $\hat{T}_w = 1.6$, $Z_R = 25$ 92

42. Geometry and Coordinate System for the Two Dimensional Leading Edge Problem. 98

43. Flat Plate Density Profiles for $M_\infty = 6.1$, $T_w/T_o = 0.11$ and $\hat{x} = 18$. 111

44. Flat Plate Density Profiles for $M_\infty = 6.1$, $T_w/T_o = 0.11$ and $\hat{x} = 36$. 112

45. Flat Plate Density Profiles for the Different Wall Temperatures at $\hat{x} = 18$. 113

46. Flat Plate Density Profiles for the Different Wall Temperatures at $\hat{x} = 36$. 114

47. Flat Plate Density Profiles at Various $\hat{x}$ Station. 115

48. Flat Plate Tangential Velocity Profiles for a Monatomic Gas 116

49. Flat Plate Tangential Velocity Profiles for a Diatomic Gas. 117

50. Flat Plate Normal Velocity Profiles 119

51. Flat Plate Temperature Profiles 120

52. Normal Pressure 122

53. Skin Friction Coefficient 124

54. Heat Transfer Coefficient 125

LIST OF SYMBOLS

a	a constant, ν_{in}/ν_{el}
A	defined in Equation (52b)
α	accommodation coefficient
b	normal direction transformation constant
B	defined in Equation (52c)
c	specific heat or tangential direction transformation constant
C	defined in Equation (52d)
d	width between plates in Couette flow
f	local distribution function
E	internal energy
F	local Maxwellian equilibrium distribution function
g	first transformed distribution function
G	equilibrium form of first transformed distribution function
h	second transformed distribution function
H	equilibrium form of second transformed distribution function
R_δ	the Gauss-Laguerre weighting coefficient
j	third transformed distribution function
J	equilibrium form of third transformed distribution function
k	Boltzmann's constant
K_n	Knudsen number
m	molecular mass
M_∞	free stream Mach number
n	density

p_{ij}	stress tensor
p	pressure
Q_δ	defined in Equation (32h)
$\vec{q}$	heat flux vector with components q_x, q_y, q_z
R_{e_x}	Reynold's number at local x station
t	time
τ_o	the collision time of the gas in equilibrium
T	temperature
$\vec{u}$	macroscopic velocity with components u_x, u_y, u_z
U_∞	freestream velocity
$\vec{v}$	microscopic velocity with components v_x, v_y, v_z
V_1	characteristic velocity, $\sqrt{2RT_1}$
v_o	characteristic velocity, $\sqrt{2RT_o}$
V_∞	characteristic velocity, $\sqrt{2RT_\infty}$
$\bar{V}_{\infty,x}$	rarefaction parameter, $M_\infty(C/R_{e_x})^{1/2}$
W	velocity of upper plate for Couette flow
$\vec{x}$	position vector with components x, y, z
Z_R	a constant, $5(1 + a)/3a$
η	transformed normal position vector
ξ	transformed tangential position vector
$\bar{\ell}$	mean free path
λ	mean free path
ν	collision frequency
$\bar{\mu}$	viscosity
$\tau(y)$	universal coordinate

$\hat{\Omega}$ defined in Equation (20)

$\hat{\xi}$ defined in Equation (20)

Superscripts

$\pm$ indicates the positive and negative direction of v_x or v_y

i internal

Subscripts

f.m. free molecular quantity

i internal

ℓ internal energy state

R rotational

t translational

T total

v constant volume condition

w wall condition

x x component

y y component

z z component

∞ freestream condition

σ evaluated at x-component of microscopic velocity associated with σ discrete point

λ evaluated at y-component of microscopic velocity associated with λ discrete point

δ evaluated at internal energy state associated with δ discrete point

eq equilibrium

eℓ elastic

in	inelastic
1	lower plate condition
2	upper plate condition
0	reference condition

SUMMARY

Rarefied gasdynamic problems have been studied by many investigators in recent years. However, most of the studies have been made by considering the fluid as a monatomic gas. In practical gasdynamic problems, air must be considered as a mixture of diatomic gases which have fully excited rotational energy at ordinary temperature. Therefore, it is the purpose of this study to solve the nonlinear Boltzmann equation with the Bhatnagar-Gross-Krook type model for a rarefied diatomic gas using the method of discrete ordinates. The nonlinear Couette flow problem with heat transfer, the nonlinear Rayleigh problem, and the two-dimensional leading edge problem are considered. When possible, the solutions were compared with experimental data.

The general results of the investigation may be summarized as follows:

1. By comparing the results with experimental data, the present method is seen to give good results for both linear (small temperature differential) and nonlinear (large temperature differential) and nonlinear Couette flow problem. The accuracy and applicability of the Bhatnagar-Gross-Krook-Morse model is reasonably good for this one-dimensional problem.
2. The nonlinear Rayleigh problem in a diatomic gas has been solved, but no experimental data are available for comparison. However, the trend and the shape of the profiles are consistent with those of the monatomic gas solution.

3. The discrete ordinate method has also been applied to the two-dimensional leading edge problem for a diatomic gas by using a closed-boundary value approach. The results are found to be more reasonable than those of the initial value approach in which the up-stream effect was neglected. The thickness of the shock layer agrees fairly well with available experimental data, although the calculated shock wave is slightly weaker than that of the experimental data.

4. In existing experimental literature the surface pressure generated for the leading edge flow are measured within cavities in the surface, and so the measurements of pressure correspond to the net normal momentum transferred to the surface (p_{yy}). The calculated normal pressure (p_{yy}) distribution in the present study agrees well with experimental data.

5. In the leading edge problem the gradients (in y-direction) in density, velocity, and temperature for the diatomic gas are smaller than those for the monatomic gas. As a consequence the heat transfer coefficient and skin friction coefficient are larger for the monatomic gas than those for the diatomic gas. Since existing experimental data for the heat transfer and skin friction coefficients scatter rather widely, no firm conclusion can be drawn as to the accuracy of the present results for these two coefficients.

CHAPTER I

INTRODUCTION

Background and Review of Recent Literature

The combination of low densities, high velocities, and high temperatures, such as are encountered in hypervelocity reentry flight, has led to the study of such non-equilibrium gasdynamic phenomena as translational, rotational, vibrational, and dissociative relaxation in flows. The determination of the complete flow field around a vehicle which travels with high velocities in a rarefied gas is of practical importance, since the information is essential in the determination of drag on vehicles and in obtaining the information about the properties of the upper atmosphere.

This work will mainly be concerned with a basic study of some nonlinear rarefied gas flows with the effect of rotational relaxation.

In solving boundary value problems in rarefied gas dynamics with the full or even the linearized Bolzmann equation, difficulties with the collision integral of this equation are often encountered. To make possible the solution of various problems in rarefied gas dynamics, Bhatnagar, Gross, Krook [1] and others [2, 3] have developed simple models for the collision integral which yield plausible results. These models approximate the Boltzmann collision integral but still retain some of the gross features of the exact Boltzmann equation. The Bhatnagar-Gross-Krook model [1] (or the BGK model) has been extensively used in

numerous rarefied gas dynamics problems [4, 5, 6]. The ellipsoidal model [2, 3] which yields the correct Prandtl number for a monatomic gas has also been applied successfully to solve problems in rarefied gas dynamics [3, 7, 8]. However, these models are only for monatomic gases. Since the gases of most physical interest possess internal structure, it is important to investigate how this structure affects experimentally measured quantities.

In practical gas dynamics, air is considered as a mixture of diatomic gases, oxygen and nitrogen, which have fully excited rotational energy at ordinary temperatures. It seems more appropriate to take this rotational energy into consideration. In this study, the research problems will be to include the rotational relaxation in the theoretical calculation of boundary value problems in rarefied gas dynamics.

The first relatively successful attempt to consider the internal degrees of freedom was in the report of Wang Chang and Uhlenbeck [9]. The simple BGK type models for the collision term for polyatomic gases have been suggested by Morse [10, 11] and by Brau [12]. Hsu and Morse [13], using the linearized kinetic model equation and the half-range moment method, studied the heat transfer problem. Cipolla and Morse [14] have obtained a kinetic description for a polyatomic gas between concentric cylinders maintained at small different temperatures. Venkataraman and Morse [15] obtained an approximate solution to the kinetic model equation suggested by Morse [10] for the diatomic gas shock structure problem using the Mott-Smith method. Giddens, et al. [16], obtained the accurate solution to the same model equation, and thus they were able to evaluate the applicability of the statistical model by comparing their results

with available experimental data. To date, however, there has been no solution to the nonlinear rarefied gas dynamic problems such as the Couette flow, unsteady Rayleigh's flow, and the leading edge problem based on kinetic models for a polyatomic gas.

The method which is used to solve the Boltzmann equation will be discussed in the next section.

The review of the literature pertaining to the separate problem will be presented in the appropriate chapter.

Discussion of the Method

This study will mainly be concerned with the application of a systematic method to solve the Boltzmann equation with the BGK type model for a diatomic gas. In this work it will be demonstrated that the present method has flexibility for adaptation to many practical problems. The method used in this investigation is the discrete ordinate method which has been successfully applied to solve both the linearized [17-25] and the nonlinear [4-8, 26-29] Boltzmann equations with the BGK model for a monatomic gas. The usefulness and accuracy of the method was established in the solutions of the one-dimensional nonlinear rarefied gasdynamic problems (the Couette flow [5] and the shock structure problem [27]). In Reference 5, the results obtained by the present method were compared with Anderson's accurate numerical solutions [30] and were found to be in agreement. The applications reveal that the method yields very accurate results over a large range of Knudsen numbers with reasonably short computer time.

This discrete ordinate technique consists of replacing the

integration over velocity space of the distribution function in the Boltzmann equation by an appropriate quadrature. This requires approximating the velocity dependence of the distribution function by a set of functions, each evaluated at appropriate discrete points in velocity space. The number of discrete points used depends upon the degree of approximation desired. Thus, instead of solving a linear or nonlinear integro-differential equation for a function of space, time, and velocity, the problem is transformed to a system of linear or nonlinear first order differential equations in a set of functions which are continuous in space and time (if time-dependent problems are considered) but are point-functions in velocity space. This set is then solved simultaneously as an approximation to the true distribution function. An interesting and useful feature of applying the quadrature method to the velocity dependence of the distribution function is that the macroscopic properties of interest are all formed by taking velocity moments of this function. Hence, these moment integrations can be evaluated using the same quadrature by which the distribution function is originally solved, resulting in an extremely convenient form for calculation.

It should be noted that the proper choice of the quadrature formula to be used in the present method is very important. For instance, the Modified Gauss-Hermite quadrature [24] allows the method to give more accurate solutions to linearized gasdynamic problems [17-25] for larger values of Knudsen number than does the classical Gauss-Hermite quadrature [31]. In particular, the modified quadrature yields faster convergence for numerical quadratures than the classical quadrature does in the near free molecular flow regime in which the distribution function possesses

a streamwise character. However, the success of the application of the method with the modified quadrature to linearized gasdynamic problems is wholly based on the nature of the linear problem. The macroscopic velocities are small, resulting in a distribution function essentially centered about a zero velocity; and the temperature is constant, or nearly so, thus giving an essentially constant shape to the distribution function. Therefore, the integrals arising in linear problems allow the use of the modified quadrature which has irrationally spaced discrete ordinates. Also, the successful extension of the method to some nonlinear gasdynamic problems [4, 5] is entirely due to the development of the equally spaced quadrature [29]. However, as pointed out by Huang [32], this quadrature is only useful in the low supersonic flow case ($M_\infty < 2$) in which the distribution function has the form of a single-peaked or nearly Maxwellian distribution. In the high supersonic or hypersonic flow case, the distribution functions are usually double-peaked or highly non-Maxwellian. In order to accurately evaluate the integrations of these highly non-Maxwellian distribution functions, it is thus desirable to develop a new quadrature which is called the new "odd" equally spaced quadrature. The development of this new quadrature is presented in Appendix A.

Several significant features of the new quadrature are:

(1) The new quadrature which is similar to that of Newton-Cotes is an open type quadrature. In constrast to the equally spaced quadrature used by Hartley [29], the new quadrature does not require the shift in the molecular velocity coordinate. Namely, there is no restriction on the number of discrete points used in the velocity space,

and thus, as long as a sufficient numbers of discrete points and an apprcpriate spacing are taken, any macroscopic moments of interest can accurately be calculated.

(2) The new quadrature can be applied to calculate the collision integral of the nonlinear Boltzmann equation with the BGK type statistical models without resorting to any interpolating procedure in the numerical calculation.

(3) The weighting coefficients of the new quadrature are all constants. Thus, it is easier to apply them than those of the equally spaced quadrature [29] whose weighting coefficients are functionals of the local value of temperature.

Purpose of the Research

Since the determination of the complete flow field around a body or a vehicle which travels with high velocities in a rarefied diatomic gas has become of practical importance, and since the Navier-Stokes and other higher order macroscopic equations may be obtained as special forms of the Boltzmann transport equation, there has been considerable interest in the possibility of solving many gasdynamic problems for a diatomic gas for all flow regimes, from free molecular to continuum, using this equation.

It is the purpose of this work to solve the nonlinear Boltzmann equation with the BGK type models for a rarefied diatomic gas using the method of discrete ordinates. The solutions obtained in this study will be compared with existing experimental data in order to evaluate the accuracy of the physical model. The Couette flow with heat transfer, the

Rayleigh flow, and the two-dimensional leading edge problems will be investigated.

CHAPTER II

THE MODEL EQUATIONS FOR A GAS WITH INTERNAL STRUCTURE

As mentioned before the main effort in kinetic theory in recent years has been concerned with studies of the Boltzmann equation and the solution of various boundary problems for a monatomic gas. However, since the fluid with which the aerodynamicist is concerned is a diatomic gas mixture, such as air, there has been an increasing interest in solving the boundary value problems of kinetic theory for a diatomic gas, using the Boltzmann equation.

The first relatively successful attempt to describe inelastic collisions at a kinetic level was in the report of Wang Chang and Uhlenbeck [9]. In this description the gas is treated semi-quantum mechanically; the internal states are quantized and the velocity states are treated classically. To each internal quantum state with energy E_ℓ is assigned a velocity distribution function $f_\ell = f_\ell(\vec{x}, \vec{v}, t, E_\ell)$, where the energy E_ℓ completely specifies the internal state. The velocity distribution function f_ℓ is governed by the generalized Boltzmann equation [9]

$$\frac{\partial f_\ell}{\partial t} + \vec{v} \cdot \nabla_{\vec{x}} f_\ell + \left(\frac{\vec{F}_{ext}}{m}\right) \cdot \nabla_{\vec{v}} f_\ell = \left(\frac{\delta f_\ell}{\delta t}\right)_c \qquad (1)$$

where the velocity distribution function $f_\ell = f_\ell(\vec{x}, \vec{v}, t, E_\ell)$ depends upon space, velocity, time, and internal energy state ℓ. Here $\vec{x}$ and $\vec{v}$ are the space and velocity vectors, $\nabla_{\vec{x}}$ and $\nabla_{\vec{v}}$ are the gradient

operators in physical space and velocity space, respectively, $\vec{F}_{ext}$ is the external force vector applied to the gas of molecular mass, m, and $\left(\frac{\delta f_\ell}{\delta f}\right)_c$ is the total time rate of change of the distribution function due to collisions of the molecules. For problems of interest in this investigation it will be assumed that there are no external forces acting on the particles of the gas. Further, the Bhatnagar-Gross-Krook type model proposed by Morse [10] will be used for the collision integral. Not only is this perhaps the simplest model available, but it is also quite accurate for several gases (see, for example, the comparisons with the most recent experimental data in Chapter III of this study).

Morse [10] assumed that the elastic and inelastic contributions to the collision integral could be separated and wrote the Boltzmann equation as

$$\frac{\partial f_\ell}{\partial t} + \vec{v} \cdot \nabla_{\vec{x}} f_\ell = \left(\frac{\delta f_\ell}{\delta t}\right)_{e\ell} + \left(\frac{\delta f_\ell}{\delta t}\right)_{in} \tag{2}$$

where $\left(\frac{\delta f_\ell}{\delta t}\right)_{e\ell}$ and $\left(\frac{\delta f_\ell}{\delta t}\right)_{in}$ are the elastic and inelastic collision integrals.

For the collision terms, the approximations similar to that of Bhatnagar, Gross, Krook [1] are used by Morse

$$\left(\frac{\delta f_\ell}{\delta t}\right)_{e\ell} = \nu_{e\ell}\left(F_{t\ell} - f_\ell\right) \tag{2a}$$

$$\left(\frac{\delta f_\ell}{\delta t}\right)_{in} = \nu_{in}\left(F_{i\ell} - f_\ell\right) \tag{2b}$$

and

$$F_{t\ell} = n_\ell \left(\frac{m}{2\pi k T_t}\right)^{3/2} e^{-\frac{m}{2kT_t}(\vec{v}-\vec{u})^2} \tag{3a}$$

$$F_{i\ell} = n_{\ell eq} \left(\frac{m}{2\pi k T_T}\right)^{3/2} e^{-\frac{m}{2kT_T}(\vec{v}-\vec{u})^2} \tag{3b}$$

where k is the Boltzmann constant, n is the gas particle density, T_t is the translational temperature, T_T is the total temperature, n_ℓ is the partial density at energy level ℓ, $\vec{u}$ is the flow velocity, and $n_{\ell eq}$ is the equilibrium number density.

The elastic collision frequency, $\nu_{e\ell}$, and the inelastic collision frequency, ν_{in}, are taken to be of the form [10]

$$\nu_{e\ell} = \frac{n k T_t}{(1+a)\bar{\mu}} \tag{4a}$$

$$\nu_{in} = a\,\nu_{e\ell} \tag{4b}$$

$$Z_R = 5(1+a)/3a \tag{4c}$$

where the rotational relaxational parameter Z_R has to be obtained from experimental means. The viscosity, $\bar{\mu}$, is assumed to have a temperature dependence

$$\frac{\bar{\mu}}{\bar{\mu}_0} = \left(\frac{T_t}{T_0}\right)^S \tag{5}$$

where S is tabulated in page 223 of Reference [35]. The viscosity coefficient, $\bar{\mu}_0$, is related to the reference mean free path $\bar{\ell}_0$, by the relation

$$\bar{\mu}_0 = \frac{5}{16} m n_0 \bar{\ell}_0 \sqrt{2\pi R T_0} \tag{6}$$

where the subscript o is referred to the reference condition.

Combining Equations (4) through (6) gives

$$\nu_{e\ell} = \frac{16}{5(1+a)} \frac{n k T_t}{\bar{\ell}_0 m n_0 \sqrt{2\pi R T_0}} \left(\frac{T_t}{T_0}\right)^{-S} \tag{7a}$$

$$\nu_{in} = a\, \nu_{e\ell} \tag{7b}$$

It is seen that $F_{t\ell}$ characterizes a local Maxwellian distribution in translational states only and allows for the possibility of disparate translational and internal temperatures since elastic collisions cannot equilibrate internal quantum states. The distribution function f_ℓ then relaxes to $F_{t\ell}$ with the elastic collision time $1/\nu_{e\ell}$. Similarly, $1/\nu_{in}$ characterizes the relaxation of f_ℓ , due to inelastic collisions, to the local Maxwellian distribution $F_{i\ell}$. In this case the effect of collisions

is to thermalize both energy modes of the gas and to cause equipartition between translational and internal degrees of freedom on a time scale of the order of $1/\nu_{in}$.

The macroscopic quantities can be calculated as follows

$$n_\ell = \int f_\ell \, d^3v \tag{8a}$$

$$n = \sum_\ell n_\ell \tag{8b}$$

$$n_{\ell eq} = n \left(\frac{e^{-E_\ell / k T_T}}{\sum_s e^{-E_s / k T_T}} \right) \tag{8c}$$

$$\vec{u} = \frac{1}{n} \sum_\ell \int f_\ell \, \vec{v} \, d^3v \tag{8d}$$

$$\frac{3}{2} k T_t = \frac{1}{n} \sum_\ell \int f_\ell \, \frac{m}{2} (\vec{v} - \vec{u})^2 \, d^3v \tag{8e}$$

$$C_v^i \, T_i = \frac{1}{n} \sum_\ell n_\ell E_\ell \tag{8f}$$

$$P_{ij} = m \sum_\ell \int (v_i - u_i)(v_j - u_j) f_\ell \, d^3v \tag{8g}$$

$$\vec{q}_i = \sum_{\ell} \int f_\ell E_\ell (\vec{v} - \vec{u})\, d^3v \tag{8h}$$

$$\vec{q}_t = \sum_{\ell} \int f_\ell \frac{m}{2} (\vec{v} - \vec{u})^2 (\vec{v} - \vec{u})\, d^3v \tag{8i}$$

where p_{ij} is the stress tensor, and $\vec{q}_t$ and $\vec{q}_i$ are the translational and internal heat flux, respectively.

The total local heat flux vector is given by the contributions of energy flux from internal and translational states, $\vec{q}(\vec{x}, \vec{t}) = \vec{q}_t + \vec{q}_i$. Further, the total temperature is defined such that

$$C_V T_T = \frac{3}{2} k T_t + C_V^i T_i \tag{8j}$$

where $c_v = (\frac{3}{2})k + c_v^i$ represents the total constant volume specific heat of the gas.

The kinetic equation described in Equation (2) will be used as the governing equation for the diatomic gas flows in this study. This equation is termed as the Boltzmann equation with the Bhatnagar-Gross-Krook-Morse model or the BBGKM equation. It is seen that the present model is concerned only with the diatomic gas whose molecules have rotational energies excited. The effects of vibrational relaxation, ionization, and dissociation are neglected. This assumption is justified for the available experimental data which are used for comparisons in this investigation.

CHAPTER III

NONLINEAR COUETTE FLOW FOR A DIATOMIC GAS

Background of the Problem

In this chapter the discrete ordinate method with the new quadrature is applied to the solution of nonlinear Couette flow with heat transfer for a diatomic gas in order to test the applicability of the model equation and the proposed method by comparing the solution with the experimental data. The continuum solution of this problem is available in Schlichting [36]. However, there has been no solution of this problem for high Knudsen numbers and high Mach numbers.

Hsu and Morse [13] have solved the linearized version of the kinetic model equation in Equation (2) for the parallel plate heat transfer problem using the half-range moment method. Cipolla and Morse [14] have used the same linearized equation and obtained a kinetic description for a diatomic gas between concentric cylinders maintained at small different temperatures.

Recently, Teagan and Springer [33] have measured the heat conduction and density distributions for a diatomic rarefied gas at rest contained between two unequally heated plates at small temperature differences. Very recently, Alofs, et al. [34] have experimentally obtained the density distribution for a diatomic gas contained between parallel plates at high temperature differences. These two sets of experimental data will be used to compare with the calculated results to test the accuracy of the

model equation and the applicability of the method.

Formulation of the Problem

The geometry of this problem is shown in Fig. 1. A diatomic gas with internal degrees of freedom (rotational only) is confined between two parallel plates, y = 0 and y = d. The plate y = 0 is at rest and is maintained at a constant temperature T_1; the plate y = d is translating in its own plane with a constant velocity W and is maintained at a constant temperature T_2. The kinetic model described in Chapter II was chosen for the collision integral in each internal energy state. The Boltzmann equation for the present case can be written as

$$V_y \frac{\partial f_\ell}{\partial y} = \nu_{\ell\ell}(F_{t\ell} - f_\ell) + \nu_{in}(F_{i\ell} - f_\ell) \tag{9}$$

where $F_{t\ell}$ and $F_{i\ell}$ in this case can be written as

$$F_{t\ell} = n_\ell \left(\frac{m}{2\pi k T_t}\right)^{3/2} e^{-\frac{m}{2kT_t}\left[(V_x - u_x)^2 + V_y^2 + V_z^2\right]} \tag{10a}$$

$$F_{i\ell} = n_{\ell eq} \left(\frac{m}{2\pi k T_T}\right)^{3/2} e^{-\frac{m}{2kT_T}\left[(V_x - u_x)^2 + V_y^2 + V_z^2\right]} \tag{10b}$$

For each energy level, Equation (9) is one dimensional in physical space but is three-dimensional in velocity space. In order to reduce the

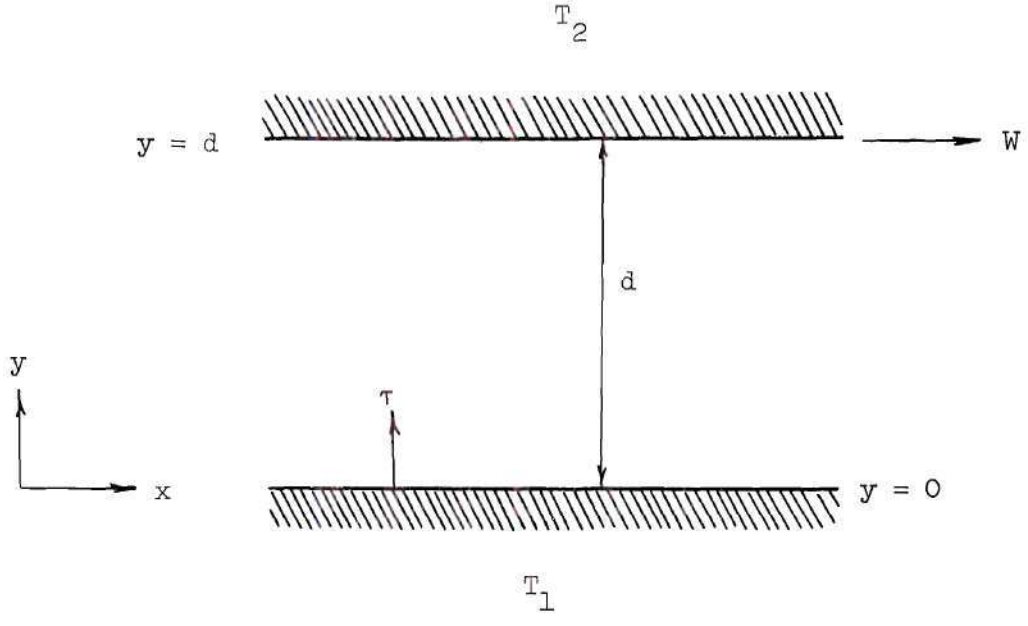

Figure 1. Geometry and Coordinate System for the Couette Flow Problem.

computer storage requirement, the following functions are defined [5]:

$$g_\ell(y;\, v_y;\, E_\ell) = \int_{-\infty}^{\infty}\int_{-\infty}^{\infty} f_\ell(y;\, \vec{v};\, E_\ell)\, dv_x\, dv_z \tag{11a}$$

$$h_\ell(y;\, v_y;\, E_\ell) = \int_{-\infty}^{\infty}\int_{-\infty}^{\infty} (v_x^2 + v_z^2)\, f_\ell(y;\, \vec{v};\, E_\ell)\, dv_x\, dv_z \tag{11b}$$

$$j_\ell(y;\, v_y;\, E_\ell) = \int_{-\infty}^{\infty}\int_{-\infty}^{\infty} v_x\, f_\ell(y;\, \vec{v};\, E_\ell)\, dv_x\, dv_z \tag{11c}$$

Multiplying Equation (9) by the weighting functions 1, v_x and $v_x^2 + v_z^2$, respectively, and integrating over $dv_x dv_z$ yield the equations:

$$v_y \frac{\partial g_\ell}{\partial y} = \nu_{e\ell}\,(G_{t\ell} - g_\ell) + \nu_{in}\,(G_{i\ell} - g_\ell) \tag{12a}$$

$$v_y \frac{\partial h_\ell}{\partial y} = \nu_{e\ell}\,(H_{t\ell} - h_\ell) + \nu_{in}\,(H_{i\ell} - h_\ell) \tag{12b}$$

$$v_y \frac{\partial j_\ell}{\partial y} = \nu_{e\ell}\,(J_{t\ell} - j_\ell) + \nu_{in}\,(J_{i\ell} - j_\ell) \tag{12c}$$

where

$$G_{tl} = \frac{n_l}{(2\pi R T_t)^{1/2}} e^{-V_y^2/2RT_t} \tag{13a}$$

$$H_{tl} = G_{tl}(2RT_t + U_x^2) \tag{13b}$$

$$J_{tl} = U_x G_{tl} \tag{13c}$$

$$G_{il} = n_{leq} \frac{1}{(2\pi R T_T)^{1/2}} e^{-V_y^2/2RT_T} \tag{13d}$$

$$H_{il} = G_{il}(2RT_T + U_x^2) \tag{13e}$$

$$J_{il} = U_x G_{il} \tag{13f}$$

The macroscopic moments are

$$n_l = \int_{-\infty}^{\infty} g_l \, dV_y \tag{14a}$$

$$n = \sum_l n_l \tag{14b}$$

$$n_{\ell eq} = n \left(\frac{e^{-E_\ell / k T_T}}{\sum_s e^{-E_s / k T_T}} \right) \tag{14c}$$

$$u_x = \frac{1}{n} \sum_\ell \int_{-\infty}^{\infty} j_\ell \, dV_y \tag{14d}$$

$$3 n R T_t = \sum_\ell \left\{ \int_{-\infty}^{\infty} h_\ell \, dV_y + \int_{-\infty}^{\infty} V_y^2 \, g_\ell \, dV_y \right\} - n u_x^2 \tag{14e}$$

$$T_i = \frac{1}{n} \sum_\ell n_\ell E_\ell \tag{14f}$$

$$T_T = \frac{3}{5} T_t + \frac{2}{5} T_i \tag{14g}$$

where c_v^i is taken to be k.

It is convenient to introduce a non-dimensional variable as follows

$$T(y) = \frac{Kn}{V_1} \int_0^y \nu_{\ell\ell}(y') \, dy' \tag{15}$$

where the global Knudsen number is defined as

$$Kn = \frac{V_1}{\int_0^d \nu_{el}(y')\,dy'} \tag{16}$$

and

$$V = \sqrt{2RT_1} \tag{17}$$

The definitions of dimensionless variables are

$$\hat{v} = \frac{v}{V_1}, \quad \hat{u} = \frac{u}{V_1}, \quad \hat{w} = \frac{w}{V_1}, \quad \hat{u}' = \sqrt{2}\,\hat{u}$$

$$\hat{w}' = \sqrt{2}\,w, \quad \hat{n} = \frac{n}{n_1}, \quad \hat{T} = \frac{T}{T_1}, \quad \hat{E} = \frac{E}{KT_1}$$

$$\hat{g}_l = \frac{V_1}{n_1} g_l, \quad \hat{h}_l = \frac{1}{n_1 V_1} h_l, \quad \hat{j}_l = \frac{1}{n_1} j_l$$

$$\hat{G}_l = \frac{V_1}{n_1} G_l, \quad \hat{H}_l = \frac{1}{n_1 V_1} H_l, \quad \hat{J}_l = \frac{1}{n_1} J_l$$

where the subscript "1" specifies the flow condition at the lower plate.

After the process of nondimensionalization of Equations (12) and (13), the discrete ordinate method outlined in Chapter I is applied. This

technique consists of approximating the integration over velocity space of the distribution function in the Boltzmann equation by the new quadrature. This requires approximating the velocity dependence of the distribution function by a set of functions, each evaluated at appropriate discrete points in velocity space. The number of discrete points which is taken depends on the degree of approximation which is desired. Thus, instead of solving a non-linear integro-differential equation for a function of space and velocity, the problem is transformed to a system of non-linear, first order differential equations in a set of functions which are continuous in space but are point-functions in velocity space. This set is then solved simultaneously as an approximation to the true distribution function.

Nondimensionalizing Equations (12) and (13), and using the discrete points in velocity space gives:

$$K_n \hat{V}_\sigma \frac{\partial \hat{g}_{\sigma,\delta}}{\partial \tau} = \hat{G}_{t,\sigma,\delta} - \hat{g}_{\sigma,\delta} + a\left(\hat{G}_{i,\sigma,\delta} - \hat{g}_{\sigma,\delta}\right) \tag{18a}$$

$$K_n \hat{V}_\sigma \frac{\partial \hat{h}_{\sigma,\delta}}{\partial \tau} = \hat{H}_{t,\sigma,\delta} - \hat{h}_{\sigma,\delta} + a\left(\hat{H}_{i,\sigma,\delta} - \hat{h}_{\sigma,\delta}\right) \tag{18b}$$

$$K_n \hat{V}_\sigma \frac{\partial \hat{J}_{\sigma,\delta}}{\partial \tau} = \hat{J}_{t,\sigma,\delta} - \hat{j}_{\sigma,\delta} + a\left(\hat{J}_{i,\sigma,\delta} - \hat{j}_{\sigma,\delta}\right) \tag{18c}$$

where

$$\hat{G}_{t,\sigma,\delta} = \hat{n}_\delta \left(\frac{1}{\pi \hat{T}_t}\right)^{1/2} e^{-\hat{v}_\sigma^2/\hat{T}_t} \tag{19a}$$

$$\hat{H}_{t,\sigma,\delta} = \left(\hat{T}_t + \hat{u}_x^2\right) \hat{G}_{t,\sigma,\delta} \tag{19b}$$

$$\hat{J}_{t,\sigma,\delta} = \hat{u}_x \hat{G}_{t,\sigma,\delta} \tag{19c}$$

$$\hat{G}_{i,\sigma,\delta} = \hat{n}_{leq} \left(\frac{1}{\sqrt{\pi \hat{T}_T}}\right) e^{-\hat{v}_\sigma^2/\hat{T}_T} \tag{19d}$$

$$H_{i,\sigma,\delta} = \left(\hat{T}_T + \hat{u}_x^2\right) \hat{G}_{i,\sigma,\delta} \tag{19e}$$

$$\hat{J}_{i,\sigma,\delta} = \hat{u}_x \hat{G}_{i,\sigma,\delta} \tag{19f}$$

$$\hat{n}_{leq} = \frac{\hat{n}}{\hat{T}_T} R_\delta e^{\hat{E}_\delta\left(1 - \frac{1}{\hat{T}_T}\right)} = \hat{n} \frac{e^{-\hat{E}_\delta/\hat{T}_T}}{\sum_s e^{-\hat{E}_s/\hat{T}_T}} \quad \text{[Appendix B]} \tag{19g}$$

the subscripts σ, δ represent functions which have been

evaluated at the discrete velocity points $\hat{v}_\sigma$ (σ = - m, -1, 1, ...n) and the discrete energy levels $\hat{E}_\delta$ (δ = 1, ...n'), respectively. Here, the new equally spaced quadrature [Appendix A] is used in the velocity space, and the Gauss-Laguerre quadrature is used in the energy space [Appendix B]. In Equation (19g), R_β and E_δ are the weighting coefficients and the discrete ordinates of the Gauss-Laguerre quadrature, respectively.

The gas-surface interaction is specified by introducing the translational accommodation coefficient α_t, and the internal accommodation coefficient α_i . Since it is important to distinguish molecules traveling toward the plate from those moving away from it within a distance of the order of several mean free paths from the plate, it is convenient to define the half-range distribution function as follows

$$\hat{f}_\ell = \hat{f}_\ell^+ + \hat{f}_\ell^-$$

$$\hat{f}_\ell^+ (\hat{y}; \hat{v}_y; \hat{E}_\ell) = 0 , \quad \text{for } \hat{v}_y < 0$$

$$\hat{f}_\ell^- (\hat{y}; \hat{v}_y; \hat{E}_\ell) = 0 , \quad \text{for } \hat{v}_y > 0$$

The normalized boundary conditions can then be written as follows, where the subscript "i" specifies the incident molecule condition

$$\hat{q}^{+}_{\sigma,\delta}(\tau=0) = \alpha_i \alpha_t \hat{\Omega}^{+}_{\tau=0} \hat{\xi}^{+}_{\tau=0}$$

$$+(1-\alpha_i)(1-\alpha_t)\hat{\Omega}^{-}_{\tau=0} \hat{\xi}^{-}_{\tau=0} + \alpha_i(1-\alpha_t)\hat{\Omega}^{+}_{\tau=0} \hat{\xi}^{-}_{\tau=0}$$

$$+(1-\alpha_i)\alpha_t \hat{\Omega}^{-}_{\tau=0} \hat{\xi}^{+}_{\tau=0}, \quad \text{for } \hat{v}_\sigma > 0$$

(20a)

$$\hat{h}^{+}_{\sigma,\delta}(\tau=0) = \alpha_i\alpha_t \hat{\Omega}^{+}_{\tau=0} \hat{\xi}^{+}_{\tau=0} + (1-\alpha_i)(1-\alpha_t)\hat{\Omega}^{-}_{\tau=0} \hat{\xi}^{-}_{\tau=0}(\hat{T}_i + \hat{u}^2_{x_i})$$

$$+\alpha_i(1-\alpha_t)\hat{\Omega}^{+}_{\tau=0} \hat{\xi}^{-}_{\tau=0}(\hat{T}_i + \hat{u}^2_{x_i})$$

$$+(1-\alpha_i)\alpha_t \hat{\Omega}^{-}_{\tau=0} \hat{\xi}^{+}_{\tau=0}, \quad \text{for } \hat{v}_\sigma > 0$$

(20b)

$$\hat{j}^{+}_{\sigma,\delta}(\tau=0) = (1-\alpha_i)(1-\alpha_t)\hat{\Omega}^{-}_{\tau=0} \hat{\xi}^{-}_{\tau=0} \hat{u}_{xi}$$

$$+\alpha_i (1-\alpha_t)\, \hat{\Omega}^{+}_{\tau=0}\, \hat{\xi}^{-}_{\tau=0}\, \hat{u}_{xi}$$

$$\text{for } \hat{v}_\sigma > 0 \qquad (20c)$$

where

$$\hat{\Omega}^{+}_{\tau=0} = \frac{e^{-\hat{E}_\delta}}{\sum_s e^{-\hat{E}_s}} = H_\delta$$

$$\hat{\Omega}^{-}_{\tau=0} = \frac{\hat{n}_i\, e^{-\hat{E}_\delta/\hat{T}_i}}{\sum_s e^{-\hat{E}_s/\hat{T}_i}} = \frac{\hat{n}_i}{\hat{T}_i} H_\delta\, e^{\hat{E}_\delta\left(1-\frac{1}{\hat{T}_i}\right)}$$

$$\hat{\xi}^{+}_{\tau=0} = \frac{1}{\sqrt{\pi}}\, e^{-\hat{v}_\sigma^2}$$

and

$$\hat{\xi}^{-}_{\tau=0} = \frac{1}{\sqrt{\pi \hat{T}_i}} e^{-\hat{v}_\sigma^2 / \hat{T}_i}$$

$$\hat{g}^{-}_{\sigma,s}(\tau=1) = \alpha_i \alpha_t \hat{\Omega}^{-}_{\tau=1} \hat{\xi}^{-}_{\tau=1} + (1-\alpha_i)(1-\alpha_t) \hat{\Omega}^{+}_{\tau=1} \hat{\xi}^{+}_{\tau=1}$$

$$+\alpha_i (1-\alpha_t) \hat{\Omega}^{-}_{\tau=1} \hat{\xi}^{+}_{\tau=1} + (1-\alpha_i)\alpha_t \hat{\Omega}^{+}_{\tau=1} \hat{\xi}^{-}_{\tau=1} \quad \text{for } \hat{v}_\sigma < 0$$

(20d)

$$\hat{h}^{-}_{\sigma,s}(\tau=1) = \alpha_i \alpha_t \hat{\Omega}^{-}_{\tau=1} \hat{\xi}^{-}_{\tau=1} (\hat{T}_2 + \hat{W}^2) + (1-\alpha_i)(1-\alpha_t) \hat{\Omega}^{+}_{\tau=1} \hat{\xi}^{+}_{\tau=1} (\hat{T}_i + \hat{u}^2_{xi})$$

$$+\alpha_i (1-\alpha_t) \hat{\Omega}^{-}_{\tau=1} \hat{\xi}^{+}_{\tau=1} (\hat{T}_i + \hat{u}^2_{xi}) + (1-\alpha_i)\alpha_t \hat{\Omega}^{+}_{\tau=1} \hat{\xi}^{-}_{\tau=1} (\hat{T}_2 + \hat{W}^2)$$

$$\text{for } \hat{v}_\sigma < 0 \qquad (20e)$$

$$\hat{j}^{-}_{\sigma,s}(\tau=1) = \alpha_i \alpha_t \hat{\Omega}^{-}_{\tau=1} \hat{\xi}^{-}_{\tau=1} \hat{W}$$

$$+(1-\alpha_i)(1-\alpha_t)\hat{\Omega}^{+}_{\tau=1}\hat{\xi}^{-}_{\tau=1}\hat{u}_{xi}+\alpha_i(1-\alpha_t)\hat{\Omega}^{-}_{\tau=1}\hat{\xi}^{+}_{\tau=1}\hat{u}_{xi}$$

$$+(1-\alpha_i)\alpha_t\hat{\Omega}^{+}_{\tau=1}\hat{\xi}^{-}_{\tau=1}\hat{W}, \quad \text{for } \hat{v}_\sigma < 0 \qquad (20f)$$

where

$$\hat{\Omega}^{-}_{\tau=1}=\frac{\hat{n}_2\, e^{-\hat{E}_s/\hat{T}_2}}{\sum_s e^{-\hat{E}_s/\hat{T}_2}}=\frac{\hat{n}_2}{\hat{T}_2}H_s\, e^{\hat{E}_s\left(1-\frac{1}{\hat{T}_2}\right)}$$

$$\hat{\Omega}^{+}_{\tau=1}=\frac{\hat{n}_i\, e^{-\hat{E}_s/\hat{T}_i}}{\sum_s e^{-\hat{E}_s/\hat{T}_i}}=\frac{\hat{n}_i}{\hat{T}_i}H_s\, e^{\hat{E}_s\left(1-\frac{1}{\hat{T}_i}\right)}$$

$$\hat{\xi}^{-}_{\tau=1}=\frac{1}{\sqrt{\pi\hat{T}_2}}e^{-\hat{v}_\sigma^2/\hat{T}_2}$$

and

$$\hat{\xi}^{+}_{\tau=1}=\frac{1}{\sqrt{\pi\hat{T}_i}}e^{-\hat{v}_\sigma^2/\hat{T}_i}$$

Another condition to determine the parameter $\hat{n}_2$ is that the net mass flux normal to the plates be zero at the plates, i.e.,

$$\sum_\ell\left\{\int_0^\infty \hat{v}_y\,\hat{g}^{+}_\ell(\hat{v}_y,\hat{E}_\ell)\,d\hat{v}_y-\int_{-\infty}^0 \hat{v}_y\,\hat{g}^{-}_\ell(\hat{v}_y,\hat{E}_\ell)\,d\hat{v}_y\right\}=0 \qquad (21)$$

Applying the new quadrature, Equation (21) then becomes

$$-\sum_{\delta=1}^{n'}\sum_{\sigma=-1}^{-m} k_\sigma \hat{V}_\sigma \hat{g}^{-}_{\sigma,\delta}(\hat{V}_\sigma, \hat{E}_\delta) + \sum_{\delta=1}^{n'}\sum_{\sigma=1}^{n} k_\sigma \hat{V}_\sigma \hat{g}^{+}_{\sigma,\delta}(\hat{V}_\sigma, \hat{E}_\delta) = 0 \tag{22}$$

where k_σ is the new weighting coefficient for the velocity component $\hat{v}_\sigma$ [Appendix A].

The new quadrature is similarly applied to find moments defined in Equations (14).

Thus, the problem leads to solving Equations (18) subject to the boundary conditions in Equations (20) and (22).

Computational Procedures

One of the advantages of applying the discrete ordinate method is to remove the microscopic velocity dependence from the distribution functions. This is to say that the system of nonlinear first order partial differential equation in Equation (12) has been transformed to a system of nonlinear, first order ordinary differential equation in Equations (18). The resulting set of equations can be solved by incorporating a finite difference technique coupled with an iterative scheme.

The distribution function at each discrete point is calculated by using the predictor-corrector method. Since the problem exhibits a "two stream" character, i.e., the distribution functions of the molecular stream coming toward the wall are significantly different from the distribution functions of the molecular stream going away from the wall at

the zero ordinate, the difference equations must be separated for the two-stream distribution functions. The grid points described below are used in the physical space.

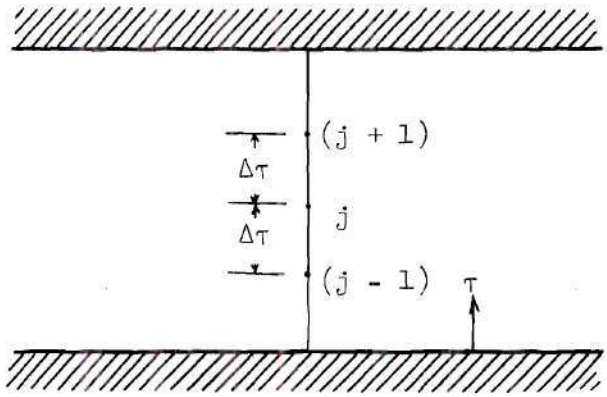

Starting from the lower wall with the known values of $\hat{g}^{+}_{\sigma,\delta}(\tau = 0)$ stated in Equation (20a), the difference form of Equation (18a) is applied as follows

$$\hat{g}^{+}_{\sigma,\delta}(j) = \left\{ \frac{1}{2}\left[\hat{G}^{+}_{t,\sigma,\delta}(j) + \hat{G}^{+}_{t,\sigma,\delta}(j-1) \right.\right.$$

$$\left. + a\left(\hat{G}^{+}_{\lambda,\sigma,\delta}(j) + \hat{G}^{+}_{\lambda,\sigma,\delta}(j-1) \right) \right]$$

$$\left. - \left(\frac{1+a}{2} - \frac{K_n \hat{V}_\sigma}{\Delta\tau} \right) \hat{g}^{+}_{\sigma,\delta}(j-1) \right\} \Big/ \left(\frac{1+a}{2} + \frac{K_n \hat{V}_\sigma}{\Delta\tau} \right) \tag{23}$$

The $\hat{h}^{+}_{\sigma,\delta}$ and $\hat{j}^{+}_{\sigma,\delta}$ equations are similarly transformed.

The resulting values of $\hat{g}^{+}_{\sigma,\delta}$ ($\tau = 1$) obtained from the solution of Equation (23) are integrated to apply the no normal mass flux boundary condition, Equation (22). This yields $\hat{n}_2$, which, in turn, generates values of $\hat{g}^{-}_{\sigma,\delta}$ ($\tau = 1$), Equation (20d). Starting with these values of $\hat{g}^{-}_{\sigma,\delta}$ ($\tau = 1$), Equation (23) is rearranged and applied in the following form marching from the upper plate to the lower plate:

$$\hat{g}^{-}_{\sigma,\delta}(j) = \left\{ \frac{1}{2}\left[\hat{G}^{-}_{t,\sigma,\delta}(j) + \hat{G}^{-}_{t,\sigma,\delta}(j+1) \right.\right.$$

$$\left. + a\left(\hat{G}^{-}_{i,\sigma,\delta}(j) + \hat{G}^{-}_{\sigma,\delta}(j+1) \right) \right]$$

$$\left. - \left(\frac{1+a}{2} + \frac{K_n \hat{V}_\sigma}{\Delta\tau} \right) \hat{g}^{-}_{\sigma,\delta}(j+1) \right\} \Big/ \left(\frac{1+a}{2} - \frac{K_n \hat{V}_\sigma}{\Delta\tau} \right) \tag{24}$$

The $\hat{h}^{-}_{\sigma,\delta}$ and $\hat{j}^{-}_{\sigma,\delta}$ equations are similarly transformed.

The equilibrium distribution function values $\hat{G}^{\pm}_{t,\sigma,\delta}$, $\hat{G}^{\pm}_{i,\sigma,\delta}$, $\hat{H}^{\pm}_{t,\sigma,\delta}$, $\hat{H}^{\pm}_{i,\sigma,\delta}$, $\hat{J}^{\pm}_{t,\sigma,\delta}$ and $\hat{J}^{\pm}_{i,\sigma,\delta}$ are determined from the moments of the previous iterate. The zeroth iterate is the free molecular solution. This yields a system of $3x(m+n)xn'$ nonlinear algebraic equation in $3x(m+n)xn'$ unknowns ($\hat{g}_{\sigma,\delta}$, $\hat{h}_{\sigma,\delta}$, and $\hat{j}_{\sigma,\delta}$; $\sigma = -m, \ldots, -1, 1, \ldots, n$; $\delta = 1, \ldots, n'$) which is solved by the method of successive approximations.

Owing to the presence of the Knudsen number K_n in Equations (23) and (24), the following procedures are applied: first, the free molecular

value of $\hat{n}$, $\hat{u}_x$, and $\hat{T}$ are assigned to the functions $\hat{G}_{t,\sigma,\delta}$, $\hat{G}_{i,\sigma,\delta}$, $\hat{H}_{t,\sigma,\delta}$, $\hat{H}_{i,\sigma,\delta}$, $\hat{J}_{t,\sigma,\delta}$ and $\hat{J}_{i,\sigma,\delta}$ in Equations (19) and then Equations (18) are solved using the iterative method for the Knudsen number, say 100. Once convergence is obtained for $K_n = 100$, the newly calculated values of $\hat{n}$, $\hat{u}_x$, and $\hat{T}$ are used as the zeroth iterates to solve Equations (18) for $K_n = 10$. The same procedure is repeated to solve Equations (18) for smaller Knudsen number cases; i.e., $K_n = 1$, 0.1, 0.05, and so on. In this way, the results for the transition, slip, and continuum flow regimes are obtained. Convergence is assumed to have occurred when the difference in successive iterates of the macroscopic variables is $\leq 10^{-4}$. A UNIVAC 1108 digital computer was used for all the computations.

Results

Although there have been no theoretical results available for the nonlinear Couette flow in a diatomic gas so far, there are experimental data obtained by Teagan and Springer [33] for the linear heat transfer case (i.e., small temperature difference between two plates) and by Alofs, Flagan and Springer [34] for the nonlinear case. These experimental data are used for comparisons in order to test the usefulness of the proposed method.

The Linear Heat Transfer Case

The accuracy of the present nonlinear method is first tested against some experimental data of the linear case. The exact experimental conditions ($T_2 = 1.32\ T_1$, and K_n as indicated in Figures 2 through 5) of Teagan and Springer's work [33] are used in the calculations for the

density profiles. The results are compared with the experimental data in Figures 2 through 5. The results are seen to be in reasonably good agreement for all flow regimes except possibly $1/K_n = 2.58$ where a rather low value of α is needed to fit with the experimental data. Also, the results seem to indicate that the accommodation coefficients needed to fit the experimental data decrease as the kinetic region is entered. This seems reasonable because the number of molecule-molecule communication is limited in kinetic region, and more specular reflection is expected to occur. The relaxation parameter "a" is taken to be 0.4 which is equivalent to $Z_R = 5.8$. It was found that the change of "a" only slightly changes the density profiles close to the plate. Based on these comparisons, the present method is seen to give reasonable solutions for the linear case.

The results shown in Figure 2 through 5 were obtained using a spacing of 0.02 in τ , five sets of the new equally spaced quadrature of order n = 8 with a spacing of 0.1 and 12 energy levels with a spacing of 0.5. Similar results have been obtained using a spacing of 0.01 in τ, quadrature of order n = 3, and 15 energy levels.

The heat transfer results are also obtained for the linearized case (the conditions are the same as those of Reference 33, where the accommodation coefficients are not experimentally measured.). The calculated heat flux solutions normalized by the free molecular quantity $(q_y/q_{f.m.})$ are compared with the experimental data in Figure 6. The calculated results seem to be always lower than the experimental data. In fact, Willis [37] has also pointed out the same conclusion for the monatomic case (see, for instance, Figure 7). In Figure 7 the heat flux

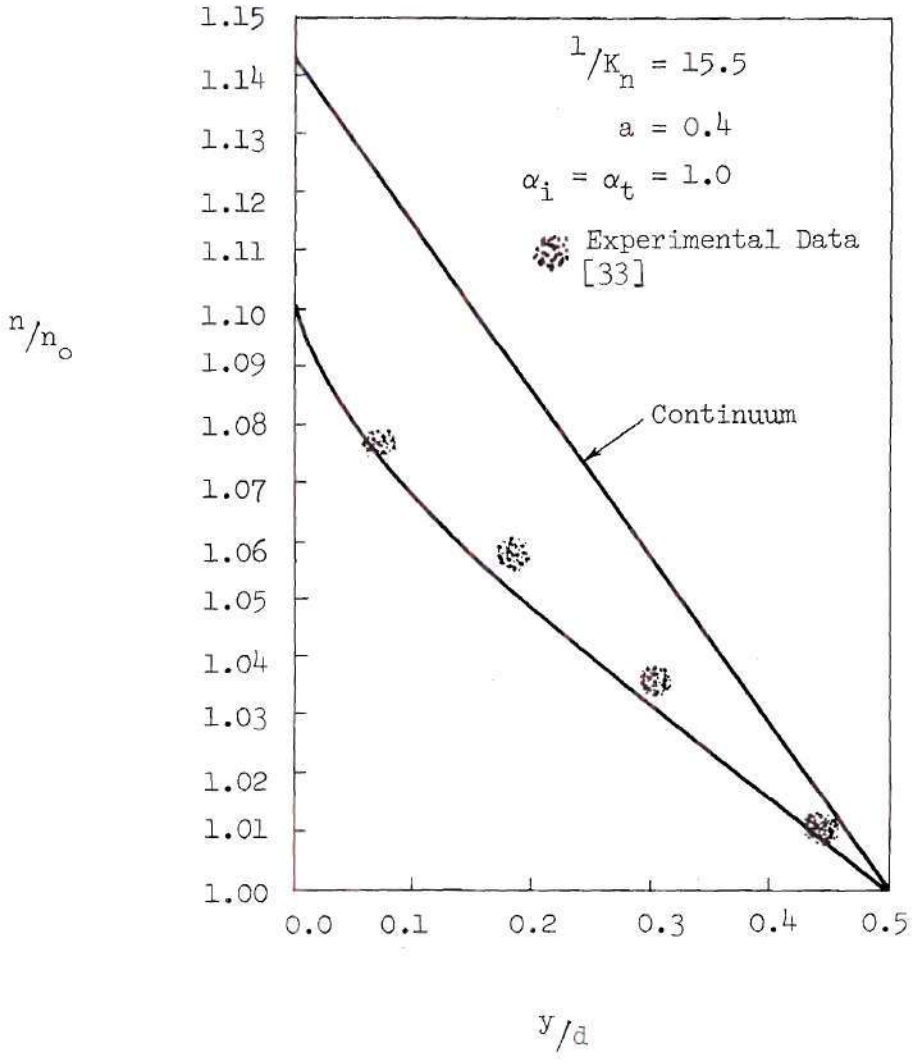

Figure 2. Comparisons of Density Profiles with Experimental Data ($1/K_n = 15.5$).

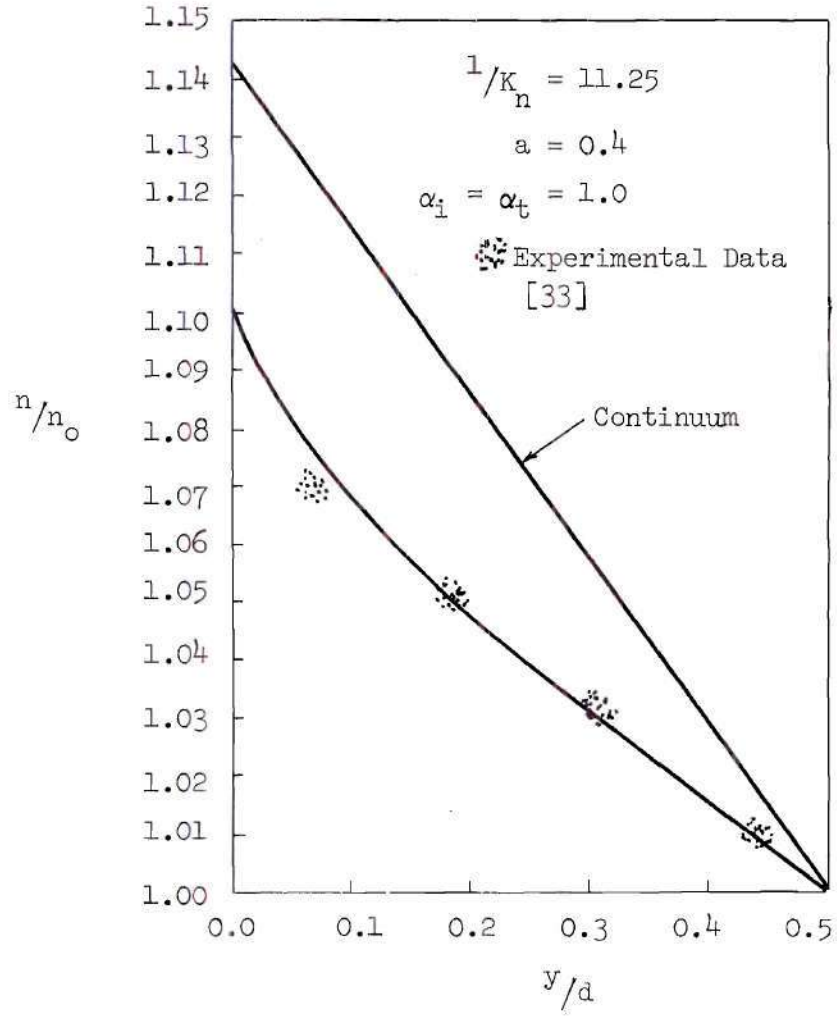

Figure 3. Comparisons of Density Profiles with Experimental Data ($1/K_n = 11.25$).

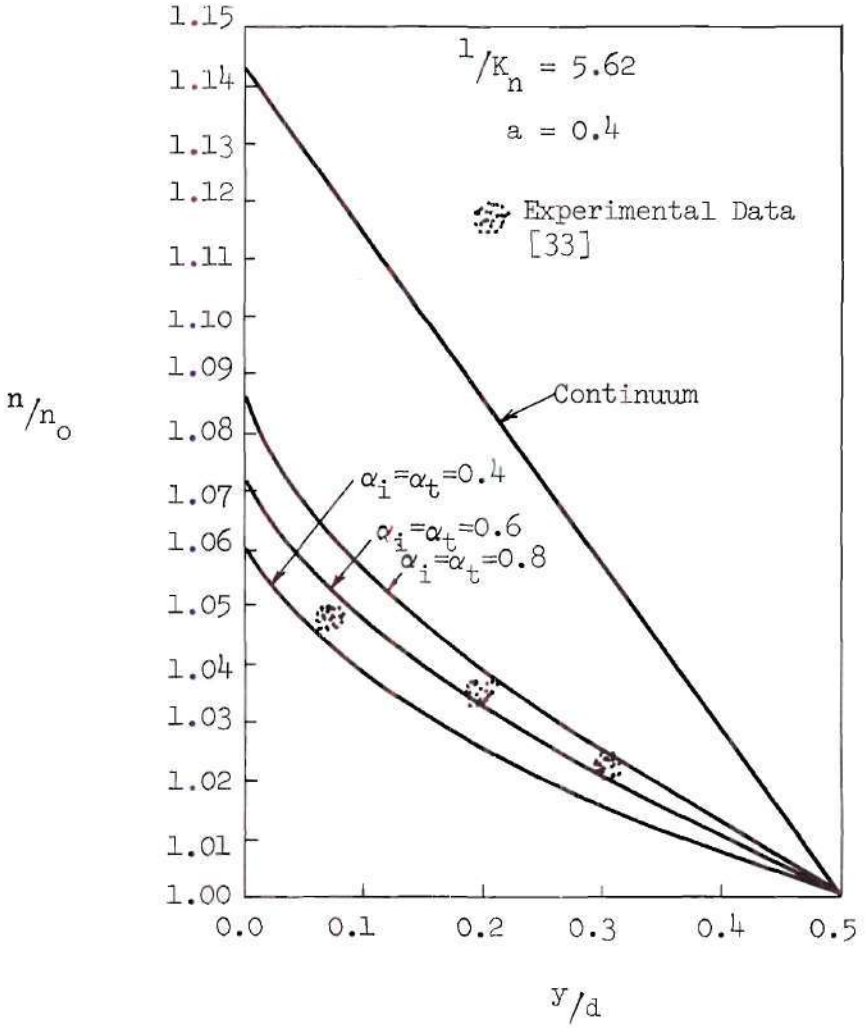

Figure 4. Comparisons of Density Profiles with Experimental Data ($1/K_n = 5.62$).

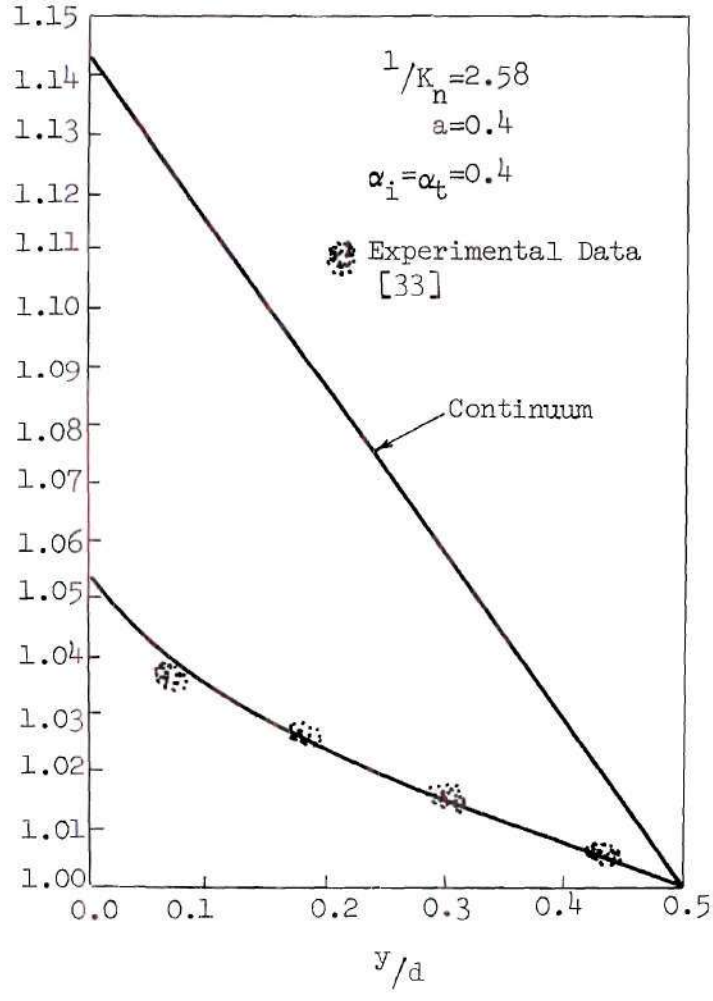

Figure 5. Comparisons of Density Profiles with Experimental Data ($1/K_n = 2.58$).

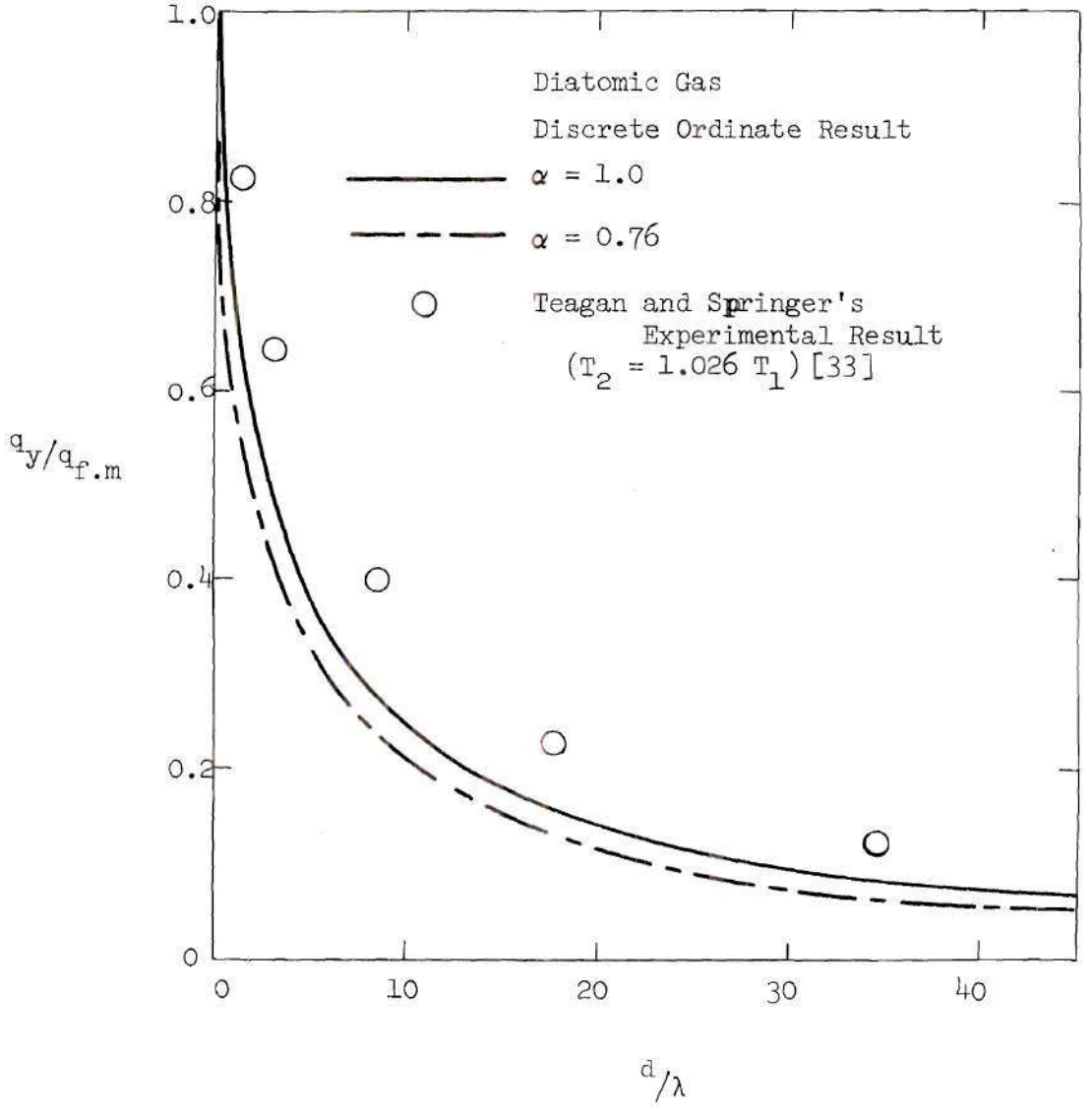

Figure 6. Comparisons of Heat Transfer with Experimental Data (Diatomic Gas).

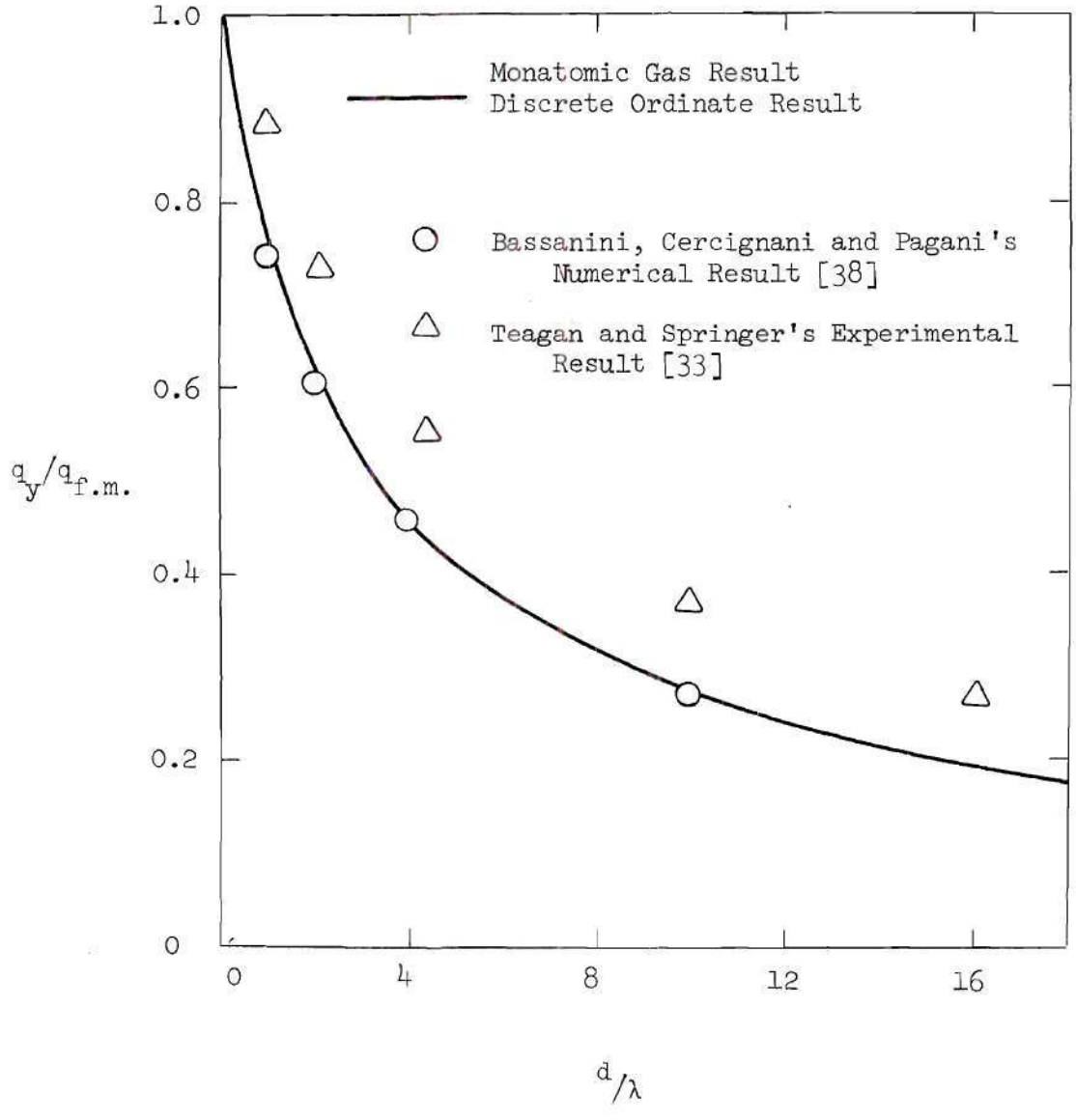

Figure 7. Comparisons of Heat Transfer with Experimental Data (Monatomic Gas).

solutions based on the BGK model and the discrete ordinate method for the monatomic gas are compared with the accurate numerical solutions of Bassanini, et al. [38] and the experimental data of Teagan and Springer [33]. It is seen that the solutions based on the present method agree very well with the accurate numerical solutions, but are always lower than the experimental data. There appear to be two possible reasons for this discrepancy. In the first place it is possible that the true Boltzmann equation for a realistic molecular model will yield results that are higher than those using the BGK model. The second possibility is that the experimental data are reduced using the assumption that the chamber pressure is the same as the pressure between the two plates while actually there may be a difference between these two pressures [39].

The results shown in Figure 6 through 7 were obtained using a spacing of 0.02 in τ , 30 sets of the new equally spaced quadrature of order n = 3 with a spacing of 0.1 for both $-\hat{v}_\sigma$ and $+\hat{v}_\sigma$ and the Gauss-Laguerre quadrature of order n = 4 for $\hat{E}_\delta$. The relaxation parameter "a" is taken to be 0.4 which is equivalent to $Z_R = 5.8$. The accommodation coefficients, α_n and α_t, are taken to be 1. Similar results have been obtained using a spacing of 0.01 in τ , quadrature of order n = 3, and the Gauss-Laguerre quadrature of order n = 4 for $\hat{E}_\delta$.

The Nonlinear Heat Transfer Case

The present method is next applied to calculate the nonlinear heat transfer case (large temperature difference between two plates). The same experimental conditions of Alofs, et al. [34], are used in the calculations ($\hat{T}_2 = 3.72$, $\alpha = 0.82$). The calculated density distributions

are compared with the experimental data [34] in Figures 8 through 12. The Knudsen number here (K_{n_o}) is defined as the ratio of the mean free path at the center plane ($\hat{y} = 0.5$, Figure 1) to the distance between the plates. The translational accommodation coefficient α_t and the internal accommodation coefficient α_i at both plates are taken to be 0.82 which is the measured value in Reference 34. In Figures 8 through 12 the continuum results [36] are also plotted for comparisons. It is seen that the calculated results are in excellent agreement with the experimental data for all flow regimes indicated.

The results from Figure 8 through 12 show that the density approaches to the continuum limit as Knudsen number decreases. The density near the cold plate ($\hat{y} = 0$) is higher than that near the hot plate ($\hat{y} = 1$). Consequently, the density near the cold plate is closer to the continuum limit than that near the hot plate due to the smaller Knudsen number near the cold plate. At $K_{n_o} = 0.053$, the density of the lower half of the channel ($0 \leq \hat{y} \leq 0.5$) is very close to that of the continuum limit, whereas the density of the upper half ($0.5 \leq \hat{y} \leq 1.0$) is still slightly away from the continuum limit.

The results shown in Figures 8 through 12 were obtained using a spacing of 0.033 in $\hat{y}$, 20 sets of new quadrature of order n = 3 with a spacing of 0.1 for $+\hat{v}_\sigma$, 18 sets for $-\hat{v}_\sigma$, and the Gauss-Laguerre quadrature of order n = 4 for $\hat{E}_\delta$. The relaxation parameter "a" is taken to be 0.4 which is equivalent to $Z_R = 5.8$.

The Nonlinear Couette Flow Case

The present method is also applied to calculate the nonlinear

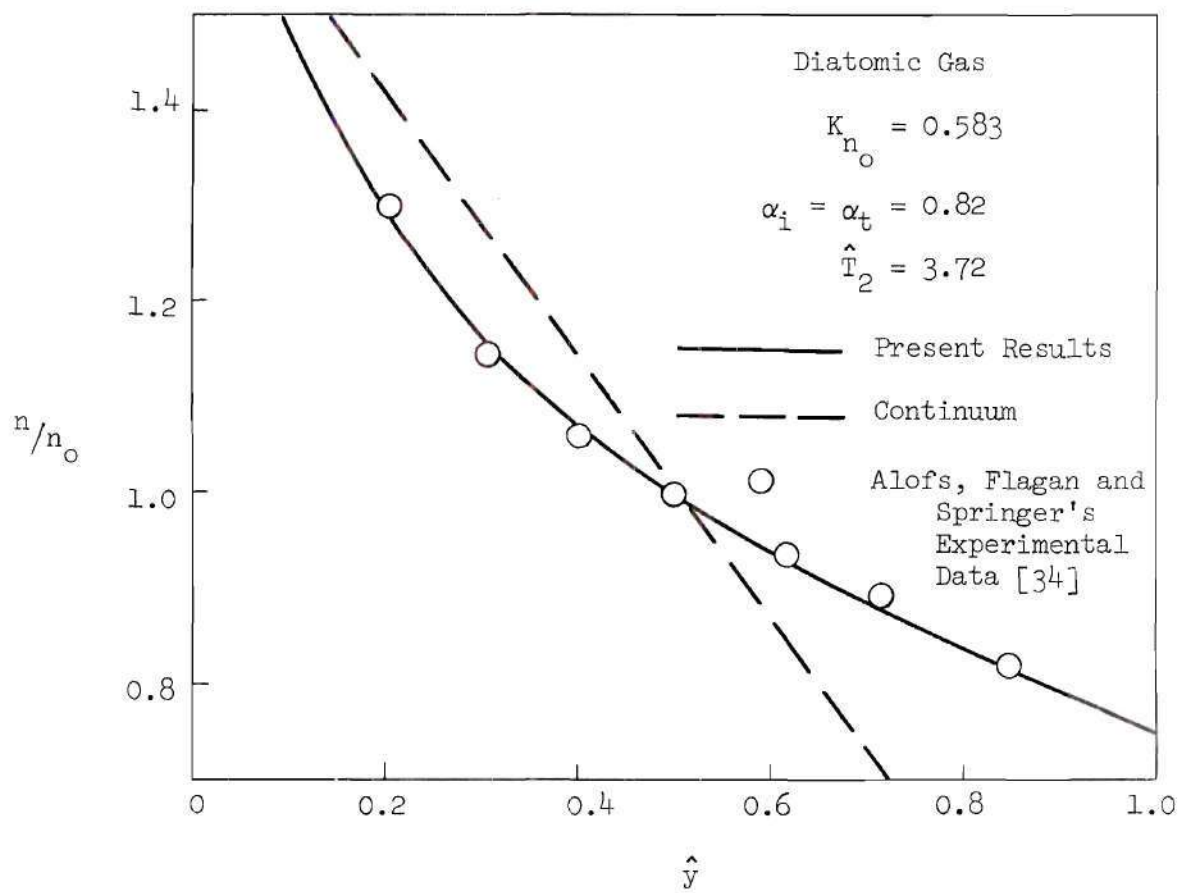

Figure 8. Comparisons of Density Profiles with Experimental Data ($K_{n_o} = 0.583$).

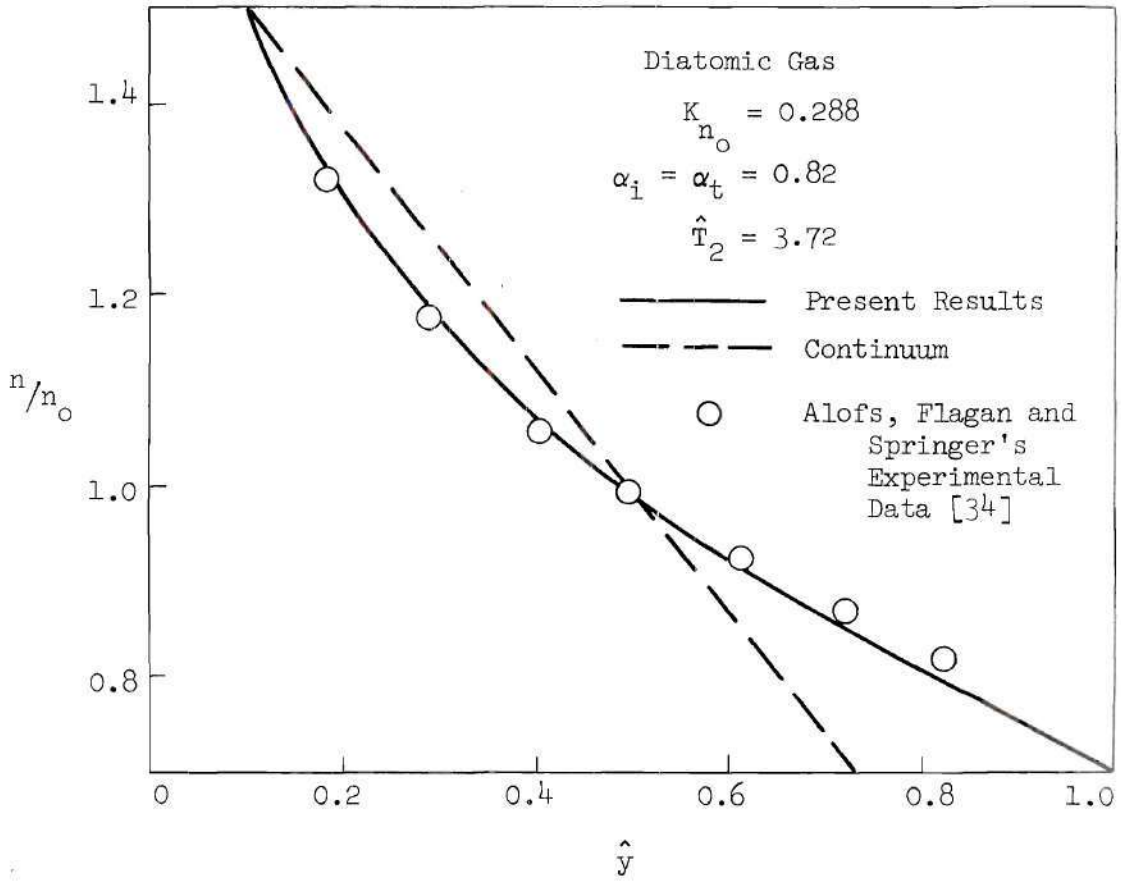

Figure 9. Comparisons of Density Profiles with Experimental Data (K_{n_o} = 0.288).

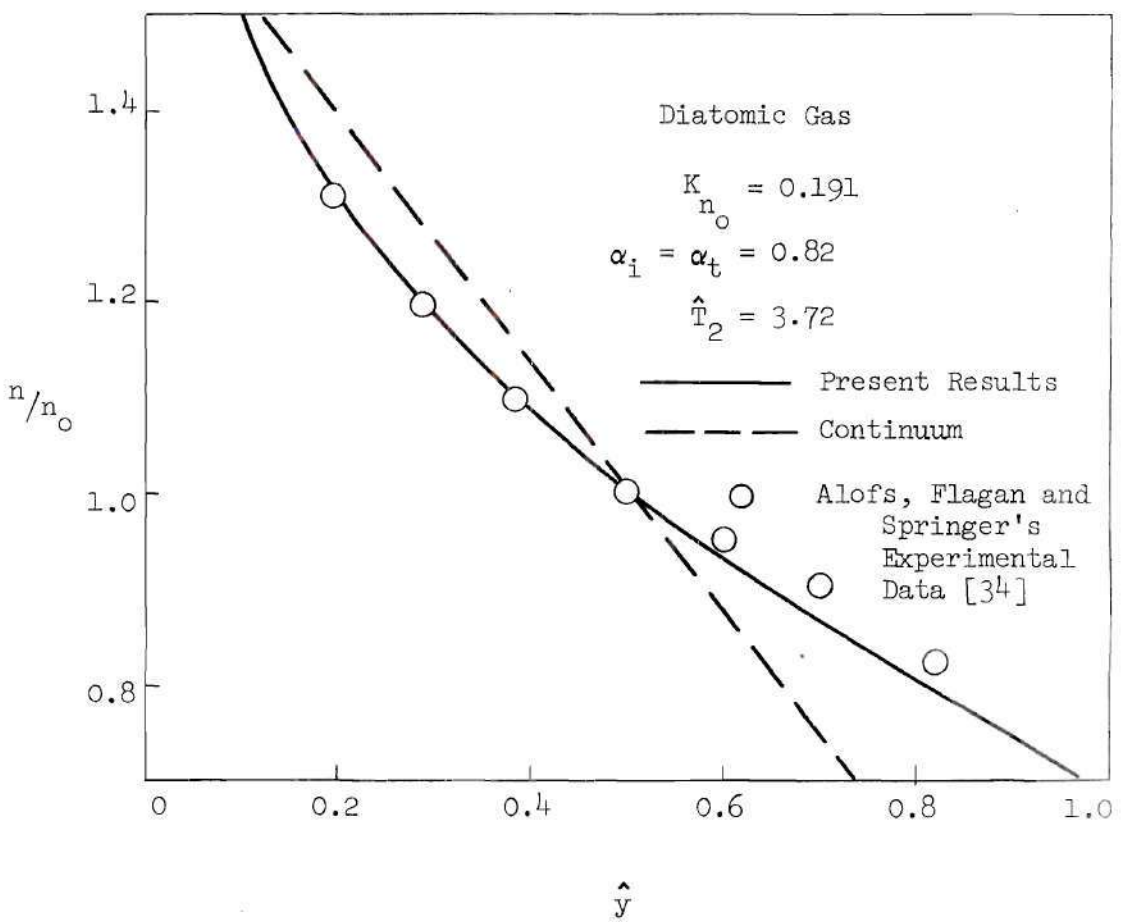

Figure 10. Comparisons of Density Profiles with Experimental Data (K_{n_o} = 0.191).

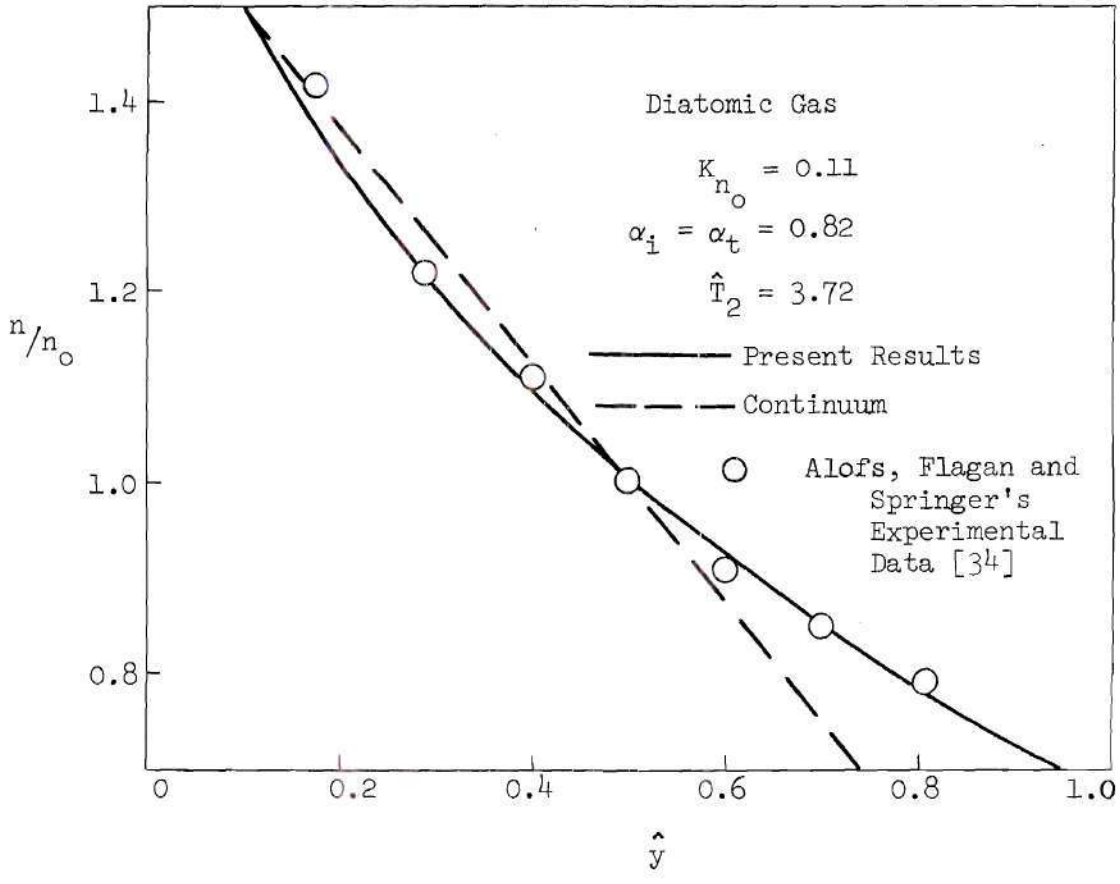

Figure 11. Comparisons of Density Profiles with Experimental Data (K_{n_o} = 0.11).

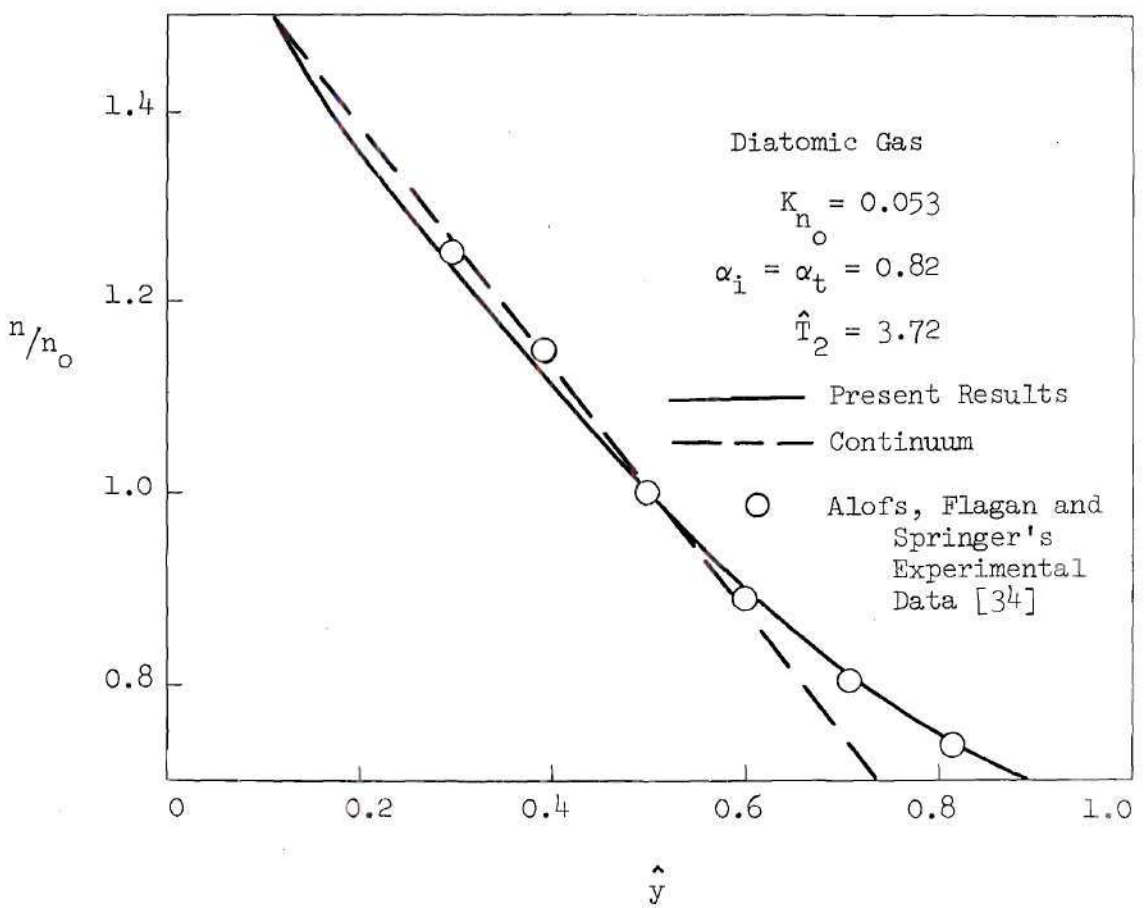

Figure 12. Comparisons of Density Profiles with Experimental Data ($K_{n_o} = 0.053$).

Couette flow case. Some typical results on the case $\hat{W}' = 1$ are shown in Figures 13 through 17. There have been no theoretical and experimental results available for comparisons. The results are compared with those of the monatomic gas case [5]. The results are seen to be very reasonable for all flow regimes. An inspection of the various profiles presented in Figures 13 through 17 reveals that some interesting changes arise with respect to the monatomic gas solutions. At $K_n = 100$, both diatomic and monatomic gasses give identical profiles in density and velocity because the flow is essentially free molecular and the molecule collisions are not important in this flow regime. It should be noted that in Figure 15 the monatomic gas gives a higher free molecule temperature than the diatomic gas does. This is because the specific heat capacity of the monatomic gas is lower than that of the diatomic gas, and it is easier for the monatomic gas to transfer the mechanical energy induced from the upper plate into the internal energy of the gas.

The results shown in Figures 13 through 17 were obtained using a spacing of 0.02 in τ , eight sets of the new equally spaced quadrature of order n = 3 with a spacing of 0.1 for $-\hat{v}_\sigma$, ten sets of the new equally spaced quadrature of order n = 3 with a spacing of 0.1 for $+\hat{v}_\sigma$, and the Gaussian Laguerre quadrature of order n = 4 for $\hat{E}_\delta$. The computer time needed (using a UNIVAC 1108 computer) for the entire calculation from $K_n = 100$ to $K_n = 0.05$ is approximately 15 minutes. The relaxation parameter "a" is taken to be 0.4. Also, $\alpha_i = \alpha_t = 1$.

Figures 18 through 25 report calculated results for $\hat{W}' = 5$. These results were obtained using a spacing of 0.02 in $\hat{\tau}$, 13 sets of the new equally spaced quadrature of order n = 3 with a spacing of 0.1

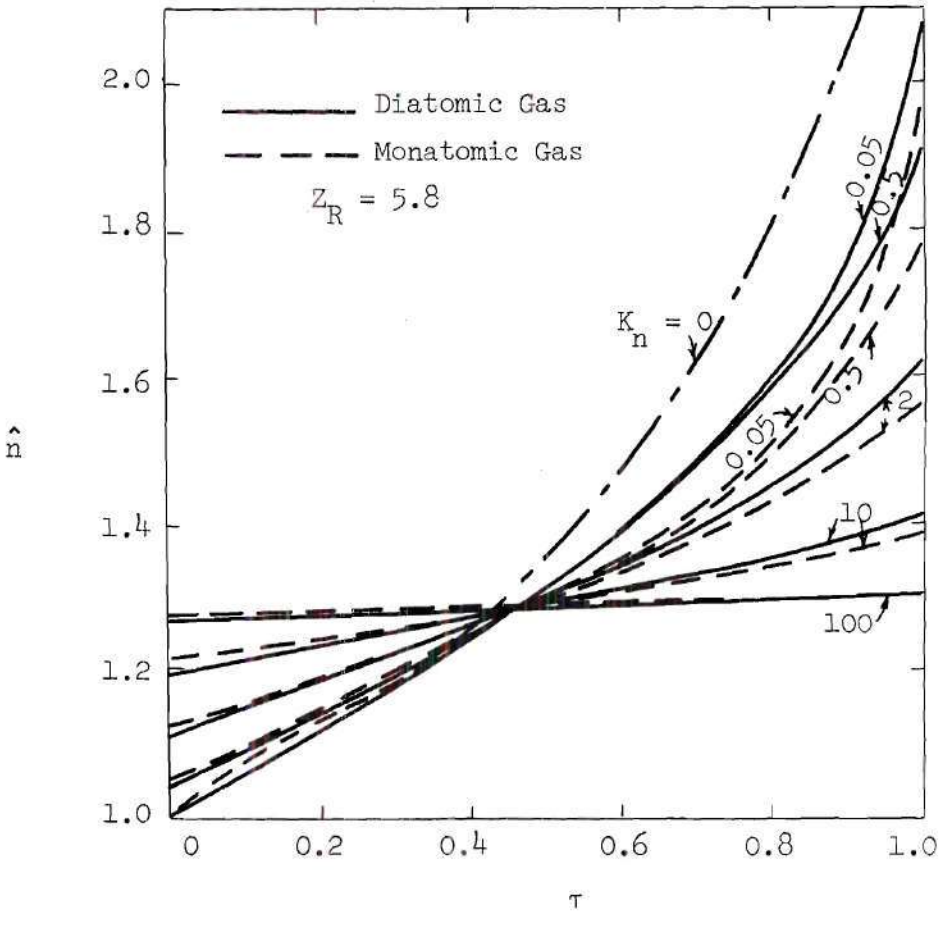

Figure 13. Couette Flow Density Profiles for $\hat{W}' = 1$, $\hat{T}_2 = 0.4$.

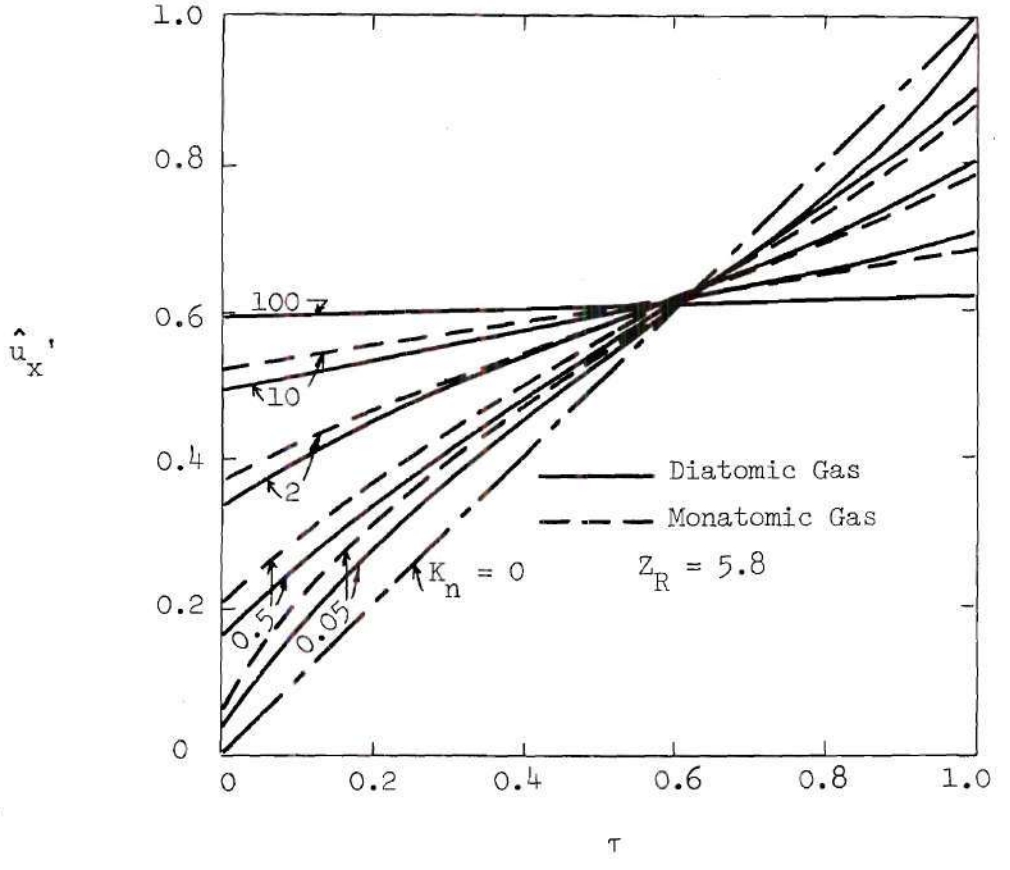

Figure 14. Couette Flow Velocity Profiles for $\hat{W}' = 1$, $\hat{T}_2 = 0.4$.

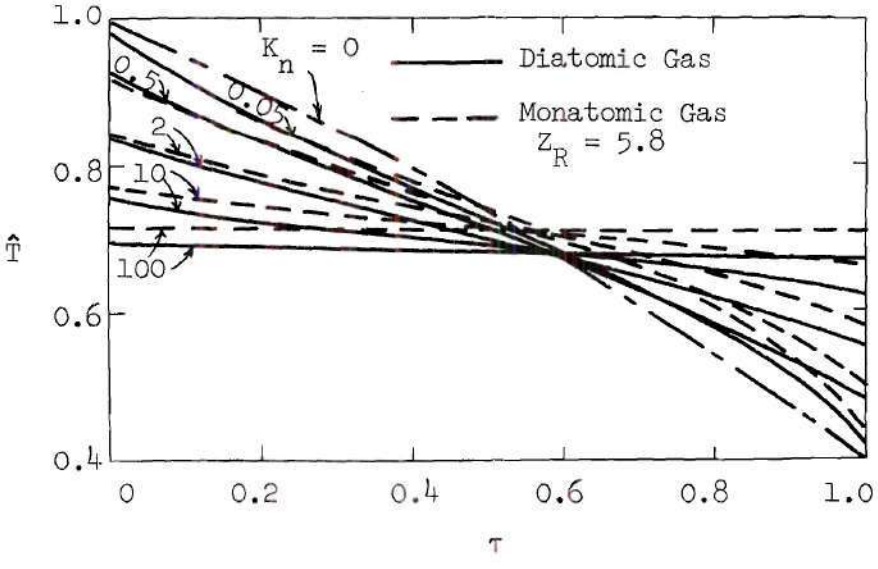

Figure 15. Couette Flow Temperature Profiles for $\hat{W}' = 1$, $\hat{T}_2 = 0.4$.

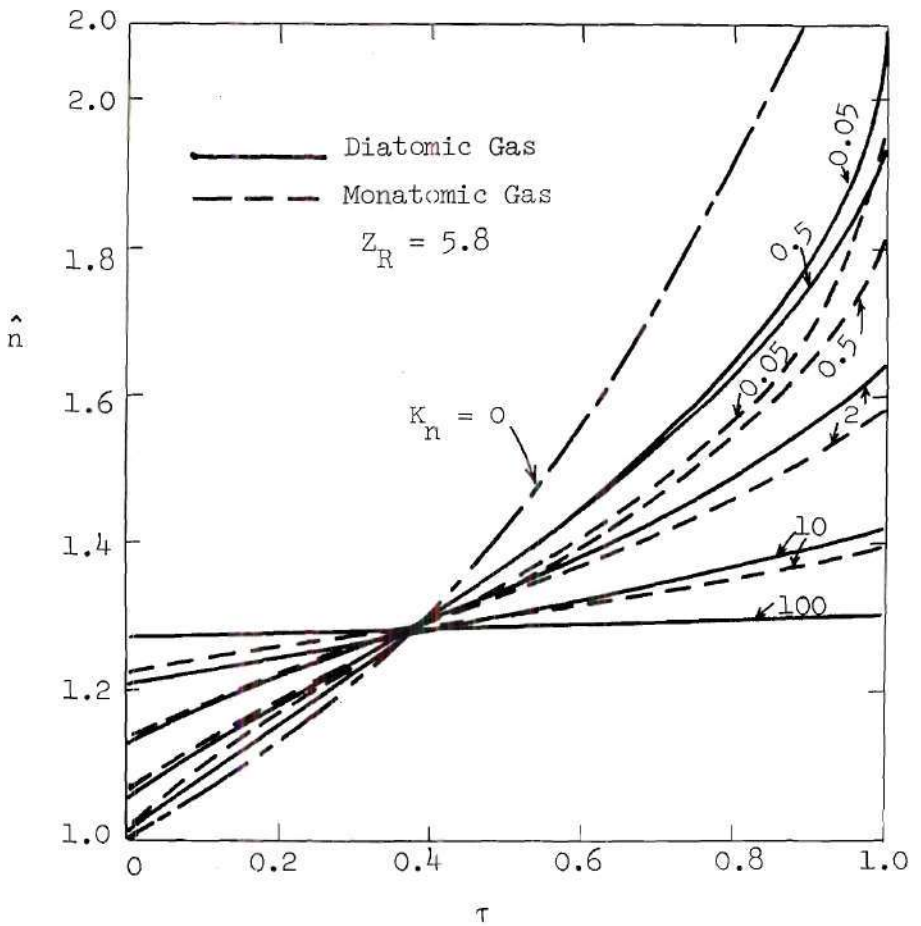

Figure 16. Couette Flow Density Profiles for $\hat{W}' = 0$, $\hat{T}_2 = 0.4$.

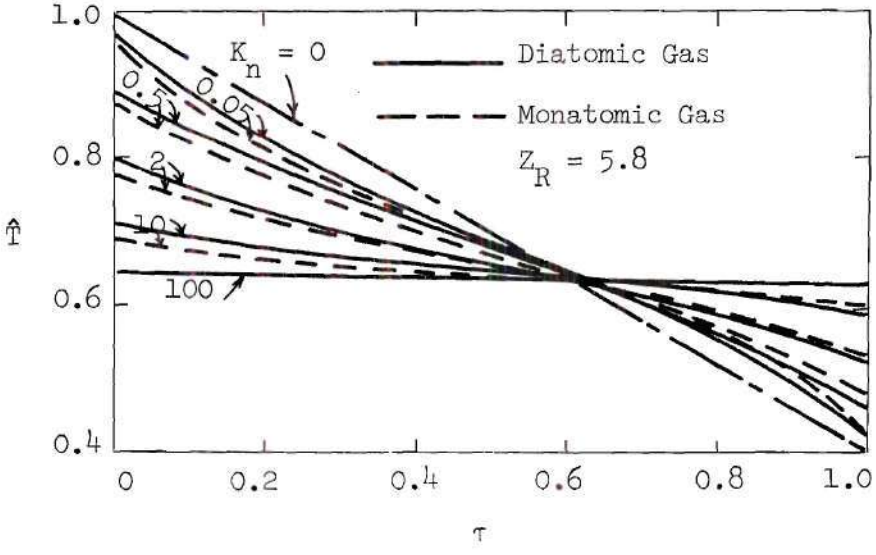

Figure 17. Couette Flow Temperature Profiles for $\hat{W}' = 0$, $\hat{T}_2 = 0.4$.

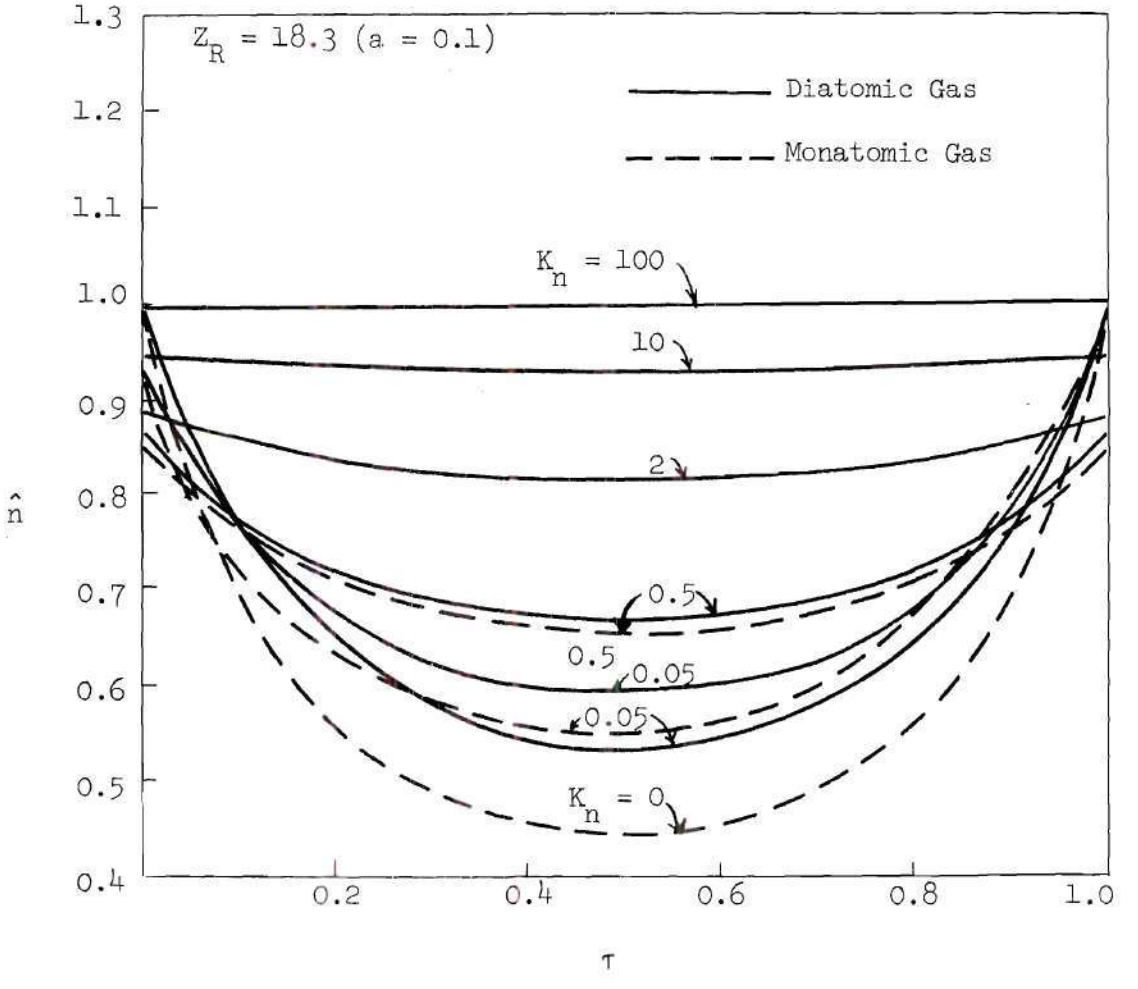

Figure 18. Couette Flow Density Profiles for $\hat{W}' = 5$, $T_2 = 1$.

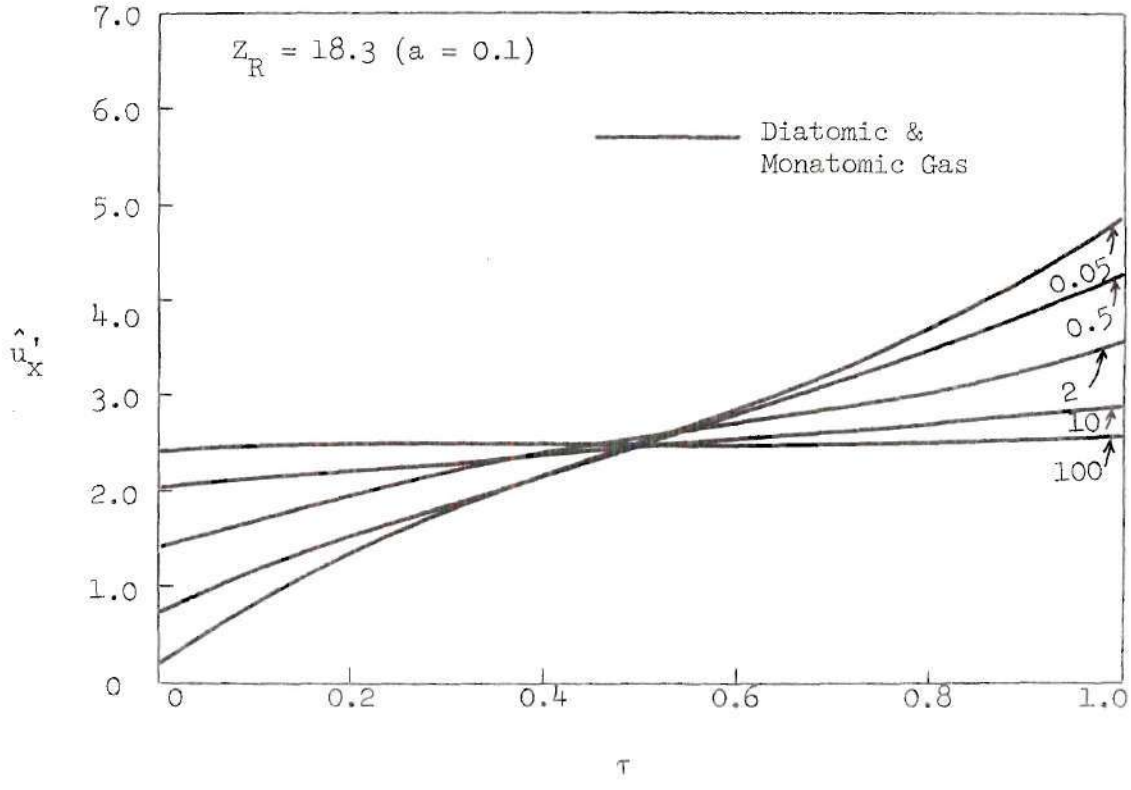

Figure 19. Couette Flow Velocity Profiles for $\hat{W}' = 5$, $\hat{T}_2 = 1$.

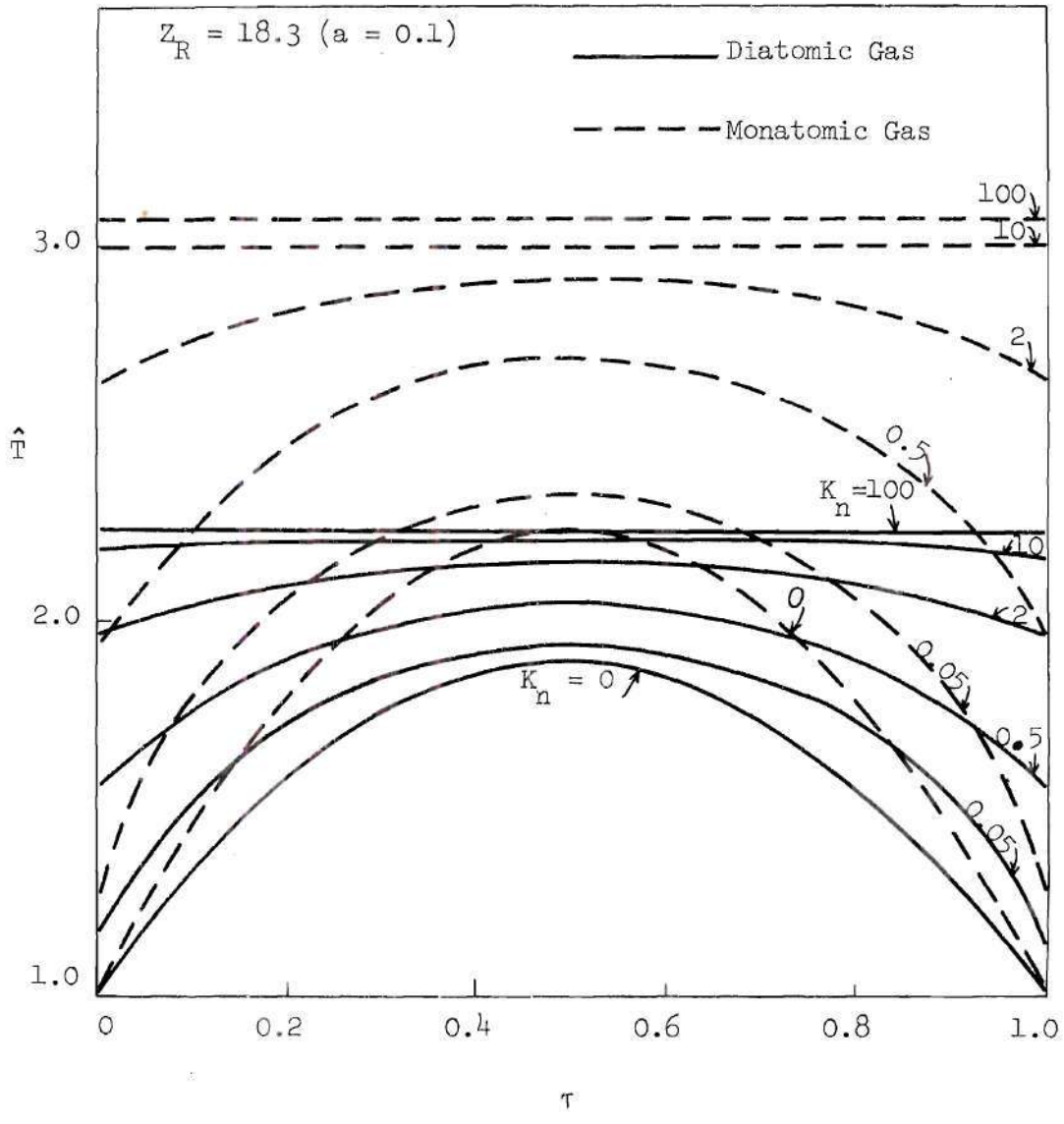

Figure 20. Couette Flow Temperature Profiles for $\hat{W}' = 5$, $\hat{T}_2 = 1$.

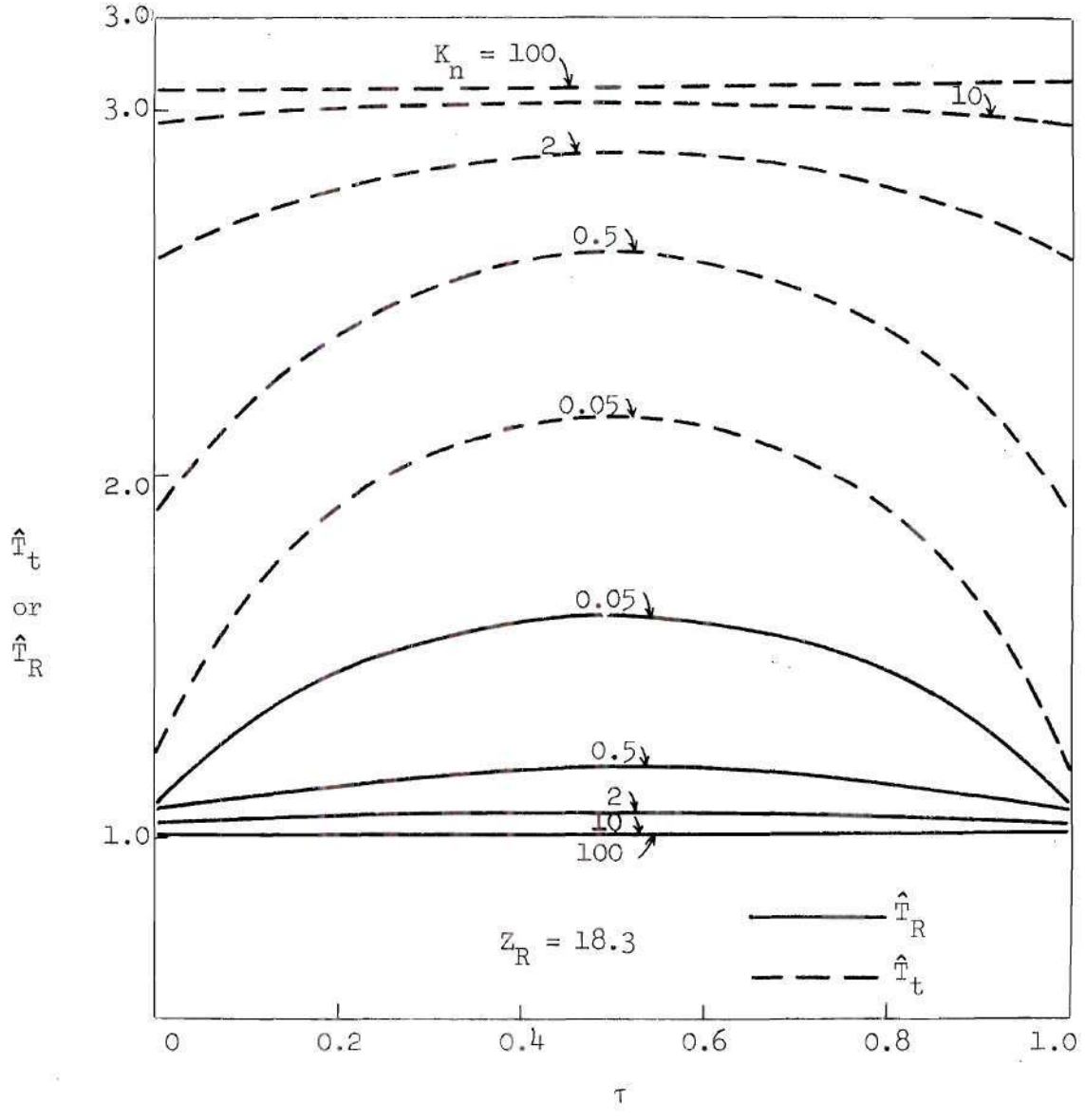

Figure 21. Couette Flow Translational and Rotational Temperature Profiles for $\hat{W}' = 5$, $\hat{T}_2 = 1$.

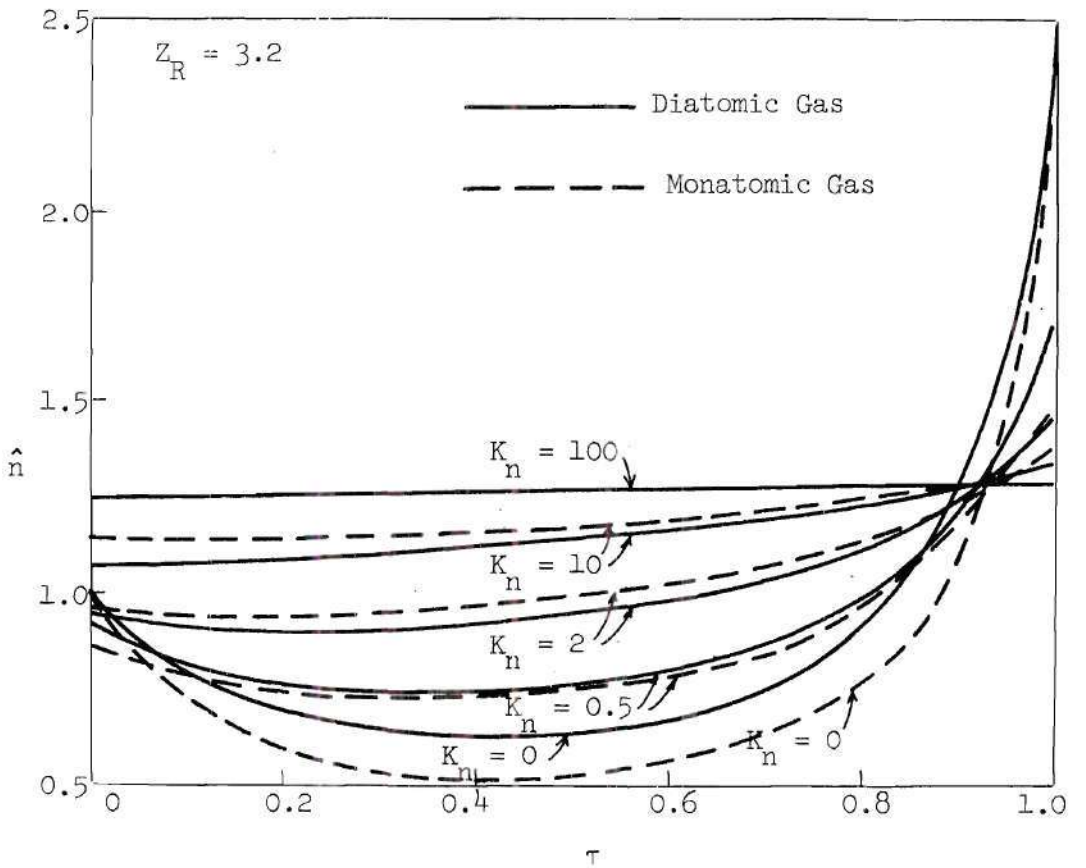

Figure 22. Couette Flow Density Profiles for $\hat{W}' = 5$, $\hat{T}_2 = 0.4$.

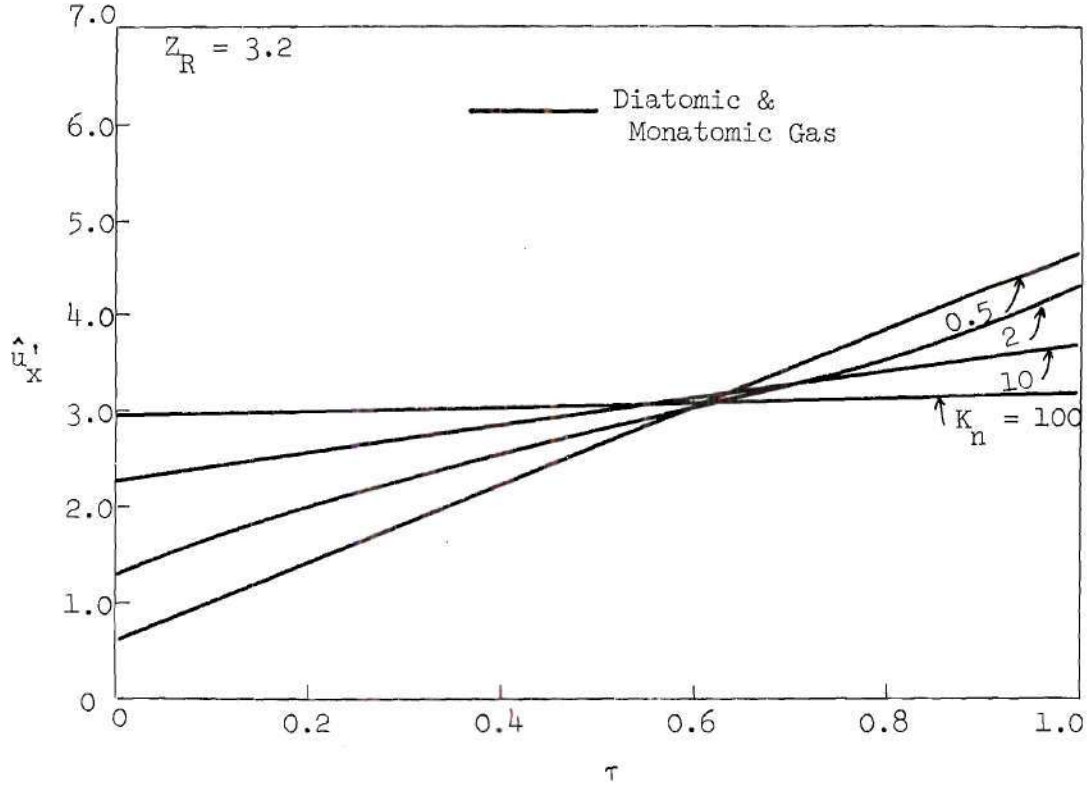

Figure 23. Couette Flow Velocity Profiles for $\hat{W}' = 5$, $\hat{T}_2 = 0.4$.

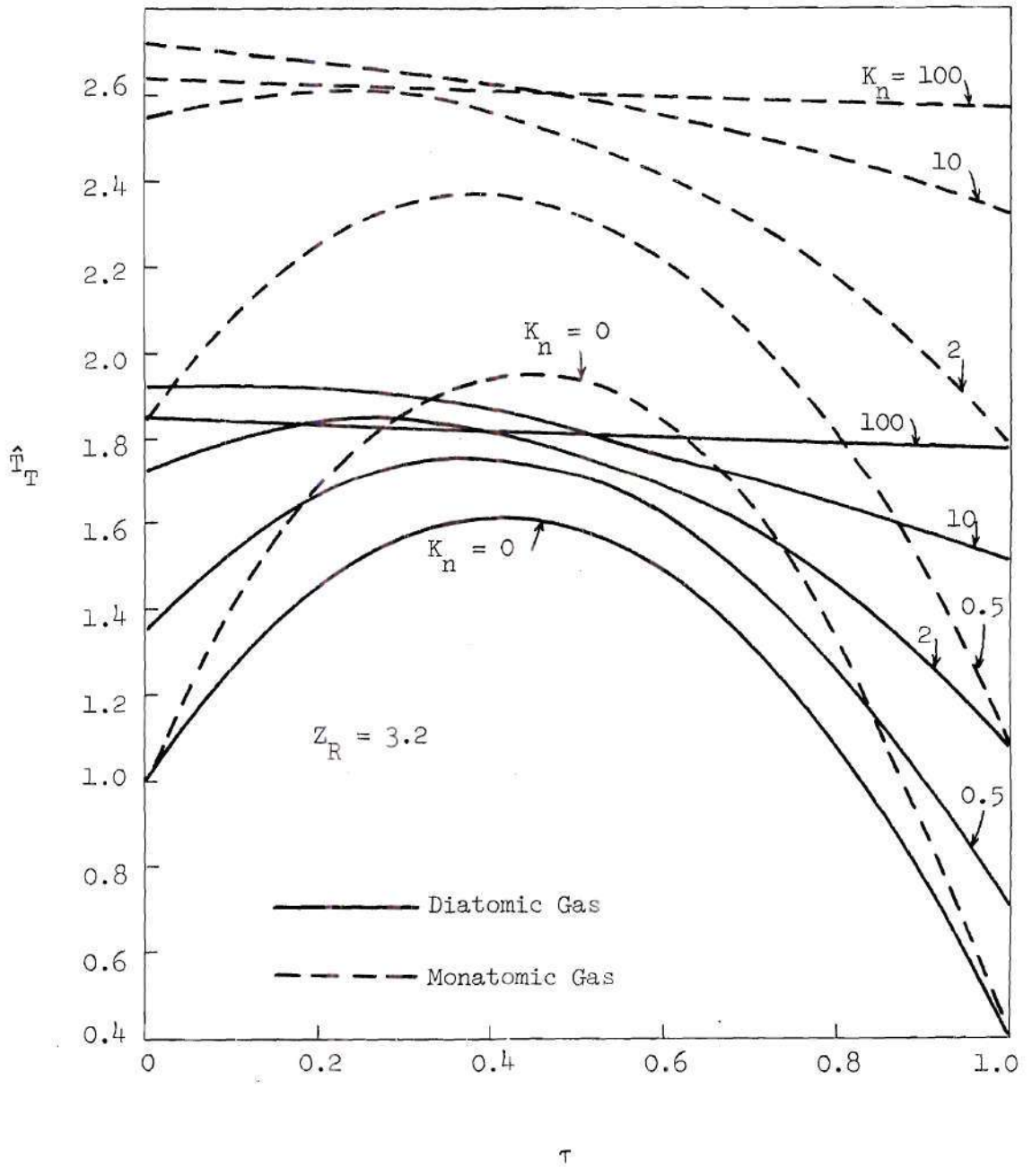

Figure 24. Couette Flow Temperature Profiles for $\hat{W}' = 5$, $\hat{T}_2 = 0.4$.

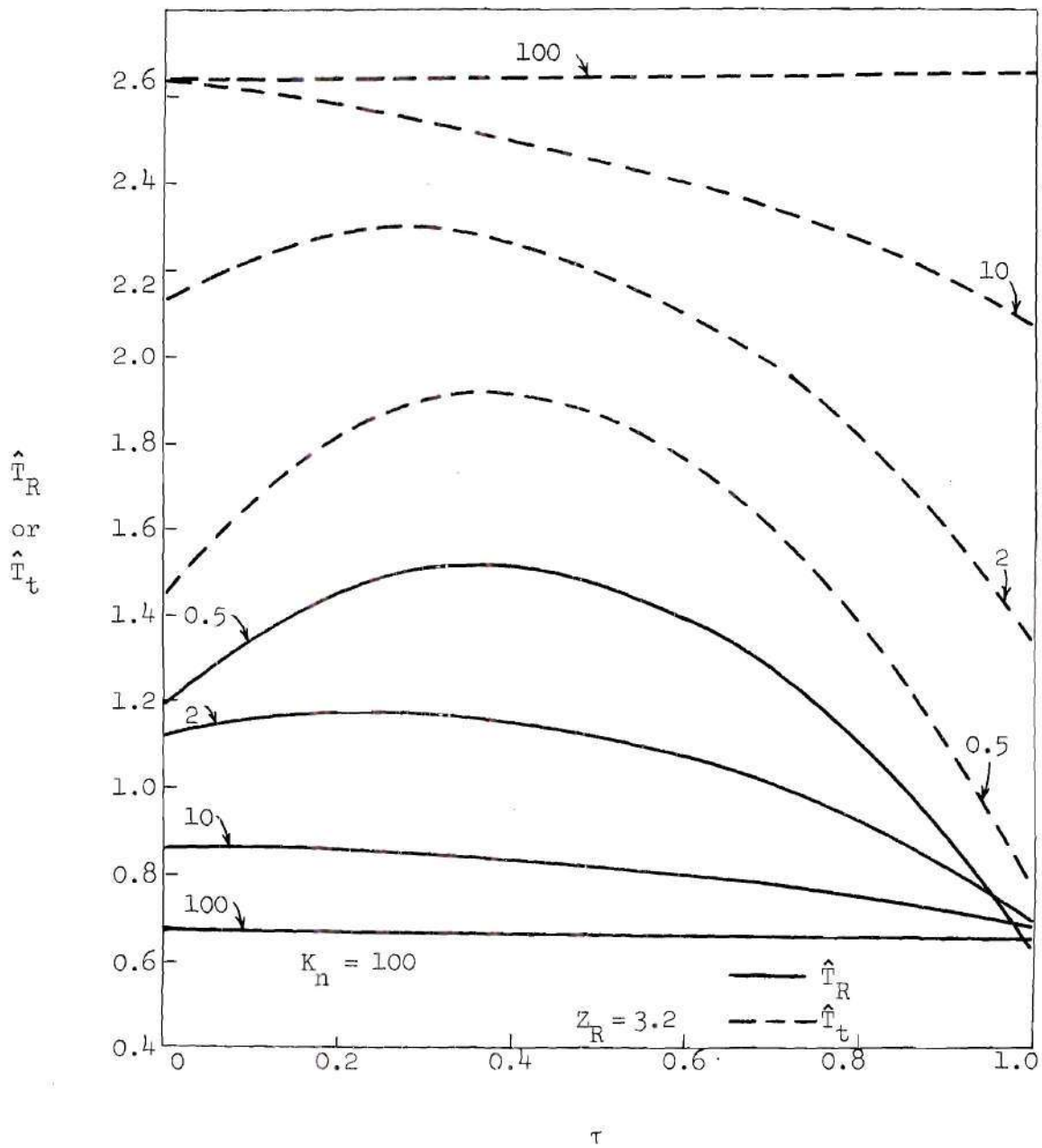

Figure 25. Couette Flow Translational and Rotational Temperature Profiles for $\hat{W}' = 5$, $\hat{T}_2 = 0.4$.

for $-\hat{v}_{\sigma}$, 15 sets of the new equally spaced quadrature of order n = 3 with a spacing of 0.1 for $+\hat{v}_{\sigma}$, and the Gaussian Laguerre quadrature of order n = 4 for $\hat{E}_{\delta}$. The relaxation parameter "a" is indicated on the graphs. The computer time needed for the entire calculation from K_n = 100 to K_n = 0.05 is approximately 15 minutes. Also, α_i and α_t are taken to be 1. Both monatomic results and diatomic results are plotted for comparison. The monatomic results which are recalculated using the new equally spaced quadrature are found to give more reasonable trends in approaching to the continuum solutions as K_n decreases than did the solutions obtained by Hartley [29] who used another "odd" equally spaced quadrature. Figures 21 and 25 indicate that T_t and T_R become closer in the continuum regime than in the kinetic region. This is reasonable because there are more molecular collisions in the continuum regime, and thus, there is more energy transfer between the translational and internal degrees of freedom.

Figure 18 through 25 reveal the fact that in the free molecular regime (K_n = 100), all profiles are identical for both diatomic and monatomic gases except the temperature profile. It is because the properties of both diatomic and monatomic gases are characterized by the same boundary (i.e., the lower and upper plates) due to the lack of collision among molecules in the free molecular regime. It is observed that in fact the translational temperature of a diatomic gas is identical to the temperature of a monatomic gas. The lower total temperature of a diatomic gas in the free molecular flow regime is contributed by the low rotational temperature for a diatomic gas. It is also observed that the flow velocity is same for diatomic and monatomic gases for all flow regimes.

In conclusion, the application of the Boltzmann equation with the Bhatnagar-Gross-Krook-Morse model using the discrete ordinate method has yielded good results for the Couette flow with heat transfer, leading the author to believe the applicability of this simple model equation.

CHAPTER IV

NONLINEAR RAYLEIGH'S FLOW FOR A DIATOMIC GAS

Background of the Problem

Rayleigh's problem in fluid dynamics relates to the evaluation of the unsteady flow which arises when an infinite flat plate, submerged in a viscous, originally quiescent fluid, is impulsively set in motion in its own plane with constant velocity. This flow, though simple for an incompressible fluid, becomes complicated when compressibility is taken into account. The heat generated by viscous dissipation produces in a compressible fluid not only temperature variation but also variations of pressure and density, and thus induces a velocity component normal to the plate. Rayleigh [40] first investigated such a flow for an incompressible fluid in order to justify boundary layer theory. Many investigators, including Howarth [41] , Illingsworth [42] , Stewartson [43] , Harlow and Meixner [44], Van Dyke [45], and Hanin [46], have studied various aspects of the problem for compressible continuum fluids. All these investigators used the Navier-Stokes equations or the boundary layer equations. However, since the flow develops in a time comparable to a molecular collision time, the no-slip condition implied by the continuum analysis gives an incorrect description for short times and particularly near the plate.

Recently, the problem has been approached by kinetic theory methods. The half range moment method was applied to the linearized

Boltzmann BGK equation by Gross and Jackson [47]; the Grad equations were investigated by Yang and Lees [48]; and the linearized BGK equation was explored by Cercignani and Sernagiotto [49], by Sone [50], and by Huang and Giddens [51]. However, when the equation is linearized, it is readily seen that the shear velocity becomes uncoupled from the normal velocity and hence also from the thermodynamic variables. Thus, from linear theory the fluid velocity is everywhere parallel to the plate and no other disturbances can be found.

More recently, the nonlinear Boltzmann BGK equation has been applied to this problem by Chu [52], who expanded the distribution function in a Taylor series in collision time and eliminated all but the first order terms. The resulting analysis yields results for several high Mach numbers. The nonlinear Boltzmann BGK equation has also been applied to this problem by Huang and Hartley [53], who used the discrete ordinate method and obtained both linear and nonlinear solutions. The results agree in the small Mach number limit with the linearized kinetic theory solutions [49], and in the nonlinear case with those of Chu [52]. However, the above analyses are all for monatomic gases only. It is the purpose of this chapter to solve the nonlinear Rayleigh problem for diatomic gases using the method of discrete ordinates which was successfully applied to the solution of the nonlinear Couette flow in the last chapter. The calculated results will be compared with those of monatomic gases [52, 53] in order to determine how the internal molecular structure affects the flow field of this unsteady problem.

Formulation of the Problem

An infinite flat plate is on the y = 0 plane and is submerged in a diatomic, originally quiescent gas with density n_o and temperature T_o (see Figure 26). The plate is at temperature T_w and is impulsively set in motion in its own plane with constant velocity W. The unsteady problem is one-dimensional in physical space in that the distribution function $f(y; \vec{v}; t)$ describing the state of the system depends only on y. The one dimensional, nonlinear unsteady BBGKM equation for this case is

$$\frac{\partial f_\ell}{\partial t} + v_y \frac{\partial f_\ell}{\partial y} = \nu_{e\ell}\left(F_{t\ell} - f_\ell\right) + \nu_{in}\left(F_{i\ell} - f_\ell\right) \tag{25}$$

where $F_{t\ell}$ and $F_{i\ell}$ in this case are

$$F_{t\ell} = n_\ell \left(\frac{m}{2\pi K T_t}\right)^{3/2} e^{-\frac{m}{2KT_t}\left[(v_x - u_x)^2 + (v_y - u_y)^2 + v_z^2\right]} \tag{26a}$$

$$F_{i\ell} = n_{\ell eq} \left(\frac{m}{2\pi K T_r}\right)^{3/2} e^{-\frac{m}{2KT_r}\left[(v_x - u_x)^2 + (v_y - u_y)^2 + v_z^2\right]} \tag{26b}$$

In order to reduce computer storage requirements, reduced distribution functions are conveniently defined, similar to the reductions in the Couette flow equations of Chapter III. After integrating out the v_x and v_z dependences in Equation (25) by using the reduced distribution functions, the single three-dimensional BBGKM equation (25) becomes the following simultaneous equations.

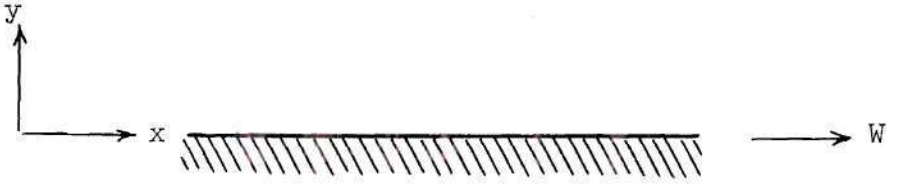

Figure 26. Geometry and Coordinate System for the Rayleigh Flow Problem.

$$\frac{\partial g_\ell}{\partial t} + v_y \frac{\partial g_\ell}{\partial y} = \nu_{e\ell}\left(G_{t\ell} + g_\ell\right) + \nu_{in}\left(G_{i\ell} + g_\ell\right) \tag{27a}$$

$$\frac{\partial h_\ell}{\partial t} + v_y \frac{\partial h_\ell}{\partial y} = \nu_{e\ell}\left(H_{t\ell} + h_\ell\right) + \nu_{in}\left(H_{i\ell} + h_\ell\right) \tag{27b}$$

$$\frac{\partial j_\ell}{\partial t} + v_y \frac{\partial j_\ell}{\partial y} = \nu_{e\ell}\left(J_{t\ell} + j_\ell\right) + \nu_{in}\left(J_{i\ell} + j_\ell\right) \tag{27c}$$

where

$$G_{t\ell} = \frac{n_\ell}{(2\pi R T_t)^{1/2}} \, e^{-(v_y - u_y)^2 / 2RT_t} \tag{28a}$$

$$H_{t\ell} = G_{t\ell}\left(2RT_t + u_x^2\right) \tag{28b}$$

$$J_{t\ell} = u_x G_{t\ell} \tag{28c}$$

$$G_{i\ell} = \frac{n_{\ell eq}}{(2\pi R T_T)^{1/2}} \, e^{-(v_y - u_y)^2 / 2RT_T} \tag{28d}$$

$$H_{i\ell} = G_{i\ell}\left(2RT_T + u_x^2\right) \tag{28e}$$

$$J_{i\ell} = u_x G_{i\ell} \tag{28f}$$

The macroscopic moments are similarly found as in Chapter III except for u_y and T_t which are given by

$$u_y = \frac{1}{n} \sum_{\ell} \int_{-\infty}^{\infty} v_y \, g_\ell \, dv_y \tag{29a}$$

$$3nRT_t = \sum_{\ell} \left\{ \int_{-\infty}^{\infty} h_\ell \, dv_y + \int_{-\infty}^{\infty} v_y^2 \, g_\ell \, dv_y \right\} - n u_x^2 - n u_y^2 \tag{29b}$$

The collision frequency $\nu_{e\ell}$ is taken to be of the form

$$\nu_{e\ell} = \frac{16 \, n k T_t}{5(1+a) \lambda_0 m n_0 \sqrt{2\pi R T_0}} \left(\frac{T_t}{T_0} \right)^{-s} \tag{30}$$

A characteristic velocity is defined as

$$v_0 = \sqrt{2RT_0}$$

The definitions of dimensionless variables are given by

$$\hat{v} = \frac{v}{v_0} \quad , \quad \hat{u} = \frac{u}{v_0} \quad , \quad \hat{w} = \frac{w}{v_0} \, ,$$

$$\hat{n} = \frac{n}{n_0} \quad , \quad \hat{T} = \frac{T}{T_0} \quad , \quad \hat{g}_\ell = \frac{v_0}{n_0} g_\ell \, ,$$

$$\hat{h}_\ell = \frac{h_\ell}{n_o V_o} , \qquad \hat{j}_\ell = \frac{j_\ell}{n_o} , \qquad \hat{G}_\ell = \frac{V_o}{n_o} G_\ell ,$$

$$\hat{H}_\ell = \frac{H_\ell}{n_o V_o} , \qquad \hat{J}_\ell = \frac{J_\ell}{n_o} , \qquad \hat{\nu} = \frac{\nu \lambda_o}{V_o} ,$$

$$\hat{y} = \frac{y}{\lambda_o} , \quad \hat{t} = \frac{t}{\tau_o}$$

where τ_o is the collision time of the gas in equilibrium.

Thus, a set of dimensionless differential equations for a specified discrete point in the velocity space $\hat{V}_\sigma$ and an energy level $\hat{E}_\delta$ can be written as

$$\frac{\partial \hat{g}_{\sigma,\delta}}{\partial \hat{t}} + \hat{V}_\sigma \frac{\partial \hat{g}_{\sigma,\delta}}{\partial \hat{y}} = \hat{\nu}_{el}\left(\hat{G}_{t,\sigma,\delta} - \hat{g}_{\sigma,\delta}\right) + \hat{\nu}_{in}\left(\hat{G}_{i,\sigma,\delta} - \hat{g}_{\sigma,\delta}\right) \tag{3la}$$

$$\frac{\partial \hat{h}_{\sigma,\delta}}{\partial \hat{t}} + \hat{V}_\sigma \frac{\partial \hat{h}_{\sigma,\delta}}{\partial \hat{y}} = \hat{\nu}_{el}\left(\hat{H}_{t,\sigma,\delta} - \hat{h}_{\sigma,\delta}\right) + \hat{\nu}_{in}\left(\hat{H}_{i,\sigma,\delta} - \hat{h}_{\sigma,\delta}\right) \tag{3lb}$$

$$\frac{\partial \hat{j}_{\sigma,\delta}}{\partial \hat{t}} + \hat{V}_\sigma \frac{\partial \hat{j}_{\sigma,\delta}}{\partial \hat{y}} = \hat{\nu}_{el}\left(\hat{J}_{t,\sigma,\delta} - \hat{j}_{\sigma,\delta}\right) + \hat{\nu}_{in}\left(\hat{J}_{i,\sigma,\delta} - \hat{j}_{\sigma,\delta}\right) \tag{3lc}$$

where

$$\hat{G}_{t,\sigma,\delta} = \hat{n}_\delta \left(\frac{1}{\pi \hat{T}_t}\right)^{1/2} e^{-(\hat{V}_\sigma - \hat{u}_y)^2 / \hat{T}_t} \tag{32a}$$

$$\hat{H}_{t,\sigma,\delta} = (\hat{T}_t + \hat{u}_x^2)\, \hat{G}_{t,\sigma,\delta} \tag{32b}$$

$$\hat{J}_{t,\sigma,\delta} = \hat{u}_x\, \hat{G}_{t,\sigma,\delta} \tag{32c}$$

$$\hat{G}_{i,\sigma,\delta} = \hat{n}_{\delta,eq} \left(\frac{1}{\pi \hat{T}_T}\right)^{1/2} e^{-(\hat{V}_\sigma - \hat{u}_y)^2 / \hat{T}_T} \tag{32d}$$

$$\hat{H}_{i,\sigma,\delta} = (\hat{T}_T + \hat{u}_x^2)\, \hat{G}_{i,\sigma,\delta} \tag{32e}$$

$$\hat{J}_{i,\sigma,\delta} = \hat{u}_x\, \hat{G}_{i,\sigma,\delta} \tag{32f}$$

$$\hat{n}_{\delta,eq} = \hat{n}\, Q_\delta \tag{32g}$$

$$Q_\delta = \frac{R_\delta\, e^{\hat{E}_\delta (1 - \frac{1}{\hat{T}})}}{\hat{T}} \tag{32h}$$

$$\hat{\nu}_{el} = \frac{8}{5(1+a)\sqrt{\pi}}\, \hat{n}\, \hat{T}_t^{1-s} \tag{32i}$$

$$\hat{v}_{in} = a\,\hat{v}_{el} \tag{32j}$$

In Equation (32h), the Gauss-Laguerre quadrature is applied in order to obtain a good approximation by taking a relatively small number of discretized energy levels [Appendix B]. R_δ and E_δ are the weighting coefficients and the discrete ordinates of the Gauss-Laguerre quadrature, respectively.

Introducing the transformation

$$\eta = 1 - e^{-b\hat{y}} \tag{33}$$

into Equations (31) then gives

$$\frac{\partial \hat{g}_{\sigma,\delta}}{\partial \hat{t}} + \hat{v}_\sigma b(1-\eta)\frac{\partial \hat{g}_{\sigma,\delta}}{\partial \eta} = \hat{v}_{el}\left[(\hat{G}_{t,\sigma,\delta} - \hat{g}_{\sigma,\delta}) + a(\hat{G}_{i,\sigma,\delta} - \hat{g}_{\sigma,\delta})\right]$$

$$\sigma = -n, \cdots, -1, 1, \cdots, n' \;;\; \delta = 1, \cdots, n'' \tag{34}$$

and the similar equations for $\hat{h}_{\sigma,\delta}$ and $\hat{j}_{\sigma,\delta}$. This transformation not only maps the infinite $\hat{y}$ region into a unit region $(0 \leq \hat{\eta} \leq 1)$ but also gives the advantage that if the region $0 \leq \hat{\eta} \leq 1$ is divided into m equal steps for the purpose of applying a finite difference scheme, the points in actual physical space are quite close together in the region near the plate where gradients are largest and are spaced further apart in regions away from the surface where there is little change in flow properties.

In order to specify the interaction of the molecules with the

surface of the plate, it is assumed that molecules which strike the surface are subsequently emitted with a Maxwellian velocity distribution characterized by the plate temperature, $\hat{T}_w$, and zero net tangential velocity. The two-stream concept introduced earlier is applied here also by defining the half-range distribution functions

$$\hat{f}_\ell = \hat{f}_\ell^{+} + \hat{f}_\ell^{-}$$

$$\hat{f}_\ell^{+}(\eta;\hat{t};\hat{v}_y;\hat{E}_\ell) = 0 \quad , \quad \text{for } \hat{v}_y < 0$$

$$\hat{f}_\ell^{-}(\eta;\hat{t};\hat{v}_y;\hat{E}_\ell) = 0 \quad , \quad \text{for } \hat{v}_y > 0$$

The non-dimensionalized boundary conditions can be written as follows

$$\hat{g}_{\sigma,s}^{-}(\eta=1) = R_s \frac{e^{-(\hat{v}_\sigma - \hat{u}_y)^2}}{\sqrt{\pi}} \tag{35a}$$

$$\hat{h}_{\sigma,s}^{-}(\eta=1) = \hat{g}_{\sigma,s}^{-}(\eta=1) \tag{35b}$$

$$\hat{j}_{\sigma,s}^{-}(\eta=1) = 0 \tag{35c}$$

$$\hat{g}_{\sigma,s}^{+}(\eta=0,\hat{t}=0) = \frac{\hat{n}_w Q_{s,w}}{\sqrt{\pi\,\hat{T}_w}} e^{-\frac{1}{\hat{T}_w}\hat{V}_\sigma^2} \tag{35d}$$

$$\hat{g}_{\sigma,s}^{+}(\eta=0,\hat{t}>0) = \frac{\hat{n}_w Q_{s,w}}{\sqrt{\pi\,\hat{T}_w}} e^{-\frac{1}{\hat{T}_w}\hat{V}_\sigma^2} \tag{35e}$$

$$\hat{h}^{+}_{\sigma,\delta}\,(\eta=0,\hat{t}=0)=\hat{g}^{+}_{\sigma,\delta}\,(\eta=0,\hat{t}=0) \tag{35f}$$

$$\hat{h}^{+}_{\sigma,\delta}(\eta=0,\hat{t}>0)=\hat{g}^{+}_{\sigma,\delta}\,(\eta=0,\hat{t}>0)(\hat{T}_w+\hat{w}^2) \tag{35g}$$

$$\hat{j}^{+}_{\sigma,\delta}\,(\eta=0,\hat{t}=0)=0 \tag{35h}$$

$$\hat{j}^{+}_{\sigma,\delta}\,(\eta=0,\hat{t}>0)=\hat{g}^{+}_{\sigma,\delta}\,(\eta=0,\hat{t}>0)\,\hat{w} \tag{35i}$$

where

$$Q_{\delta,w}=\frac{R_\delta\, e^{\hat{E}_\delta\left(1-\frac{1}{\hat{T}_w}\right)}}{\hat{T}_w}$$

The density of the molecules diffusing from the plate, $\hat{n}_w$, is not known a priori and can be found by applying the condition of zero mass flux normal to the plate at the surface, i.e.,

$$\int_{-\infty}^{\infty}\int_{-\infty}^{\infty}\int_{-\infty}^{\infty} v_y\, f\, dv_x\, dv_y\, dv_z = 0$$

In the non-dimensionalized discrete ordinate form the above condition yields the relation

$$\hat{n}_w=-\frac{2\sqrt{\pi}}{\sqrt{\hat{T}_w}}\sum_{\delta=1}^{n''}\sum_{\sigma=-n}^{-1} k_\sigma \hat{v}_\sigma\, \hat{g}^{-}_{\sigma,\delta} \tag{36}$$

where k_σ is the weighting coefficients of the new equally spaced quadrature [Appendix A] for velocity component $\hat{V}_\sigma$.

Thus, the problem reduces to solving Equation (34) subject to conditions (35) and (36). This yields 3 x (n + n') x n" equations with 3 x (n + n') x n" discrete unknowns.

Computational Procedure

Equation (34) can be solved by incorporating a finite-difference technique in physical space coupled with an iterative scheme.

Consider the grid formation shown below.

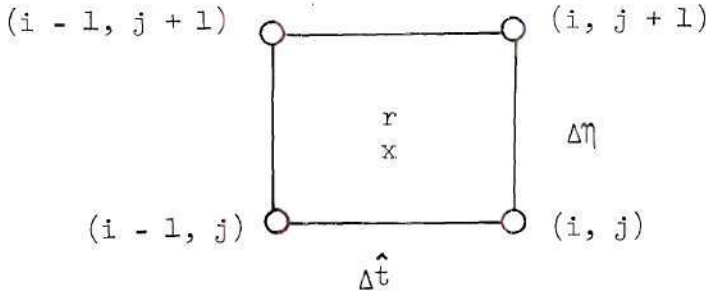

The difference equations are written about the point "r", averaging values from the four points (i, j), (i, j + 1), (i - 1, j), and (i - 1, j + 1), i.e.,

$$\left.\frac{\partial \hat{g}_{\sigma,\delta}}{\partial t}\right|_r = \frac{1}{2\Delta\hat{t}}\left[\hat{g}_{\sigma,\delta}(i,j+1) - \hat{g}_{\sigma,\delta}(i-1,j+1) + \hat{g}_{\sigma,\delta}(i,j) - \hat{g}_{\sigma,\delta}(i-1,j)\right]$$

$$\left.\hat{g}_{\sigma,\delta}\right|_r = \frac{\hat{g}_{\sigma,\delta}(i,j) + \hat{g}_{\sigma,\delta}(i-1,j) + \hat{g}_{\sigma,\delta}(i,j+1) + \hat{g}_{\sigma,\delta}(i-1,j+1)}{4}$$

and similarly for $\left.\frac{\partial \hat{g}_{\sigma,\delta}}{\partial \eta}\right|_r$, $\left.\hat{G}_{t,\sigma,\delta}\right|_r$, $\left.\hat{G}_{i,\sigma,\delta}\right|_r$, $\left.\hat{h}_{\sigma,\delta}\right|_r$, and $\left.\hat{j}_{\sigma,\delta}\right|_r$.

Substituting the above expressions into Equation (34) and solving for $\hat{g}^{-}_{\sigma,s}(i,j)$ yield

$$\hat{g}^{-}_{\sigma,s}(i,j) = \Big\{\Big(-COX - COY - \frac{(1+a)\hat{\nu}_{el}(i,j+1)}{4}\Big)\hat{g}_{\sigma,s}(i,j+1)$$

$$+\Big(COX - COY - (1+a)\frac{\hat{\nu}_{el}(i-1,j+1)}{4}\Big)\hat{g}_{\sigma,s}(i-1,j+1)$$

$$+\Big(COX + COY - (1+a)\frac{\hat{\nu}_{el}(i-1,j)}{4}\Big)\hat{g}_{\sigma,s}(i-1,j)$$

$$+\frac{1}{4}\Big[\hat{\nu}_{el}(i,j)\big(\hat{G}_{t,\sigma,s}(i,j) + a\,\hat{G}_{i,\sigma,s}(i,j)\big)$$

$$+\hat{\nu}_{el}(i,j+1)\big(\hat{G}_{t,\sigma,s}(i,j+1) + a\,\hat{G}_{i,\sigma,s}(i,j+1)\big)$$

$$+\hat{\nu}_{el}(i-1,j+1)\big(\hat{G}_{t,\sigma,s}(i-1,j+1) + a\,\hat{G}_{i,\sigma,s}(i-1,j+1)\big)$$

$$+\hat{\nu}_{el}(i-1,j)\big(\hat{G}_{t,\sigma,s}(i-1,j) + a\,\hat{G}_{i,\sigma,s}(i-1,j)\big)\Big]\Big\} \qquad (37)$$

$$/\,(COX - COY + (1+a)\hat{\nu}_{el}(i,j)/4)$$

where

$$COX = 1/2\Delta\hat{t}$$

$$COY = \hat{V}_y\, b\,(1-\eta)\,2\Delta\eta$$

The $\hat{h}^{-}_{\sigma,s}(i,j)$ and $\hat{j}^{-}_{\sigma,s}(i,j)$ equations are similarly reduced.

One unique feature of this problem is that at time $\hat{t}+\Delta\hat{t}$ the distribution functions $\hat{g}^{+}_{\sigma,s}$ and $\hat{g}^{-}_{\sigma,s}$ are both known at $\eta = 1$ $(y=\infty)$ to be equilibrium freestream values. The distribution function $\hat{g}^{+}_{\sigma,s}$ is known at $\eta = 0$ $(y=0)$ once $\hat{g}^{-}_{\sigma,s}$ has been determined there from a downward marching finite difference technique. Consequently, the solution of $\hat{g}^{-}_{\sigma,s}$ as a function of η is an initial value problem

starting at $\eta = 1$ and marching down to $\eta = 0$ using Equation (37). The solution of $\hat{g}^{+}_{\sigma,\delta}$, however, is a closed-boundary value problem and this feature can be used to derive a more appropriate finite difference scheme.

For $\hat{g}^{+}_{\sigma,\delta}$ the following grid formation is used

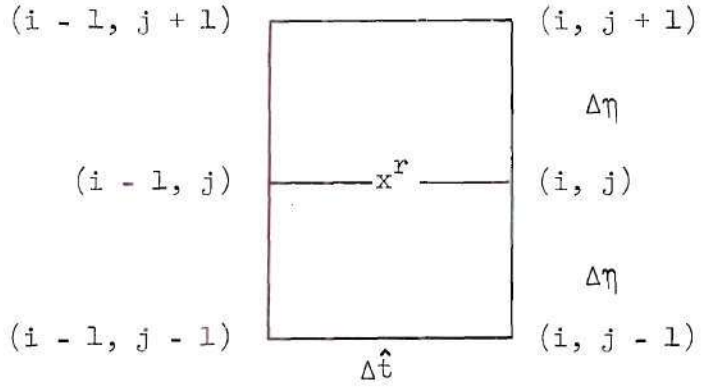

The difference equations are written about the point "r", as follows

$$\left.\frac{\partial \hat{g}_{\sigma,\delta}}{\partial \hat{t}}\right|_r = \frac{1}{\Delta \hat{t}}\left[\hat{g}_{\sigma,\delta}(i,j) - \hat{g}_{\sigma,\delta}(i-1,j)\right]$$

$$\left.\frac{\partial \hat{g}_{\sigma,\delta}}{\partial \eta}\right|_r = \frac{1}{4\Delta\eta}\left[\hat{g}_{\sigma,\delta}(i,j+1) - \hat{g}_{\sigma,\delta}(i,j-1) + \hat{g}_{\sigma,\delta}(i-1,j+1) - \hat{g}_{\sigma,\delta}(i-1,j-1)\right]$$

and similarly for the others.

Substituting the above expressions into Equation (34) and solving for $\hat{g}^{+}_{\sigma,\delta}(i,j)$ yield

$$\hat{g}^{+}_{\sigma,\delta}(i,j) = \left\{\left[1/\Delta\hat{t} - \frac{(1+a)\hat{v}_{el}(i-1,j)}{2}\right]\hat{g}^{+}_{\sigma,\delta}(i-1,j)\right.$$

$$-AC\,\hat{g}_{\sigma,\delta}(i,j+1) + AC\,\hat{g}_{\sigma,\delta}(i,j-1) - AC\,\hat{g}_{\sigma,\delta}(i-1,j+1)$$

$$+AC\,\hat{g}_{\sigma,\delta}(i-1,j-1) + \frac{1}{2}\hat{v}_{el}(i-1,j)\left(\hat{G}_{t,\sigma,\delta}(i-1,j)\right.$$

$$\left.+a\,\hat{G}_{i,\sigma,\delta}(i-1,j)\right) + \frac{1}{2}\hat{v}_{el}(i,j)\left(\hat{G}_{t,\sigma,\delta}(i,j)\right.$$

$$\left.\left.+a\,\hat{G}_{i,\sigma,\delta}(i,j)\right)\right\} \Big/ \left[1/\Delta\hat{t} + \frac{1}{2}(1+a)\hat{v}_{el}(i,j)\right] \qquad (38)$$

where $AC = v_y\, b\,(1-\eta)/4\Delta\eta$

Starting with the freestream values of $\hat{g}^{-}_{\sigma,\delta}(\eta=1)$ [Equation (35a)] Equation (37) is applied to solve $\hat{g}^{-}_{\sigma,\delta}(i,j)$. The resulting values of $\hat{g}^{-}_{\sigma,\delta}$ $(\eta=0)$ are integrated to apply the condition of no normal mass flux at $\eta=0$. This yields $\hat{n}_w$ [Equation (36)], which in turn generates values of $\hat{g}^{+}_{\sigma,\delta}(\eta=0)$, Equation (35e). Starting with these values of $\hat{g}^{+}_{\sigma,\delta}(\eta=0)$ and the known values of $\hat{g}^{+}_{\sigma,\delta}(i,j+1)$, Equation (38) is applied to solve $\hat{g}^{+}_{\sigma,\delta}(i,j)$. The $\hat{h}^{\pm}_{\sigma,\delta}$ and $\hat{j}^{\pm}_{\sigma,\delta}$ equations are similarly solved. The equilibrium distribution function values, $\hat{G}^{\pm}_{t,\sigma,\delta}$, $\hat{G}^{\pm}_{i,\sigma,\delta}$, $\hat{H}^{\pm}_{t,\sigma,\delta}$, $\hat{H}^{\pm}_{i,\sigma,\delta}$, $\hat{J}^{\pm}_{t,\sigma,\delta}$ and $\hat{J}^{\pm}_{i,\sigma,\delta}$ are all determined from moments of the previous iterate. The zeroth iterate at time $\hat{t}_i$ is the time $\hat{t}_{i-1}$ solution. This yields a system

of 3x (n + n') x n" nonlinear algebraic equations with 3x (n + n') x n" unknowns, ($\hat{g}_{\sigma,\delta}$, $\hat{h}_{\sigma,\delta}$ and $\hat{j}_{\sigma,\delta}$; $\sigma = -n, \cdots, -1, 1, \cdots, n'$; $\delta = 1, \cdots, n''$) which is solved by the method of successive approximations. Convergence is assumed to have occurred when the difference between successive iterates of the macroscopic variables at a particular $\hat{t}$ station is $\leq 10^{-4}$. This normally requires five iterations.

A UNIVAC 1108 digital computer was used for the calculations. Seven sets of the new equally spaced quadrature with n = 3 was used for both positive and negative $\hat{v}_y$ integrations. The grid size in the physical η space was taken to be $\Delta\eta = 0.033$ (30 space steps), and the grid size in the $\hat{t}$ space was chosen to be $\Delta\hat{t} = 0.25$. The step size in the velocity space was taken to be 0.2. The same results were obtained by using the smaller grid size, $\Delta\eta = 0.0167$ (60 space steps) and $\Delta\hat{t} = 0.1$.

The constant "b" in Equation (33) was chosen to be 0.03356.

The constant "S" in Equation (32i) was taken to be 0.756, which is the value for Nitrogen, a diatomic gas.

The plate velocity $\hat{W}$ was chosen to be $\hat{W} = 2$ in order to compare with the monatomic solution of Chu [52].

Results

Figures 27 through 41 show the distribution of the flow variables at different instants of time for a wall velocity $\hat{W} = 2$, and wall temperatures $\hat{T}_w = 1$, and 1.6. The shear velocity u (Figures 28 and 34) propagates in the fluid dynamic boundary layer region, with thickness proportional to $\sqrt{t}$. On the plate, the slip and its decrease with time are evident. The other variables are disturbed considerably further away from the plate,

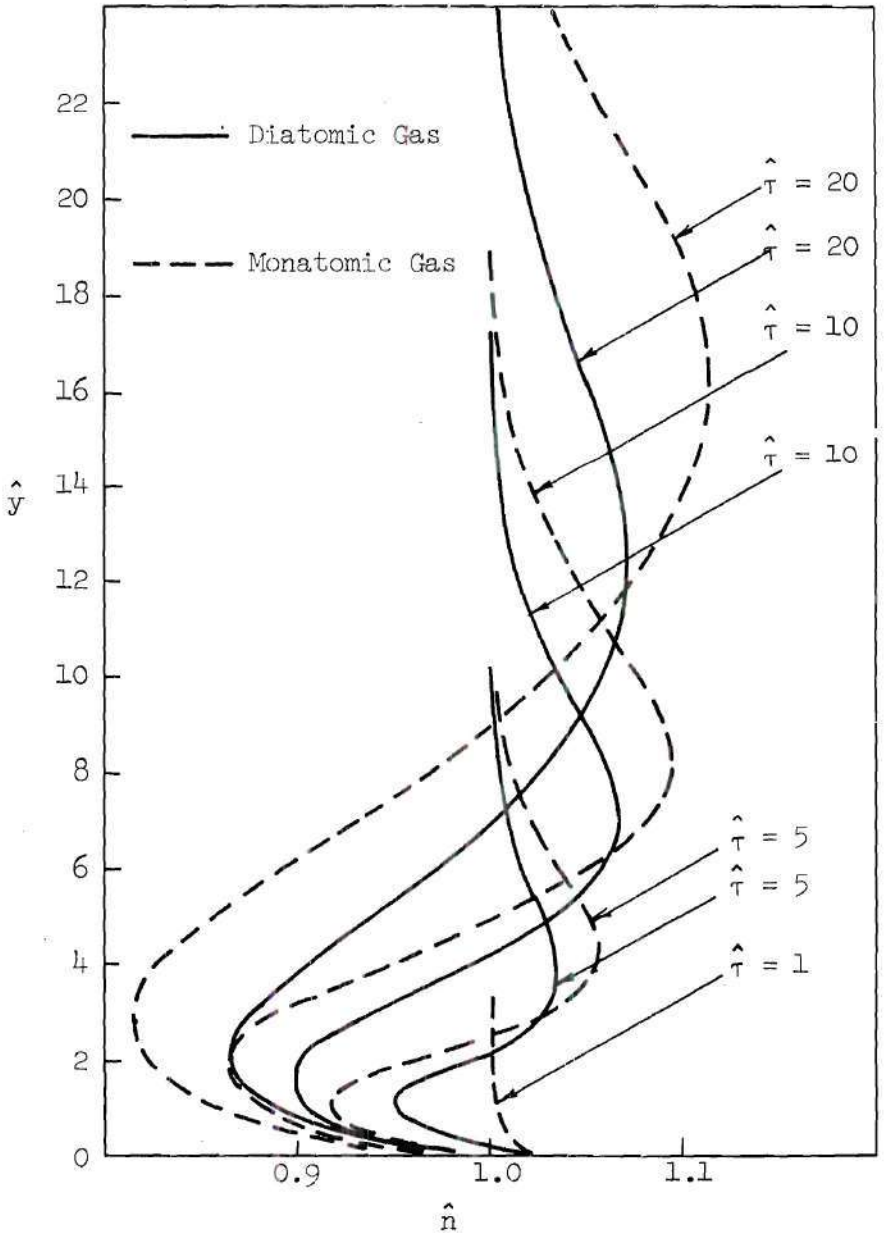

Figure 27. Rayleigh Flow Density Profiles for $\hat{W} = 2$, $T_w = 1$, $Z_R = 3.2$.

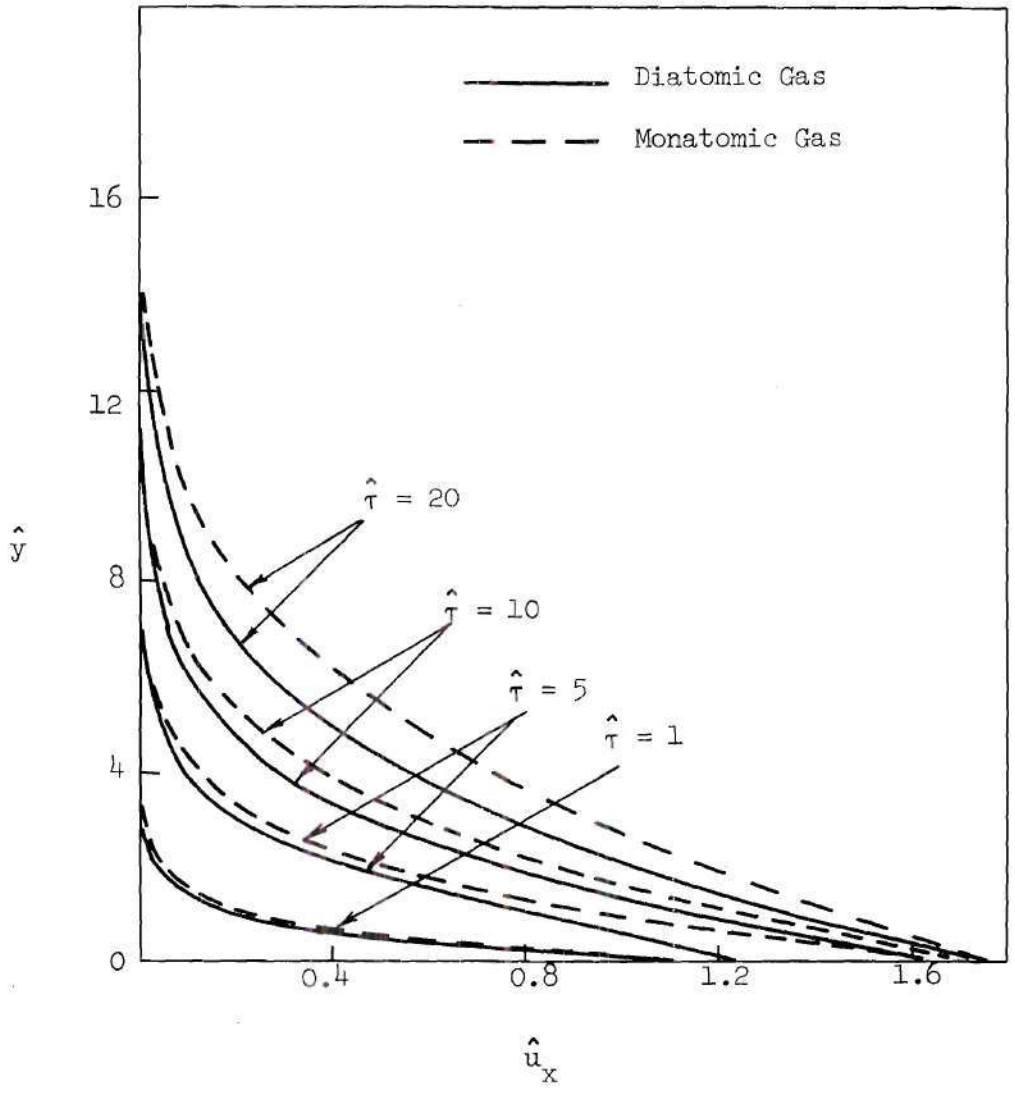

Figure 28. Rayleigh Flow Tangential Velocity Profiles for $\hat{W} = 2$, $\hat{T}_w = 1$, $Z_R = 3.2$.

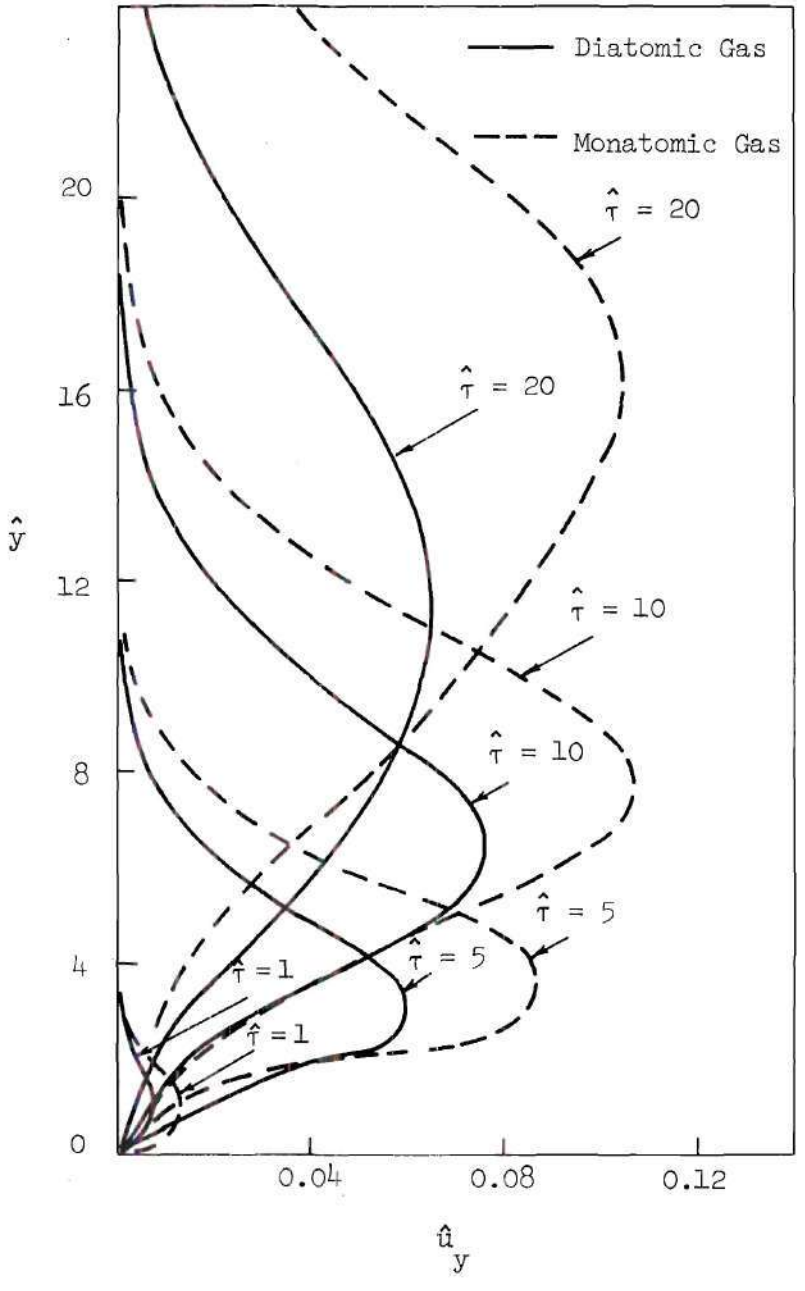

Figure 29. Rayleigh Flow Normal Velocity Profiles for $\hat{W} = 2$, $\hat{T}_w = 1$, $Z_R = 3.2$.

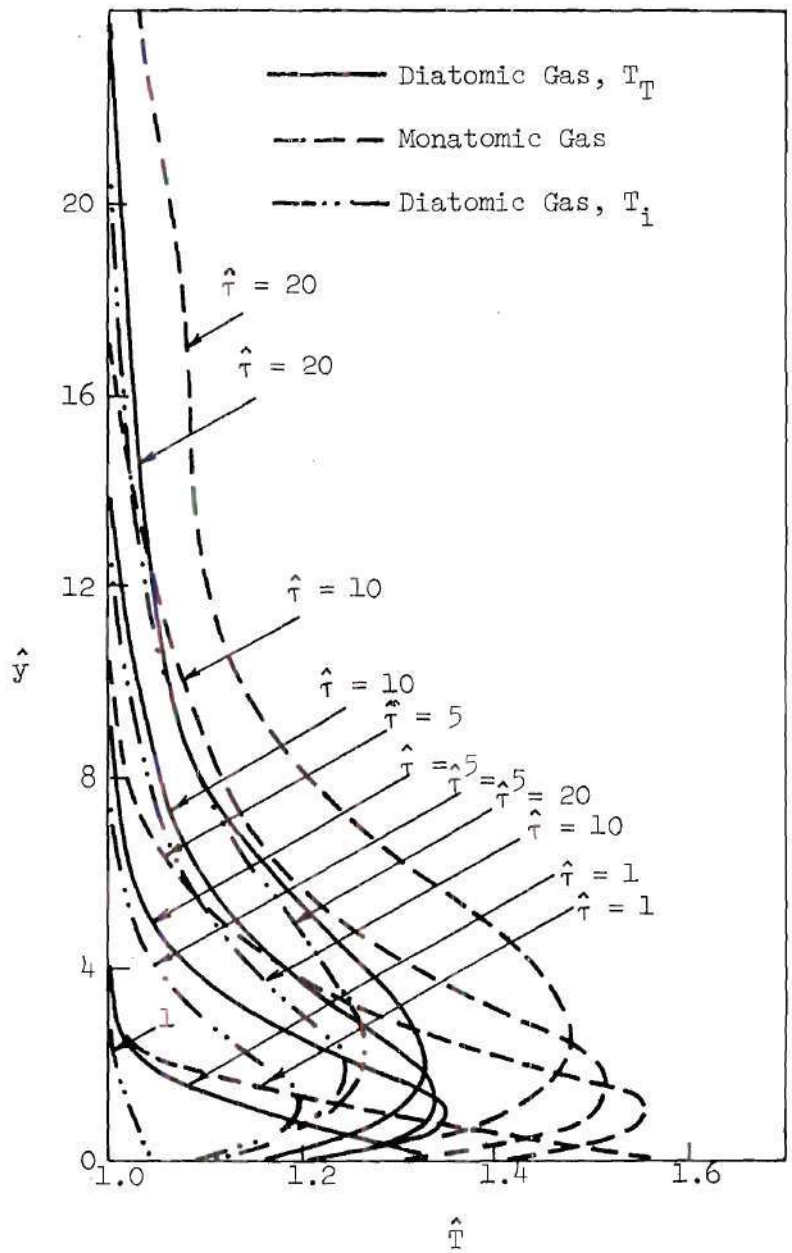

Figure 30. Rayleigh Flow Total Temperature Profiles and Internal Temperature Profiles for $\hat{W} = 2$, $\hat{T}_w = 1$, $Z_R = 3.2$.

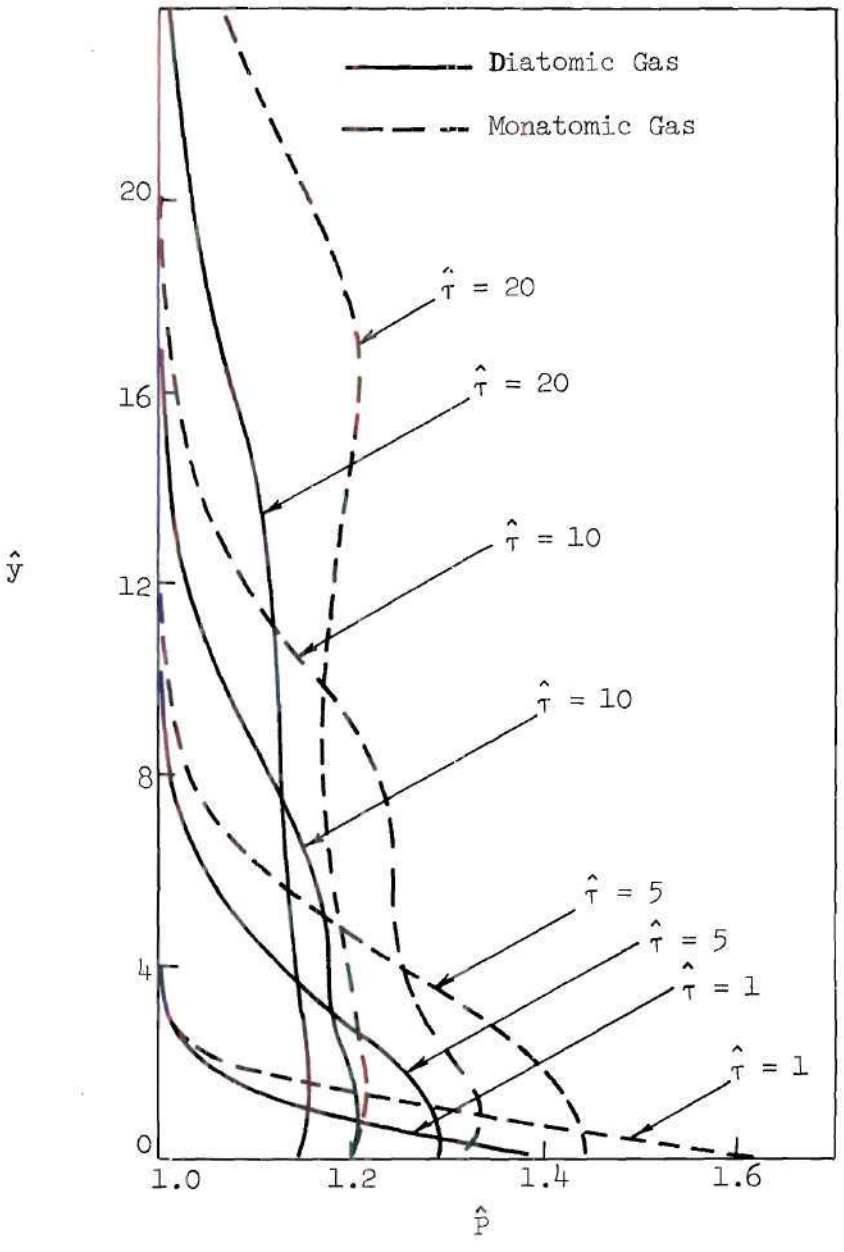

Figure 31. Rayleigh Flow Pressure Profiles for $\hat{W} = 2$, $\hat{T}_w = 1$, $Z_R = 3.2$.

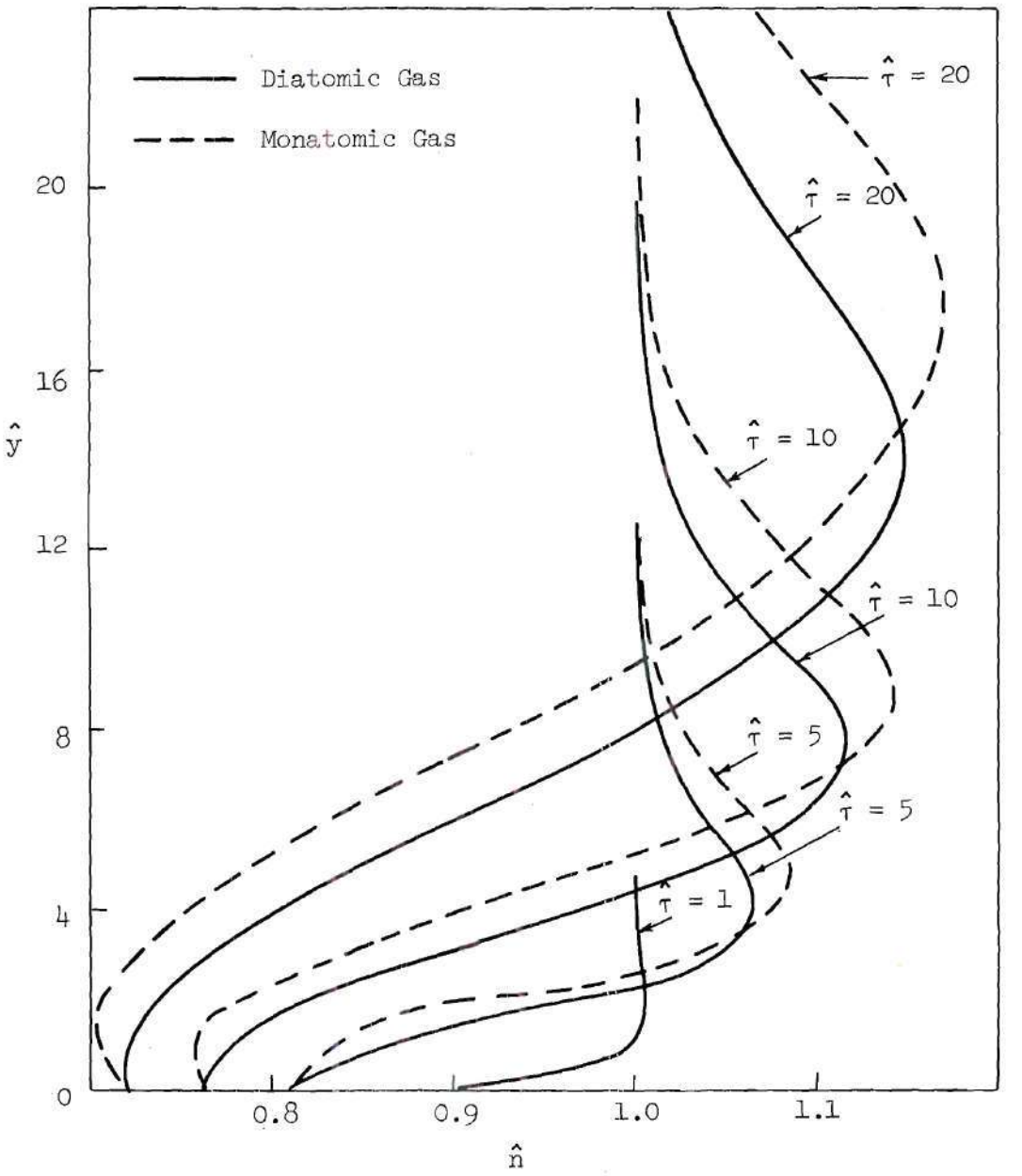

Figure 32. Rayleigh Flow Density Profiles for $\hat{W} = 2$, $\hat{T}_w = 1.6$, $Z_R = 3.2$.

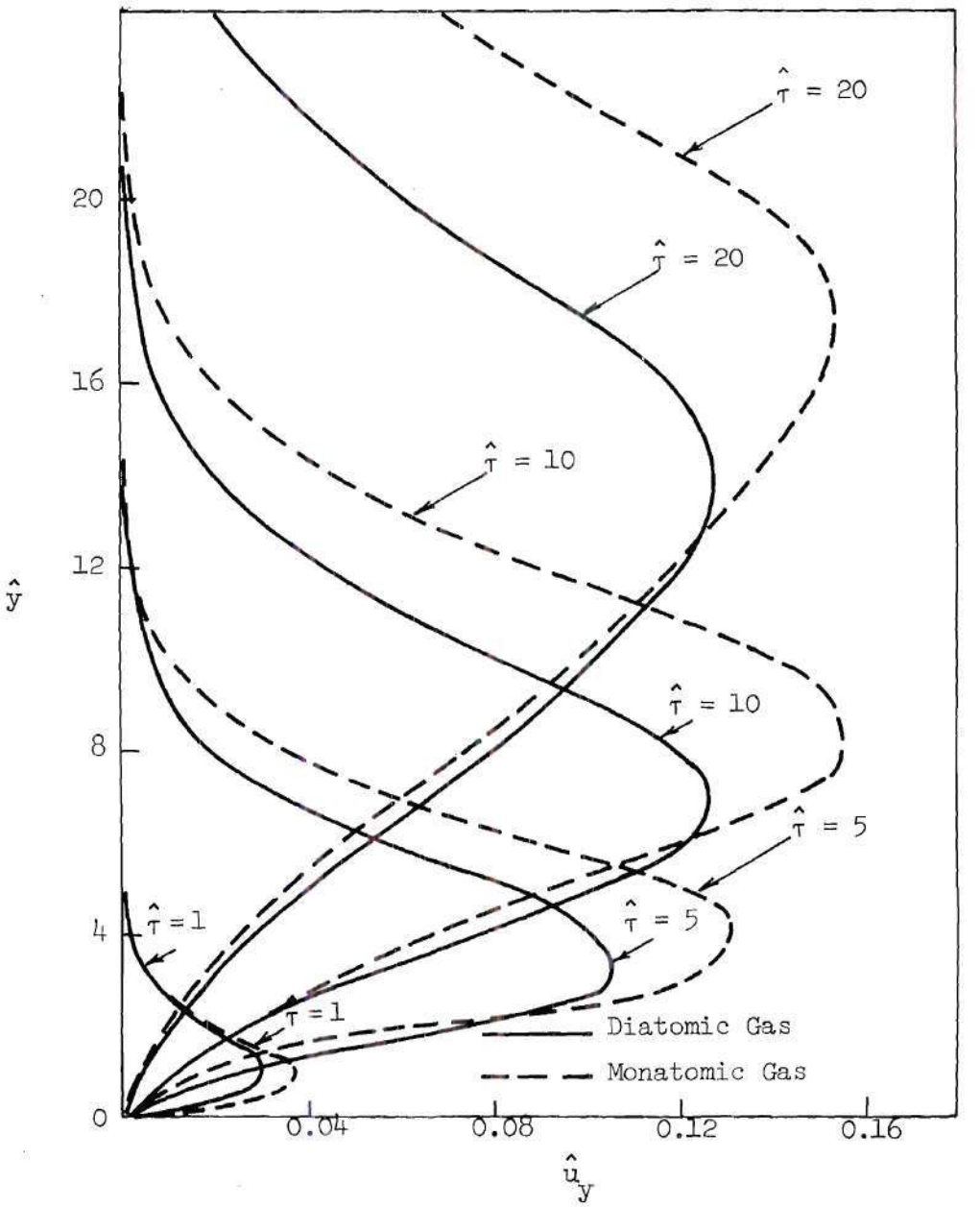

Figure 33. Rayleigh Flow Normal Velocity Profiles for $\hat{W} = 2$, $\hat{T}_w = 1.6$, $Z_R = 3.2$.

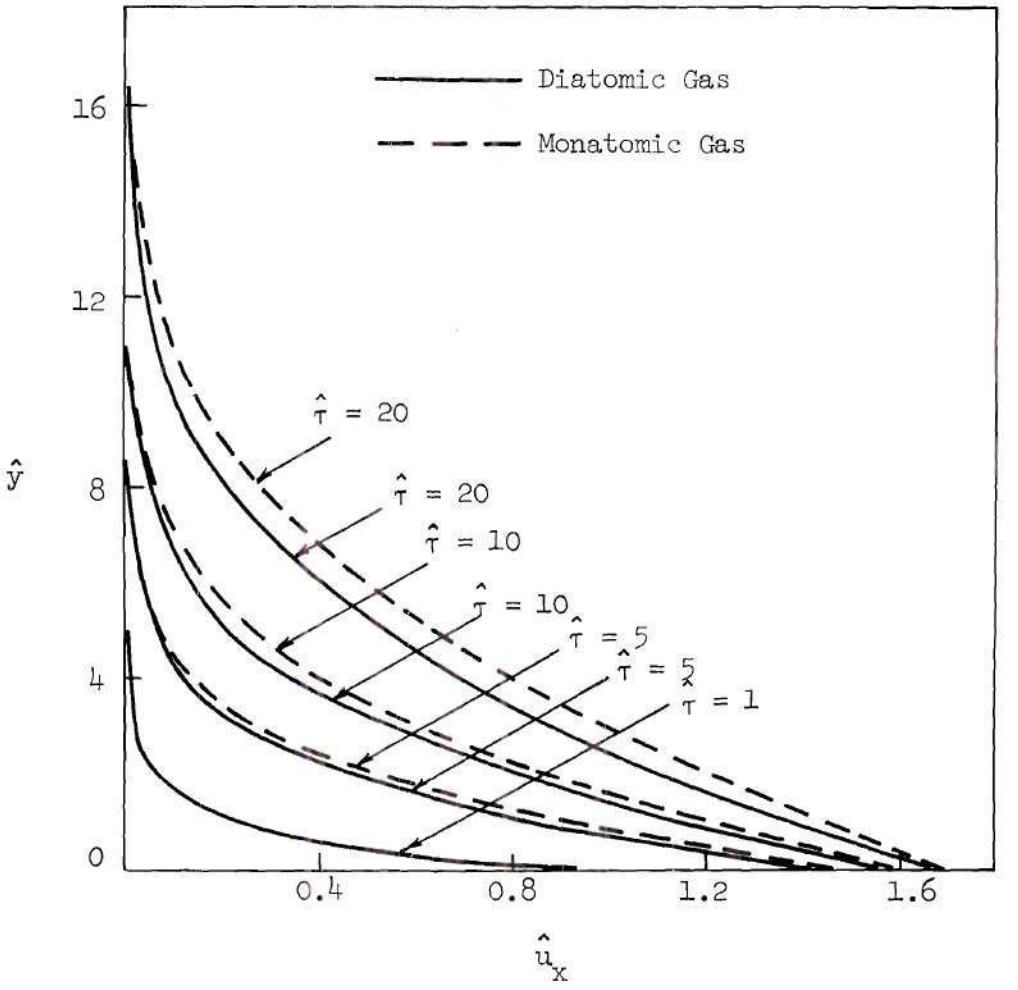

Figure 34. Rayleigh Flow Tangential Velocity Profiles for $\hat{W} = 2$, $\hat{T}_w = 1.6$, $Z_R = 3.2$.

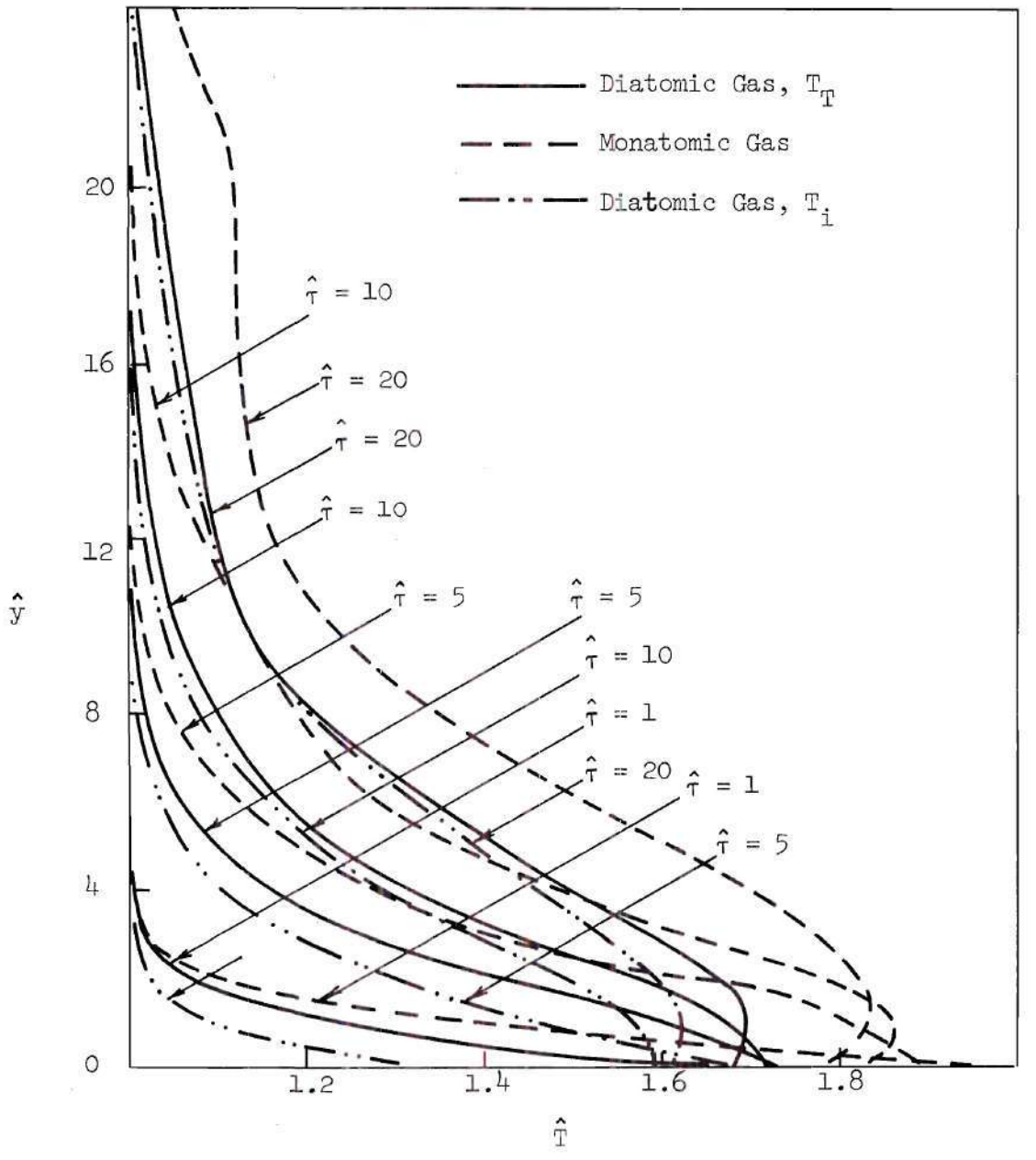

Figure 35. Rayleigh Flow Temperature Profiles for $\hat{W} = 2$ $\hat{T}_w = 1.6$, $Z_R = 3.2$.

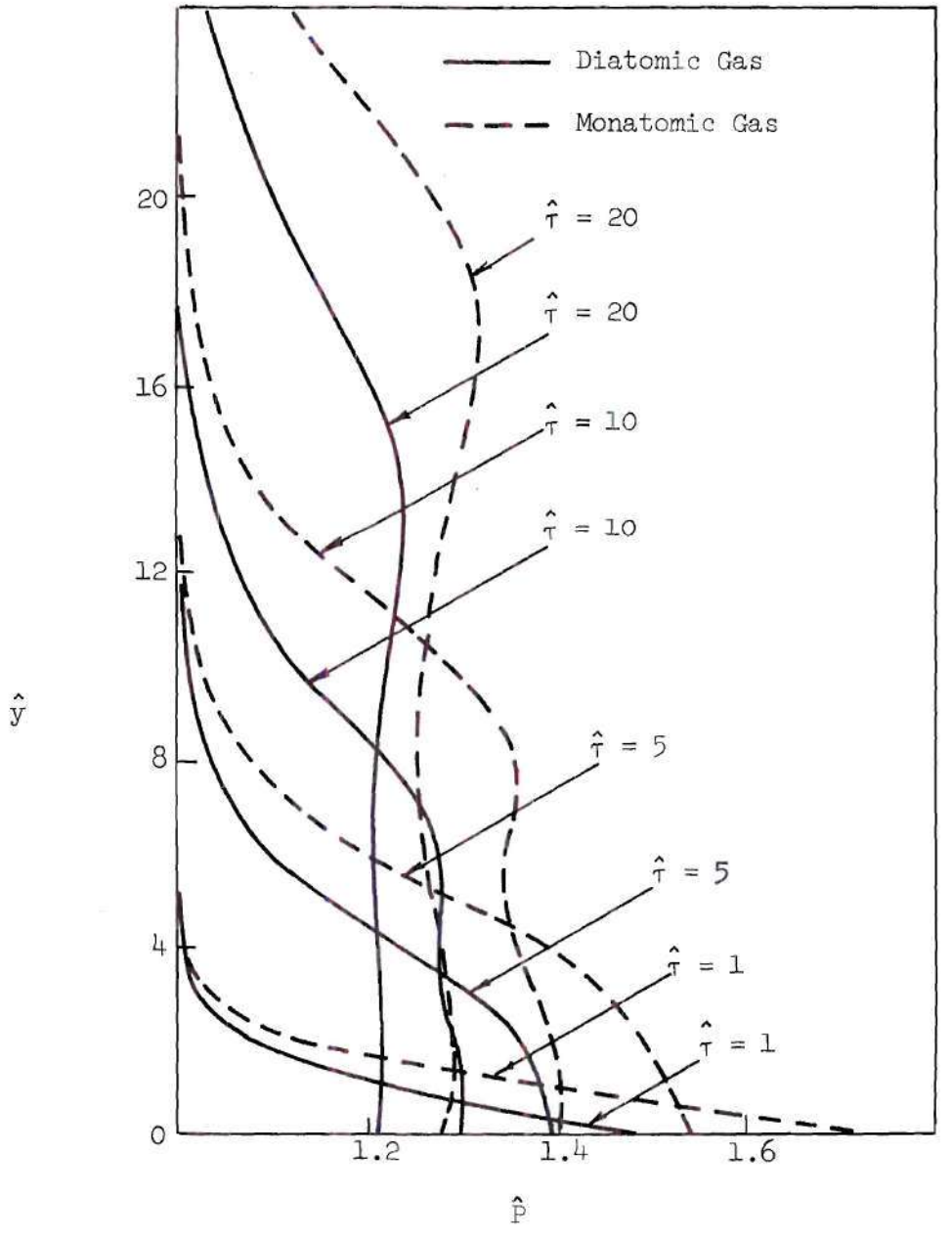

Figure 36. Rayleigh Flow Pressure Profiles for $\hat{W} = 2$, $\hat{T}_w = 1.6$, $Z_R = 3.2$.

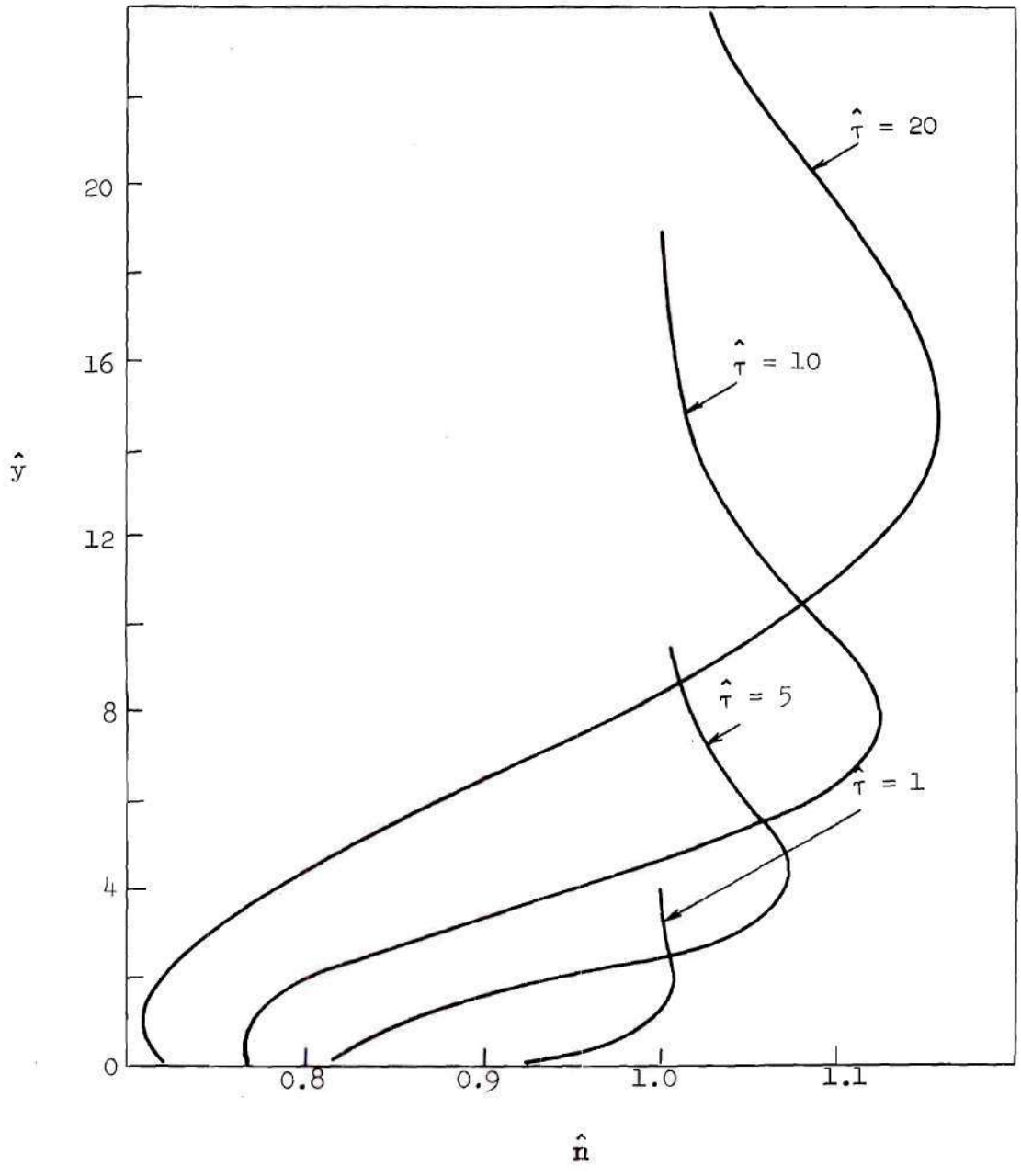

Figure 37. Rayleigh Flow Density Profiles for $\hat{W} = 2$, $\hat{T}_w = 1.6$, $Z_R = 25$.

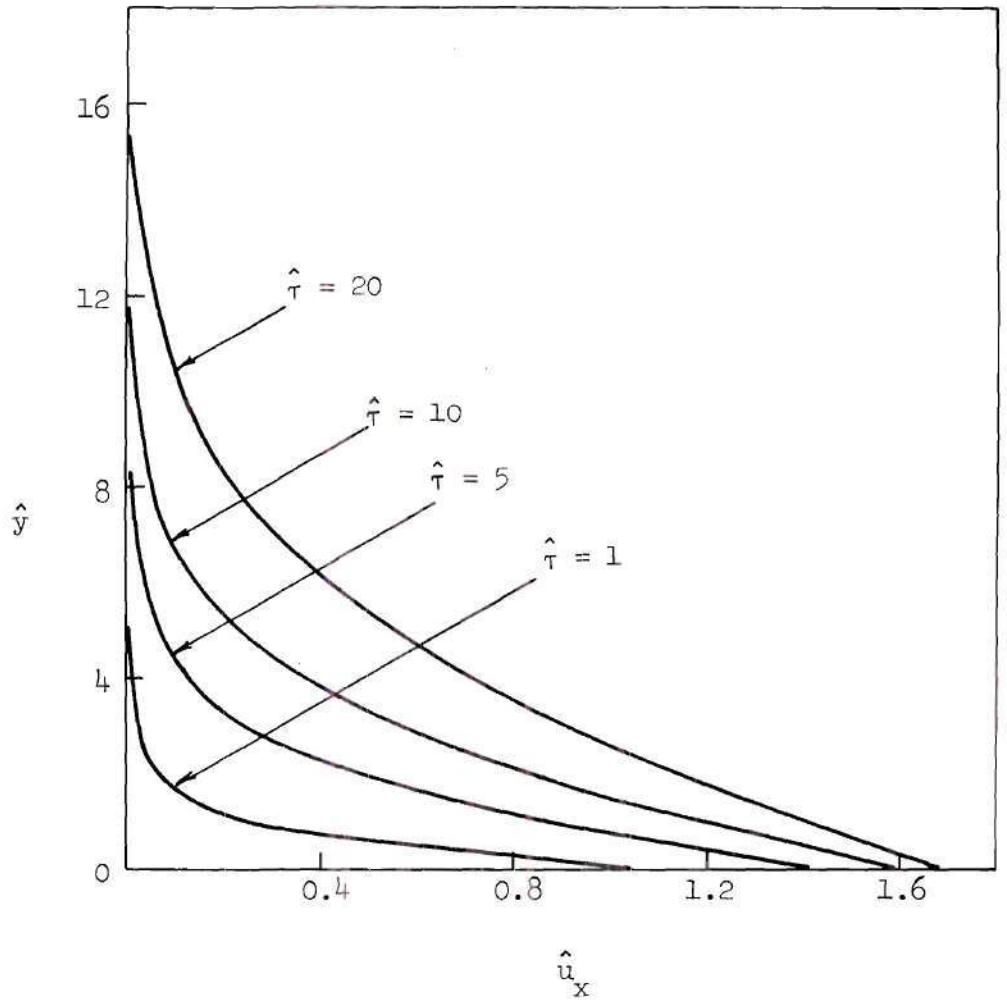

Figure 38. Rayleigh Flow Tangential Velocity Profiles for $\hat{W} = 2$, $\hat{T}_w = 1.6$, $Z_R = 25$.

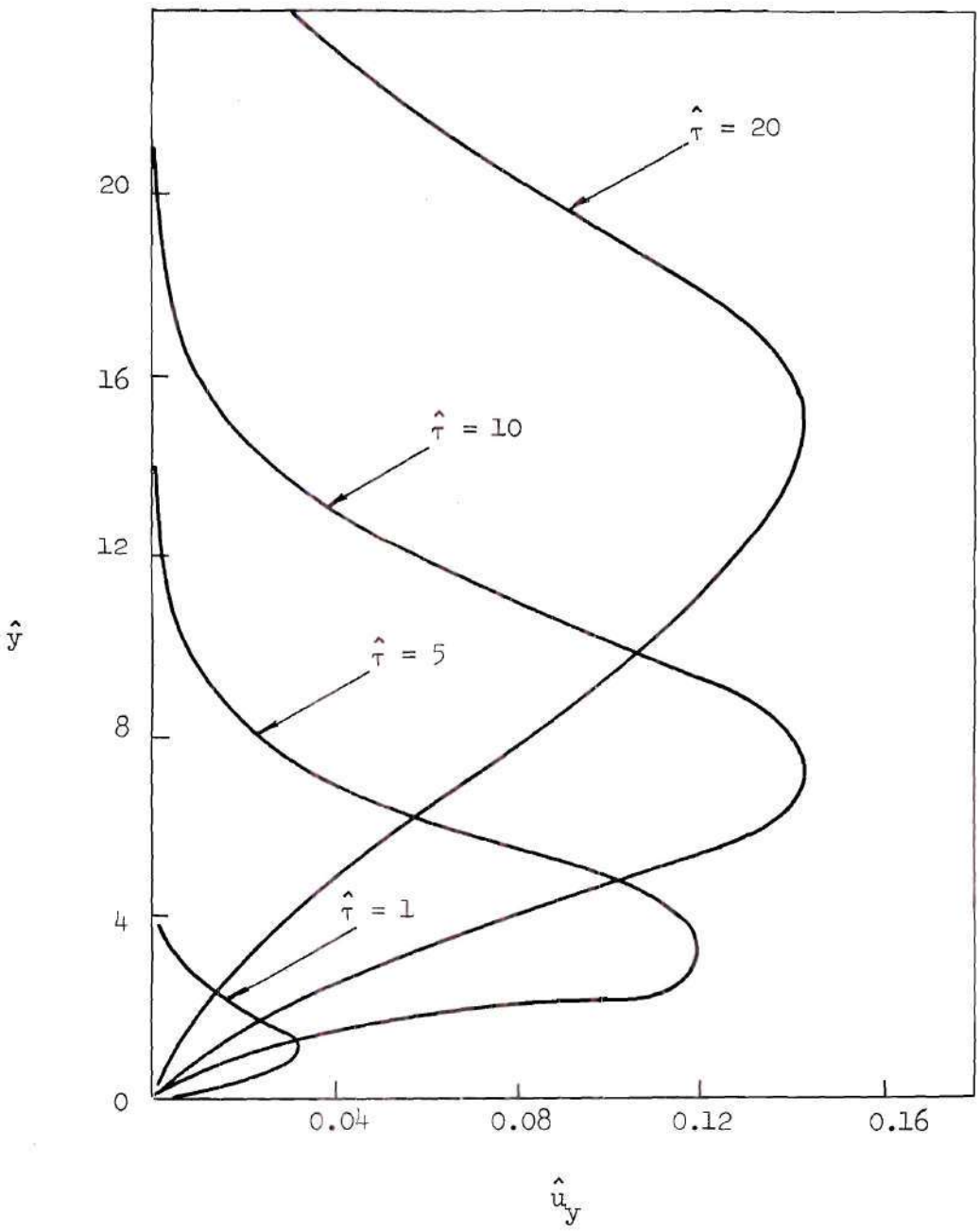

Figure 39. Rayleigh Flow Normal Velocity Profiles for $\hat{W} = 2$, $\hat{T}_w = 1.6$, $Z_R = 25$.

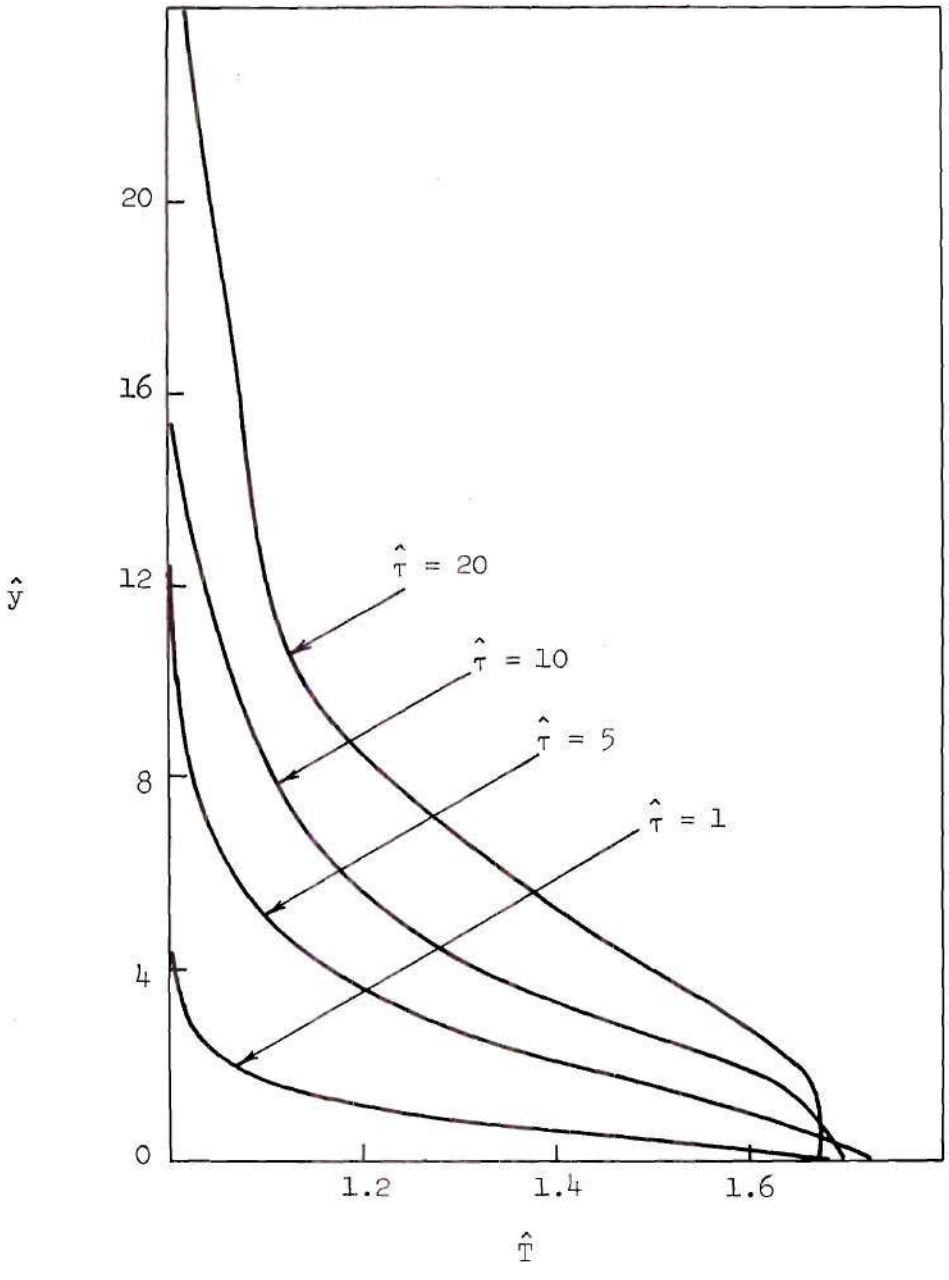

Figure 40. Rayleigh Flow Temperature Profiles for $\hat{W} = 2$, $T_w = 1.6$, $Z_R = 25$.

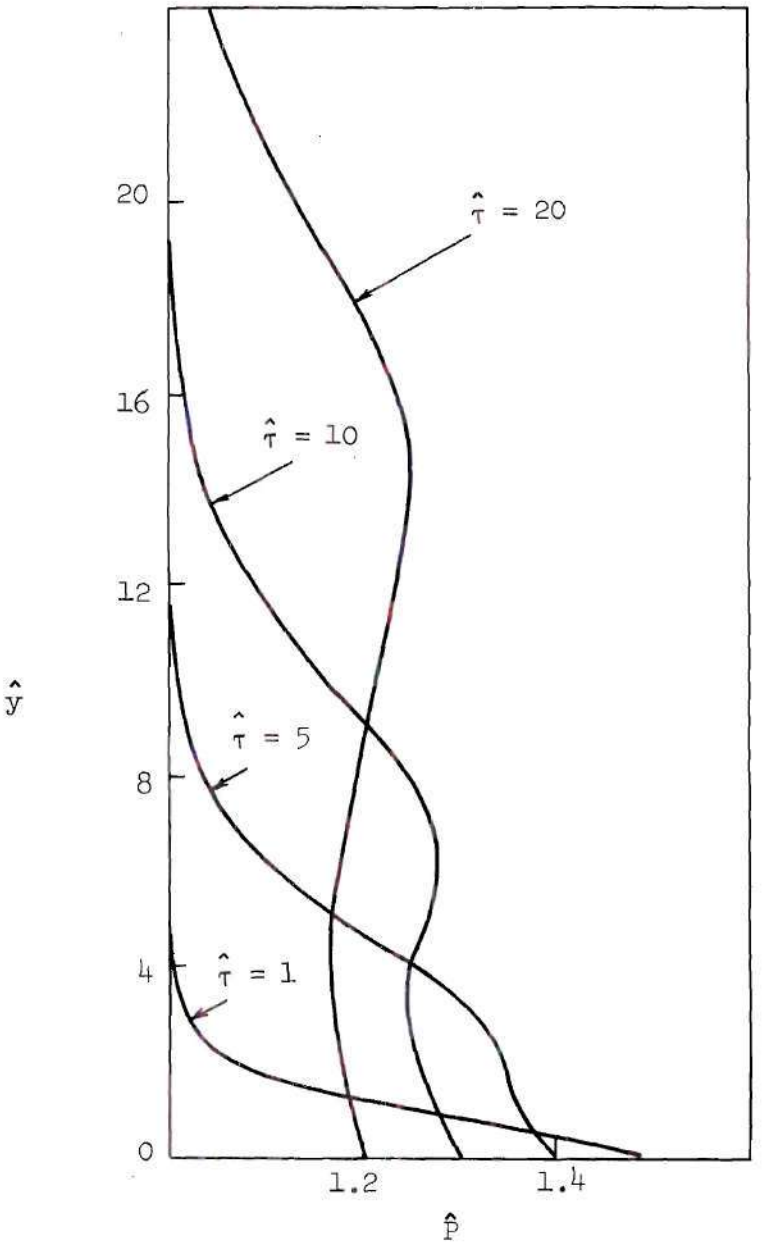

Figure 41. Rayleigh Flow Pressure Profiles for $\hat{W} = 2$, $\hat{T}_w = 1.6$, $Z_R = 25$.

as a result of the heating and shock wave induced by the boundary layer flow.

The monatomic results which were recalculated by using the new equally spaced quadrature are in good agreement with that of Chu [52] and that of Huang and Hartley [53]. The comparison between the monatomic results and that of the diatomic gas reveals the following differences.

(1) At $\hat{\tau} = 1$, both diatomic and monatomic gases give almost identical profiles in density and velocity because the flow is essentially free molecular and the molecular collisions are not important in this flow regime. The monatomic gas gives higher temperature profiles than the diatomic gas does because the specific heat capacity of the monatomic gas is lower than that of the diatomic gas. When $\hat{\tau} > 1$, the monatomic gas gives a thicker boundary layer and stronger shock profiles than the diatomic gas (see for instance Figure 27).

(2) At each instant of time, the diatomic gas gives smaller slip velocities at the plate than the monatomic gas does (see Figure 28).

(3) A comparison between the profiles with $Z_R = 3.2$ (Figures 32 through 36) and the profiles with $Z_R = 25$ (Figures 37 through 41) reveals that the effect of Z_R on the macroscopic profiles is small.

(4) The effect of the different wall temperatures is observed by comparing Figures 27 through 31 and Figures 32 through 36. The higher wall temperature gives the lower density at the wall. The stronger shock strength, the thicker shock layer and the higher surface pressure are observed in the higher wall temperature case.

CHAPTER V

THE TWO DIMENSIONAL LEADING EDGE PROBLEM

Background of the Problem

It has been recognized for a long time that the boundary layer theory is inadequate in the neighborhood of the sharp leading edge of a flat plate in a high-speed flow. One of the earliest evidences to this fact was shown by Becker [54] in 1950. Today there is still need for more experimental and theoretical work on this complex phenomenon. In the regions of the flat plate where rarefaction effects are predominant, theoretical developments are of particular importance due to the poor reliability of experimental techniques. Several theories have been developed to explain the flow behavior, but none of them adequately cover the entire flow regime. One obvious difference can be noted in comparing the available theoretical analyses in regard to the predicted surface pressure distribution. The results of Oguchi [55] and Jain and Li [56] predict a pressure plateau to exist over a substantial portion of the plate before a fall to the free molecular flow limit. The results of Pan and Probstein [57] indicate a pressure peak similar to the heat transfer results. Charwat [58] predicted the existence of a pressure plateau beginning downstream of the leading edge, while Kogan [59] and Bird [60] suggested that even very close to the leading edge, no region of true free-molecular flow exists.

The first experimental evidence of departure from strong inter-

action theory was obtained by Schaaf, Talbot, Hurlbut and Aroesty [61] in a low-density wind-tunnel using an insulated wall model. They attributed the departure to slip flow phenomena. Later Nagamatsu, et al. [62, 63] obtained evidence of the formulation of plateaus in both induced pressure and heat transfer by using cold wall models in a shock tunnel. Further evidence for the same was provided by Vidal and Wittliff [64] . The first experimental evidence showing the upstream end of a plateau curving downward towards free molecule flow values were contributed by Burke, et al. [65] . Later, Wallace and Burke [66] presented cold wall data for skin friction and heat transfer for the entire flow regimes - from continuum to free-molecular region. These results showed rather a peak in skin friction and heat transfer instead of a broad plateau. The induced pressure data in their paper did not tend towards the free molecular value. Recent experiments are directed towards the exploration of the properties of the flow field. However, there are some data available on the surface pressure distribution. One of the most important experimental data published recently is by Metcalf, Lillicrap and Berry [67, 68]. In addition to these experimental data, some theoretical calculations are also available. One of these results available is the Monte Carlo calculations by Vogenitz, Broadwell and Bird [69] . All these data show a plateau in the surface pressure.

The disagreement in various induced pressure data may be due to differences in the configurations of the pressure taps used in the models and this becomes important near the leading edge. Another important aspect to be considered in the surface pressure measurements is the "orifice effect". Under rarefied conditions, heat transfer and shear stress can

cause the surface pressure measured within the orifice to be significantly different from the actual pressure on the surface adjacent to the orifice. Normally, the pressure transducers are highly temperature sensitive and even a small disturbance near the orifice can affect the pressure measurement. Many correction schemes have been developed [70, 71, 72] for making orifice correction to the measured surface pressure. The most significant is by Potter, et al. [70]. This correction is based on a free molecular theory, in which the orifice diameter is assumed to be small compared to local mean free path of the gas and is supplemented by a correlation of transitional flow experimental data. This scheme assumes that at such an orifice, the incoming molecules do not collide with the molecules leaving the orifice. With such a model, expressions for number flux of molecules and the surface pressure have been obtained utilizing a two-stream Maxwellian distribution function. This, however, is inaccurate since the distribution function for the incoming molecules is most probably not Maxwellian. Besides, the reliability of this model is still under investigation.

There is little conclusive experimental evidence on the surface pressure measurement. Thus, there is a strong need for more theoretical work in this complex phenomenon. The present study attempts to obtain the surface pressure distribution as well as the flow field for a diatomic gas using the discrete ordinate method as a tool and the Boltzmann equation with the BGK model as a governing equation.

The surface pressure distribution has also been calculated by Huang and Hartley [4] and Huang and Hwang [6, 8] using the BGK model equation and the discrete ordinate method. However, the numerical

procedures used in References 4, 6 and 8 were that of an initial value approach. Consequently, the up-stream effect was not taken into account, and the flow field and the surface pressure distribution were not in agreement with experimental data. The numerical procedure used in this investigation is that of a closed-boundary value approach [32]. It will be shown that it is this approach that yields good results to the problem.

Formulation of the Problem

The geometry of the problem is shown in Fig. 42. A finite flat plate is kept at zero angle of attack in a high-speed rarefied flow. M_∞ is the Mach number of the freestream with density n_∞ and temperature T_∞. The plate temperature T_w is kept constant.

The governing equation for this case is

$$V_x \frac{\partial f_\ell}{\partial x} + V_y \frac{\partial f_\ell}{\partial y} = \nu_{e\ell} (F_{t\ell} - f_\ell) + \nu_{in} (F_{i\ell} - f_\ell) \tag{39}$$

where

$$F_{t\ell} = n_\ell \left(\frac{m}{2\pi k \bar{T}_t}\right)^{3/2} e^{-\frac{m}{2k\bar{T}_t}\left[(V_x - U_x)^2 + (V_y - U_y)^2 + V_z^2\right]} \tag{40a}$$

$$F_{i\ell} = n_{\ell_{eq}} \left(\frac{m}{2\pi k \bar{T}_T}\right)^{3/2} e^{-\frac{m}{2kT_T}\left[(V_x - U_x)^2 + (V_y - U_y)^2 + V_z^2\right]} \tag{40b}$$

$\nu_{e\ell}$ and ν_{in} are defined in Equation (4a) and (4b).

For the purpose of reduction in computer storage requirements, the reduced distribution functions which are similar to the case of Couette

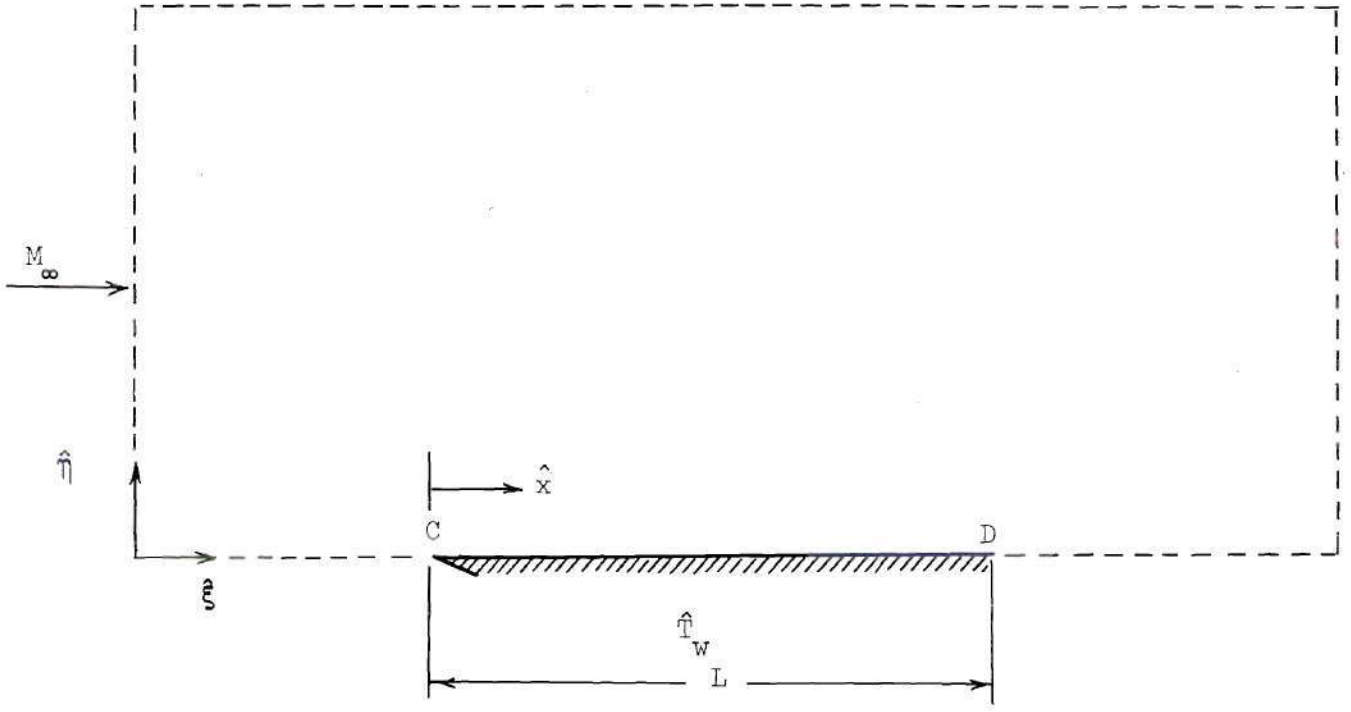

Figure 42. Geometry and Coordinate System for the Two Dimensional Leading Edge Problem.

flow are conveniently introduced.

$$g_\ell(x, y; V_x, V_y; E_\ell) = \int_{-\infty}^{\infty} f_\ell(x, y; \vec{V}; E_\ell)\, dV_z \tag{41a}$$

$$h_\ell(x, y; V_x, V_y; E_\ell) = \int_{-\infty}^{\infty} V_z^2\, f_\ell(x, y; \vec{V}; E_\ell)\, dV_z \tag{41b}$$

Thus, integrating out the v_z dependence in Equation (39) by using Equations (41), the single three-dimensional (in velocity space) Boltzmann equation reduces to the following two simultaneous two-dimensional (in velocity space) equations

$$V_x \frac{\partial g_\ell}{\partial x} + V_y \frac{\partial g_\ell}{\partial y} = \nu_{e\ell}(G_{t\ell} - g_\ell) + a\,\nu_{e\ell}(G_{i\ell} - g_\ell) \tag{42a}$$

$$V_x \frac{\partial h_\ell}{\partial x} + V_y \frac{\partial h_\ell}{\partial y} = \nu_{e\ell}(H_{t\ell} - h_\ell) + a\,\nu_{e\ell}(H_{i\ell} - h_\ell) \tag{42b}$$

where

$$G_{t\ell} = \frac{n_\ell}{2\pi R T_t}\, e^{-\frac{1}{2RT_t}\left[(V_x - U_x)^2 + (V_y - U_y)^2\right]} \tag{43a}$$

$$H_{t\ell} = R T_t\, G_{t\ell} \tag{43b}$$

$$G_{i\ell} = \frac{n_{\ell eq}}{2\pi R T_T}\, e^{-\frac{1}{2RT_T}\left[(V_x - U_x)^2 + (V_y - U_y)^2\right]} \tag{43c}$$

$$H_{il} = R\, T_T\, G_{il} \tag{43d}$$

the moments are found as follows

$$n_l = \int_{-\infty}^{\infty} g_l \, dV_x \, dV_y \tag{44a}$$

$$n = \sum_l n_l \tag{44b}$$

$$n_{leq} = n \left(\frac{e^{-\bar{E}_l / k T_T}}{\sum_s e^{-\bar{E}_s / k T_T}} \right) \tag{44c}$$

$$u_x = \frac{1}{n} \sum_l \int_{-\infty}^{\infty} V_x \, g_l \, dV_x \, dV_y \tag{44d}$$

$$u_y = \frac{1}{n} \sum_l \int_{-\infty}^{\infty} V_y \, g_l \, dV_x \, dV_y \tag{44e}$$

$$\frac{3}{2} n R \bar{T}_t = \frac{1}{2} \sum_l \left\{ \int_{-\infty}^{\infty} \int_{-\infty}^{\infty} h_l \, dV_x \, dV_y + \frac{1}{2} \int_{-\infty}^{\infty} \int_{-\infty}^{\infty} \left[(V_x - u_x)^2 + (V_y - u_y)^2 \right] g_l \, dV_x \, dV_y \right\} \tag{44f}$$

$$q_{yt} = \sum_l \left\{ \frac{m}{2} \int_{-\infty}^{\infty} \int_{-\infty}^{\infty} V_y V_x^2 \, g_l \, dV_x \, dV_y - m u_x \int_{-\infty}^{\infty} \int_{-\infty}^{\infty} V_x V_y \, g_l \, dV_x dV_y \right.$$

$$+\frac{m}{2}\int_{-\infty}^{\infty}\int_{-\infty}^{\infty} V_y^3\, g_\ell\, dV_x dV_y - m u_y \int_{-\infty}^{\infty}\int_{-\infty}^{\infty} V_y^2\, g_\ell\, dV_x dV_y$$
$$+\frac{m}{2}\int_{-\infty}^{\infty}\int_{-\infty}^{\infty} V_y h_\ell\, dV_x dV_y\Big\} - \frac{3}{2} nRTu_y + \frac{mn u_y (u_x^2 + u_y^2)}{2} \tag{44g}$$

$$q_{yi} = \sum_\ell \int g_\ell E_\ell V_y\, dV_y \tag{44f}$$

$$q_y = q_{yt} + q_{yi} \tag{44i}$$

$$p = mnkT \tag{44j}$$

$$\tau_{xy} = -m\sum_\ell \int_{-\infty}^{\infty}\int_{-\infty}^{\infty} V_x V_y\, g_\ell\, dV_x dV_y + mn u_x u_y \tag{44k}$$

$$C_v^i T_i = \frac{1}{n}\sum_\ell E_\ell n_\ell \tag{44l}$$

$$C_v T_T = \frac{3}{2} k T_t + C_v^i T_i \tag{44m}$$

where $C_v = \frac{3}{2}k + C_v^i$. τ_{xy} is the shear stress in the x-y plane, q_{yt}, q_{yi}, q_y are translational, internal and total heat flux normal to the plate, respectively.

$\nu_{\ell\ell}$ and ν_{in} are defined in Equations (4a) and (4b).

A characteristic velocity is defined as

$$V_\infty = \sqrt{2RT_\infty} \tag{45}$$

The definitions of dimensionless variables are introduced as follows

$$\hat{u}_x = \frac{u_x}{V_\infty}\ ,\quad \hat{u}_y = \frac{u_y}{V_\infty}\ ,\quad \hat{n} = \frac{n}{n_\infty}\ ,\quad \hat{T} = \frac{T}{T_\infty}\ ,$$

$$\hat{p} = \frac{p}{p_\infty}\ ,\quad \hat{\tau}_{xy} = \tau_{xy}/m n_\infty U_\infty^2\ ,\quad \hat{q}_y = q_y/c_p T_\infty m n_\infty U_\infty\ ,$$

$$\hat{x} = \frac{x}{\bar{\ell}_\infty}\ ,\quad \hat{y} = \frac{y}{\bar{\ell}_\infty}\ ,\quad \hat{g}_\ell = g_\ell V_\infty^2/n_\infty\ ,\quad \hat{h}_\ell = h_\ell/n_\infty\ ,$$

$$\hat{\nu} = \nu\bar{\ell}_\infty/V_\infty\ ,\qquad \hat{G}_\ell = G_\ell V_\infty^2/n_\infty\ ,\qquad \hat{H}_\ell = H_\ell/n_\infty\ ,$$

$$\hat{E}_\ell = E_\ell/kT_\infty$$

Thus a set of dimensionless differential equations for a specified discrete point in the velocity space $(\hat{v}_\sigma, \hat{v}_\lambda)$ and an evergy level $\hat{E}_\delta$ can be written as

$$\hat{V}_\sigma \frac{\partial \hat{g}_{\sigma,\lambda,\delta}}{\partial \hat{x}} + \hat{V}_\lambda \frac{\partial \hat{g}_{\sigma,\lambda,\delta}}{\partial \hat{y}} = \hat{\nu}_{el}\left(\hat{G}_{t,\sigma,\lambda,\delta} - \hat{g}_{\sigma,\lambda,\delta}\right) + a\hat{\nu}_{il}\left(\hat{G}_{i,\sigma,\lambda,\delta} - \hat{g}_{\sigma,\lambda,\delta}\right) \tag{46a}$$

$$\hat{V}_\sigma \frac{\partial \hat{h}_{\sigma,\lambda,\delta}}{\partial \hat{x}} + \hat{V}_\lambda \frac{\partial \hat{h}_{\sigma,\lambda,\delta}}{\partial \hat{y}} = \hat{\nu}_{el}\left(\hat{H}_{t,\sigma,\lambda,\delta} - \hat{h}_{\sigma,\lambda,\delta}\right) + a\hat{\nu}_{il}\left(\hat{H}_{i,\sigma,\lambda,\delta} - \hat{h}_{\sigma,\lambda,\delta}\right) \tag{46b}$$

where

$$\hat{G}_{t,\sigma,\lambda,\delta} = \frac{\hat{n}_s}{\pi \hat{T}_t} e^{-\frac{1}{\hat{T}_t}\left[(\hat{V}_\sigma - \hat{u}_x)^2 + (\hat{V}_\lambda - \hat{u}_y)^2\right]} \tag{47a}$$

$$\hat{H}_{t,\sigma,\lambda,\delta} = \frac{\hat{T}_t}{2} \hat{G}_{t,\sigma,\lambda,\delta} \tag{47b}$$

$$\hat{G}_{i,\sigma,\lambda,\delta} = \frac{\hat{n}_{s,eq}}{\pi \hat{T}_T} e^{-\frac{1}{\hat{T}_T}\left[(\hat{V}_\sigma - \hat{u}_x)^2 + (\hat{V}_\lambda - \hat{u}_y)^2\right]} \tag{47c}$$

$$\hat{H}_{i,\sigma,\lambda,\delta} = \frac{\hat{T}_I}{2} \hat{G}_{i,\sigma,\lambda,\delta} \tag{47d}$$

and

$$\hat{\nu}_{el} = \frac{8}{5(1+a)\sqrt{\pi}} \hat{n} \hat{T}_t^{1-s} \tag{47e}$$

Introducing the transformation

$$\hat{\eta} = 1 - e^{-b\hat{y}}$$
$$\hat{\xi} = 1 - e^{-c\hat{x}} \tag{48}$$

into Equation (46) gives

$$\hat{V}_\sigma c(1-\hat{\xi}) \frac{\partial \hat{g}_{\sigma,\lambda,\delta}}{\partial \hat{\xi}} + \hat{V}_\lambda b(1-\hat{\eta}) \frac{\partial \hat{g}_{\sigma,\lambda,\delta}}{\partial \hat{\eta}} = \hat{\nu}_{el} \left(\hat{G}_{t,\sigma,\lambda,\delta} - \hat{g}_{\sigma,\lambda,\delta}\right) + a\hat{\nu}_{el}\left(\hat{G}_{i,\sigma,\lambda,\delta} - \hat{g}_{\sigma,\lambda,\delta}\right) \tag{49}$$

$\sigma = -n', \cdots, -1, 1, \cdots, n'$; $\lambda = -n''', \cdots, -1, 1, \cdots, n'''$; $\delta = 1, \cdots, n''$;

and a similar equation for $\hat{h}_{\sigma,\lambda,\delta}$. This transformation not only maps the infinite $\hat{y}$ region into a unit region $(0 \leq \hat{\eta} \leq 1)$, but it also does so in an efficient manner. That is, if the region $0 \leq \hat{\eta} \leq 1$ is divided into M equal steps for the purpose of applying a finite difference scheme, the points in actual physical space are quite close together in the region near the plate where gradient are largest and are spaced farther apart in regions away from the surface where there is little change in flow properties.

Perfectly diffuse reflection is assumed to specify the interaction of the molecules with the surface of the plate. That is, it is assumed that molecules which strike the surface subsequently emitted with a Maxwellian velocity distribution characterized by the plate temperature, $\hat{T}_w$, and zero net tangential velocity. The two-stream concept introduced earlier is applied here also by defining the half-range distribution functions

$$\hat{f}_\ell = \hat{f}_\ell^{++} + \hat{f}_\ell^{+-} + \hat{f}_\ell^{-+} + \hat{f}_\ell^{--}$$

where

$\hat{f}_\ell^{++}$ is the distribution function for $\hat{v}_x > 0$ and $\hat{v}_y > 0$;
$\hat{f}_\ell^{+-}$ is the distribution function for $\hat{v}_x > 0$ and $\hat{v}_y < 0$;
$\hat{f}_\ell^{-+}$ is the distribution function for $\hat{v}_x < 0$ and $\hat{v}_y > 0$;
$\hat{f}_\ell^{--}$ is the distribution function for $\hat{v}_x < 0$ and $\hat{v}_y < 0$;

The non-dimensionalized boundary condition can be written as

$$\hat{g}^{+\pm}(\hat{\xi}=0,\hat{\eta};\hat{V}_\sigma,\hat{V}_\lambda;\hat{E}_s)=\hat{g}^{-\pm}(\hat{\xi}=1,\hat{\eta};\hat{V}_\sigma,\hat{V}_\lambda;\hat{E}_s)$$

$$=\hat{g}^{\pm-}(\hat{\xi},\hat{\eta}=1;\hat{V}_\sigma,\hat{V}_\lambda;\hat{E}_s)$$

$$=\frac{e^{-\hat{E}_s}}{\pi\sum_s e^{-\hat{E}_s}}\,e^{-[(\hat{V}_\sigma-\hat{U}_\infty)^2+\hat{V}_\lambda^2]}$$

$$=\frac{R_s}{\pi}\,e^{-[(\hat{V}_\sigma-\hat{U}_\infty)^2+\hat{V}_\lambda^2]} \qquad \text{[Appendix A] (50a)}$$

$$\hat{h}^{+\pm}(\hat{\xi}=0,\hat{\eta};\hat{V}_\sigma,\hat{V}_\lambda;\hat{E}_s)=\hat{h}^{-\pm}(\hat{\xi}=1,\hat{\eta};\hat{V}_\sigma,\hat{V}_\lambda;\hat{E}_s)$$

$$=\hat{h}^{\pm-}(\hat{\xi},\hat{\eta}=1;\hat{V}_\sigma,\hat{V}_\lambda;\hat{E}_s)$$

$$=\frac{e^{-\hat{E}_s}}{2\pi\sum_s e^{-\hat{E}_s}}\,e^{-[(\hat{V}_\sigma-\hat{U}_\infty)^2+\hat{V}_\lambda^2]}$$

$$=\frac{R_s}{2\pi}\,e^{-[(\hat{V}_\sigma-\hat{U}_\infty)^2+\hat{V}_\lambda^2]} \qquad (50b)$$

$$\hat{g}^{\pm+}(C\le\hat{\xi}\le D,\hat{\eta}=0;\hat{V}_\sigma,\hat{V}_\lambda;\hat{E}_s)$$

$$=\frac{\hat{n}_w\,e^{-\hat{E}_s/\hat{T}_w}}{\pi\hat{T}_w\sum_s e^{-\hat{E}_s/\hat{T}_w}}\,e^{-(\hat{V}_\sigma^2+\hat{V}_\lambda^2)/\hat{T}_w}$$

$$=\frac{\hat{n}_w R_s\,e^{\hat{E}_s(1-1/\hat{T}_w)}}{\hat{T}_w}\left(\frac{1}{\pi\hat{T}_w}\right)e^{-(\hat{V}_\sigma^2+\hat{V}_\lambda^2)/\hat{T}_w} \qquad (50c)$$

$$\hat{h}^{\pm+}\left(C \le \hat{\xi} \le D,\ \hat{\eta}=0;\ \hat{V}_\sigma, \hat{V}_\lambda;\ \hat{E}_\delta\right) = \frac{\hat{T}_w}{2}\,\hat{g}^{\pm+}\left(C \le \hat{\xi} \le D,\ \hat{\eta}=0;\ \hat{V}_\sigma, \hat{V}_\lambda;\ \hat{E}_\delta\right) \tag{50d}$$

$$\hat{g}^{\pm+}\left(\hat{\xi} < C \text{ or } \hat{\xi} > D,\ \hat{\eta}=0;\ \hat{V}_\sigma, \hat{V}_\lambda;\ \hat{E}_\delta\right) = \hat{g}^{\pm-}\left(\hat{\xi} < C \text{ or } \hat{\xi} > D,\ \hat{\eta}=0;\ \hat{V}_\sigma, \hat{V}_\lambda;\ \hat{E}_\delta\right) \tag{50e}$$

$$\hat{h}^{\pm+}\left(\hat{\xi} < C \text{ or } \hat{\xi} > D,\ \hat{\eta}=0;\ \hat{V}_\sigma, \hat{V}_\lambda;\ \hat{E}_\delta\right) = \hat{h}^{\pm-}\left(\hat{\xi} < C \text{ or } \hat{\xi} > D,\ \hat{\eta}=0;\ \hat{V}_\sigma, \hat{V}_\lambda;\ \hat{E}_\delta\right) \tag{50f}$$

$(\hat{\xi}=C, \hat{\eta}=0)$ is the point at the leading edge whereas $(\hat{\xi}=D, \hat{\eta}=0)$ is the point at the trailing edge. R_δ is the Gauss-Laguerre weighting coefficient.

The density of the molecules diffusing from the plate, $\hat{n}_w$, is not known a priori and may be found by applying the condition of zero mass flux normal to the plate at the surface. i.e.,

$$\sum_\ell \left\{ \int_{-\infty}^{\infty} \int_0^{\infty} \hat{V}_y\, \hat{g}_\ell^{+}(\hat{V}_x, \hat{V}_y, \hat{E}_\ell)\, d\hat{V}_x\, d\hat{V}_y + \int_{-\infty}^{\infty} \int_{-\infty}^{0} \hat{V}_y\, \hat{g}_\ell^{-}(\hat{V}_x, \hat{V}_y, \hat{E}_\ell)\, d\hat{V}_x\, d\hat{V}_y \right\} = 0$$

In discrete ordinate form, this condition yields the relation

$$\hat{n}_w = -\frac{2\sqrt{\pi}}{\sqrt{\hat{T}_w}} \sum_{\delta=1}^{n''} \sum_{\sigma=-n'}^{n'} \sum_{\lambda=-n''}^{-1} k_\sigma k_\lambda \hat{V}_\lambda\, \hat{g}_{\sigma,\lambda,\delta}\left(\hat{\eta}=0\right) \tag{51}$$

where k_σ and k_λ are the weighting coefficients of the new quadrature [Appendix A] for $\hat{v}_\sigma$ and $\hat{v}_\lambda$, respectively.

Thus, the problem reduces to solving Equation (46) subject to conditions (50) and (51). This yields 2x (n + n') x (2n"') x n" equations with 2x (n + n') x (2n"') x n" discrete unknowns.

Computational Procedures

The simple forward and backward difference scheme is applied in order to reduce the computer time.

The grid points used for $\hat{g}^{+-}_{\sigma,\lambda,\delta}$ are illustrated below

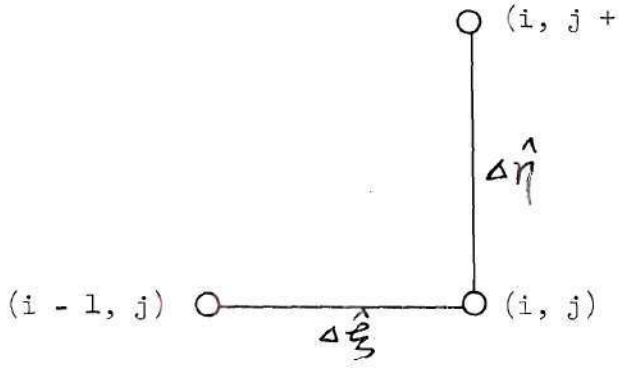

Starting from $\hat{\eta}=1$ and $\hat{\xi}=0$ with the known values of $\hat{g}^{+-}_{\sigma,\lambda,\delta}(\hat{\eta}=1)$ and $\hat{g}^{+-}_{\sigma,\lambda,\delta}(\hat{\xi}=0)$ Equation (50a), the difference form of Equation (49) is applied as follows

$$\hat{g}^{+-}_{\sigma,\lambda,\delta}(i,j) = \Big\{ A\,\hat{g}^{+-}_{\sigma,\lambda,\delta}(i-1,j) - B\,\hat{g}^{+-}_{\sigma,\lambda,\delta}(i,j+1)$$

$$+ C\Big[\hat{G}^{+-}_{t,\sigma,\lambda,\delta}(i,j) + a\,\hat{G}^{+-}_{i,\sigma,\lambda,\delta}(i,j)\Big]\Big\} \Big/ \big[A - B + (1+a)C\big] \qquad (52a)$$

where

$$A = \big[\hat{V}_\sigma\, C(1-\hat{\xi})\big] \Big/ \Delta\hat{\xi} \qquad (52b)$$

$$B = \left[\hat{V}_\lambda b\,(1-\hat{\eta})\right]/\Delta\hat{\eta} \tag{52c}$$

and

$$C = \hat{\nu}_{el} \tag{52d}$$

$\hat{g}^{--}_{\sigma,\lambda,\delta}$ is similarly applied.

To be consistant with the backward difference scheme, the derivatives are written in the direction of flow of the molecules. Appropriately, then the grid formulation for $\hat{g}^{++}_{\sigma,\lambda,\delta}$ is taken to be as illustrated below

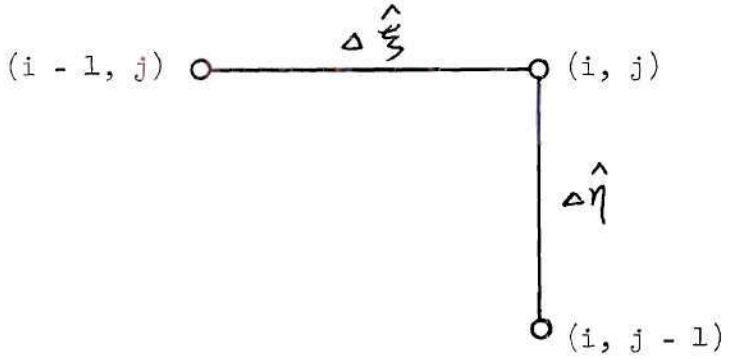

The resulting values of $\hat{g}^{\pm-}_{\sigma,\lambda,\delta}(\hat{\eta}=0)$ obtained from the solution of Equation (52) are integrated to apply the no normal mass flux boundary condition, Equation (51). This yields $\hat{n}_w$, which, in turn, generates values of $\hat{g}^{\pm+}_{\sigma,\lambda,\delta}(\hat{\eta}=0)$ along the plate, Equation (50c). The symetric condition is applied along the $\hat{\eta}=0$ plane elsewhere, Equation (50e). Equation (49) is rearranged and applied in the following form

$$\hat{g}^{++}_{\sigma,\lambda,\delta}(i,j) = \Big\{A\,\hat{g}^{++}_{\sigma,\lambda,\delta}(i-1,j) + B\,\hat{g}^{++}_{\sigma,\lambda,\delta}(i,j+1) + C\left[\hat{G}^{++}_{t,\sigma,\lambda,\delta}(i,j) + a\,\hat{G}^{++}_{i,\sigma,\lambda,\delta}(i,j)\right]\Big\}\Big/\left[A+B+(1+a)C\right] \tag{53}$$

where A, B, and C are identical to that of Equation (52).

The $\hat{h}^{\pm\pm}_{\sigma,\lambda,\delta}$ equation is similarly solved.

The equilibrium distribution values, $\hat{G}^{\pm\pm}_{t,\sigma,\lambda,\delta}$, $\hat{G}^{\pm\pm}_{i,\sigma,\lambda,\delta}$, $\hat{H}^{\pm\pm}_{t,\sigma,\lambda\delta}$ and $\hat{H}^{\pm\pm}_{i,\sigma,\lambda,\delta}$ are all determined from the moments of the previous iterate. This yields a system of $2x(n+n')\,x\,(2n"')\,xn"$ nonlinear algebraic equation with $2x(n+n')\,x\,(2n"')\,xn"$ unknowns ($\hat{g}_{\sigma,\lambda,\delta}$ and $\hat{h}_{\sigma,\lambda,\delta}$; σ = - n, ..., -1, 1, ..., n'; λ = - n"', ..., -1, 1, ..., n"'; δ = 1, ..., n").

A UNIVAC 1108 digital computer was used for the calculations. The new "odd" equally spaced quadrature with n = 3 was used for both $\hat{v}_x$ and $\hat{v}_y$ integrations. The Gauss-Laguerre quadrature with n = 4 is used for energy levels. The grid size in the physical $\hat{\eta}$ space was taken to be $\Delta\hat{\eta} = 18$ (18 space steps), and the grid size in the $\hat{\xi}$ space was chosen to be $\Delta\hat{\xi} = 41$ (41 space steps). There are 9 grid points in front of the leading edge ($\hat{\xi}$ = 10) and 11 grid points after the trailing edge ($\hat{\xi}$ = 30). The length of the plate is $51.8\ell_\infty$. Convergence is assumed to have occurred when the difference between successive iterates at every grid point is $\lesssim 10^{-3}$.

The constants "b" and "c" in Equation (48) serve as "stretching factors" and were chosen to be 0.0932 and 0.02 respectively.

The viscosity-temperature exponent in Equation (47e) was taken to be S = 0.756 which is the value for Nitrogen, a diatomic gas.

The Chapman-Rubesin constant, C, used only in the calculation of the plotting parameter, $\bar{V}_{\infty,x}$, was chosen to be unity.

The freestream Mach number was chosen to be M_∞ = 6.1. All the flow phenomena of interest in the leading edge problem are exhibited at this Mach number.

Results

As the distribution function was determined at successive stations in the flow field, all macroscopic moments of interest were obtained by applying the same quadrature used to solve the governing equations. A complete presentation of all the macroscopic phenomena of interest is offered in the followings.

Density Profiles

The density profiles at $\hat{x} = 18$ and 36 are compared with the available experimental data [68] in Figures 43 and 44, respectively. The monatomic results based on the BGK model are also presented for comparisons (these results were obtained using the present closed-boundary value approach). It should be noted that the experimental data are for a diatomic gas and that, although the calculated results are lower than the experimental data, the positions of the peak and valley agree very well with the experimental curve. In other words, the thickness of the shock layer in the present results agrees quite well with the experimental data.

The effect of the different wall temperatures is shown in Figures 45 and 46.

The density profiles at various $\hat{x}$ stations are illustrated in Figure 47. The thickness of the shock layer for the monatomic gas is always larger than that of the diatomic gas.

Tangential Velocity Profiles

Figures 48 and 49 illustrate the variation of the tangential velocity profiles along the plate for monatomic and diatomic gases

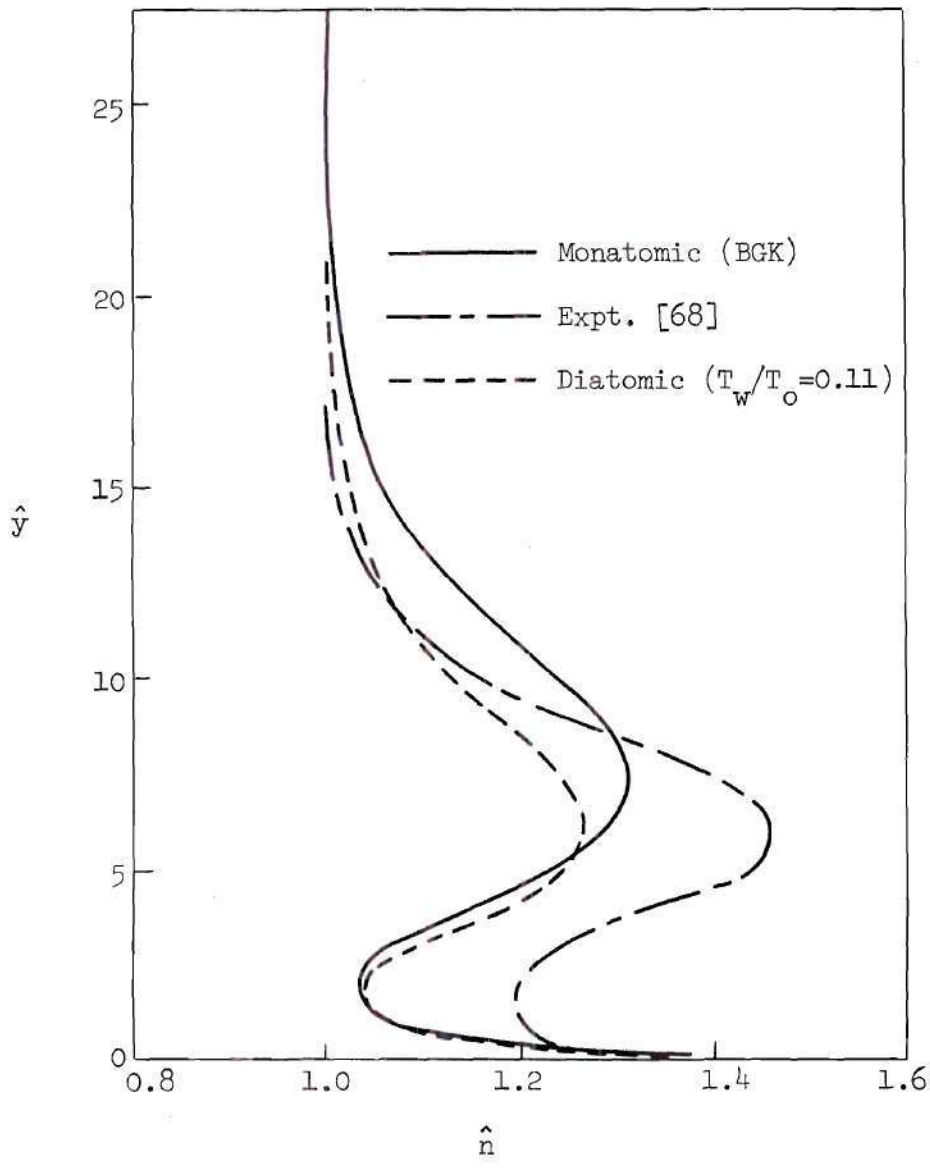

Figure 43. Flat Plate Density Profiles for $M_\infty = 6.1$, $T_w/T_o = 0.11$ and $\hat{x} = 18$.

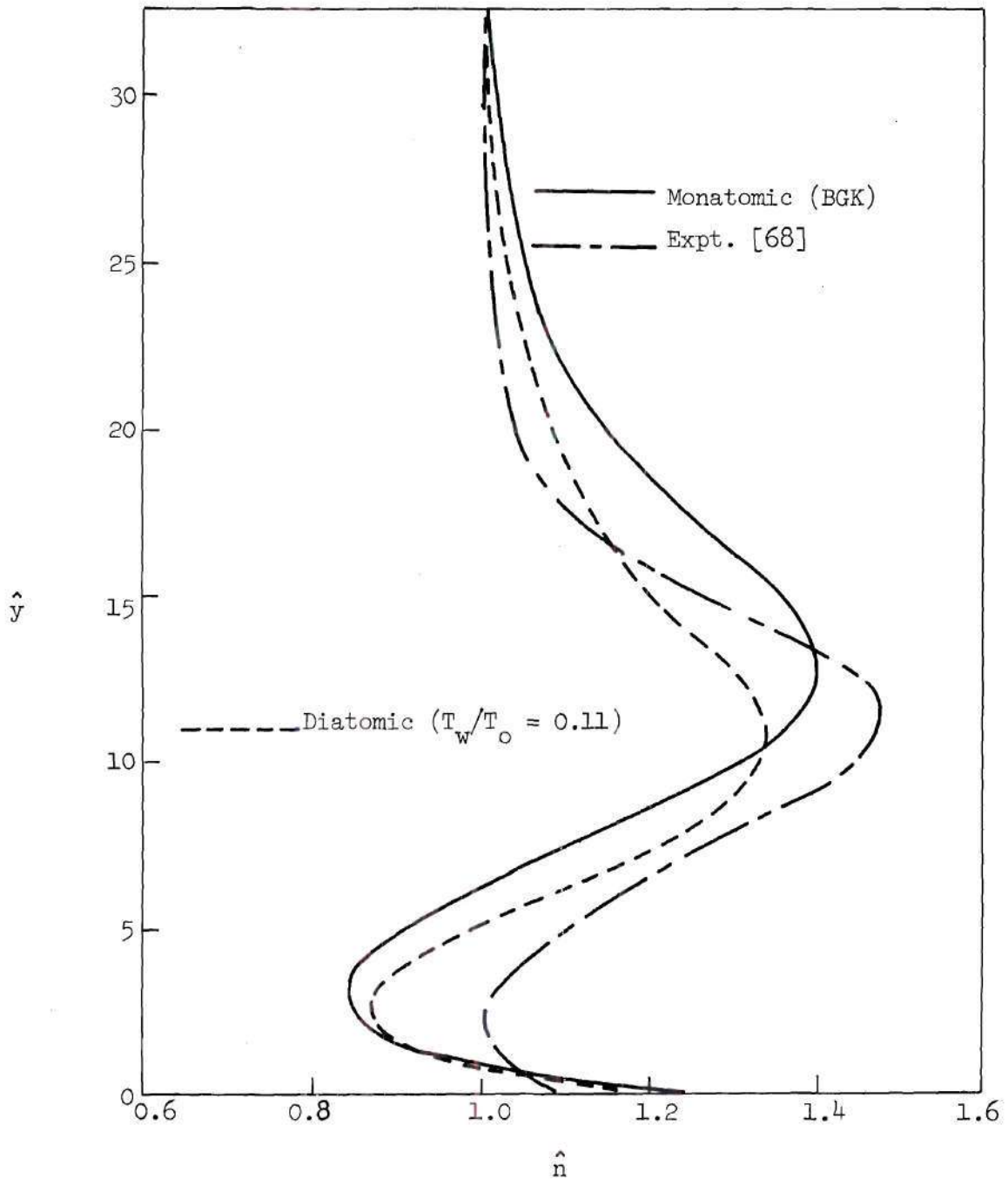

Figure 44. Flat Plate Density Profile for M_∞ = 6.1, T_w/T_o = 0.11 and $\hat{x}$ = 36.

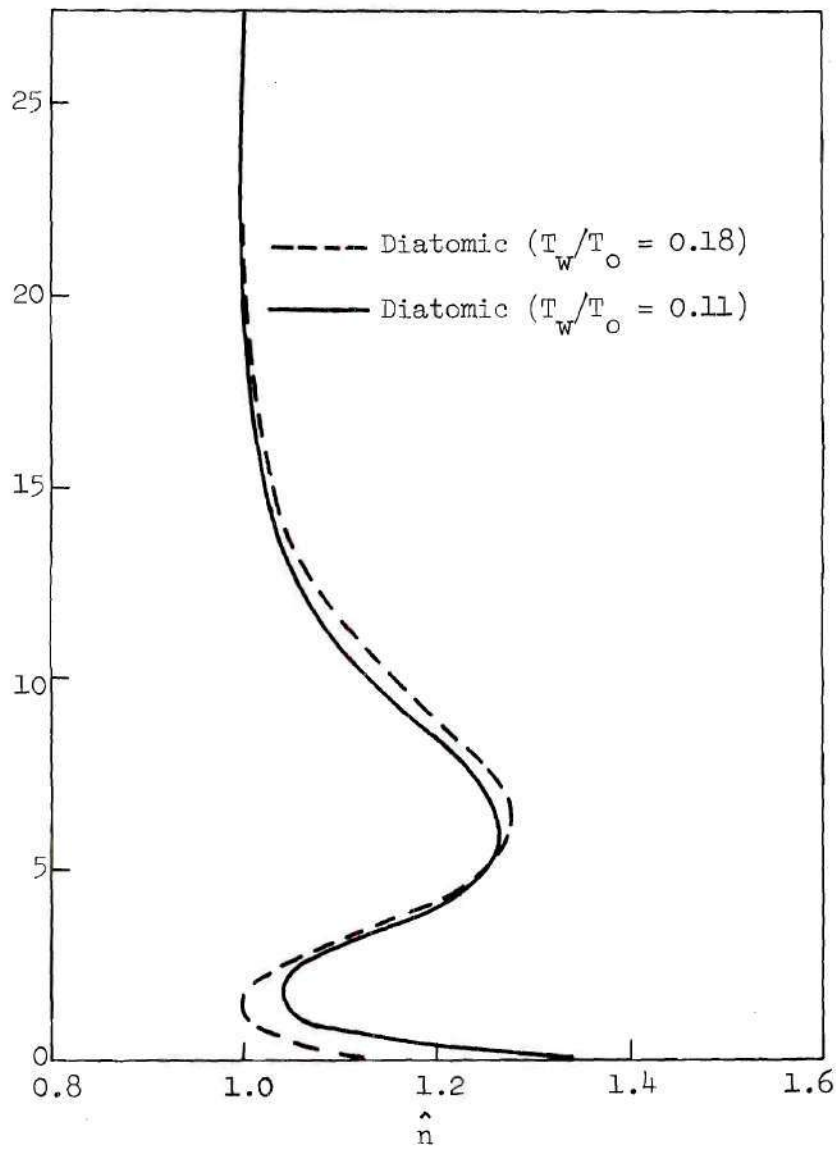

Figure 45. Flat Plate Density Profiles for the Different Wall Temperatures at $\hat{x}$ = 18.

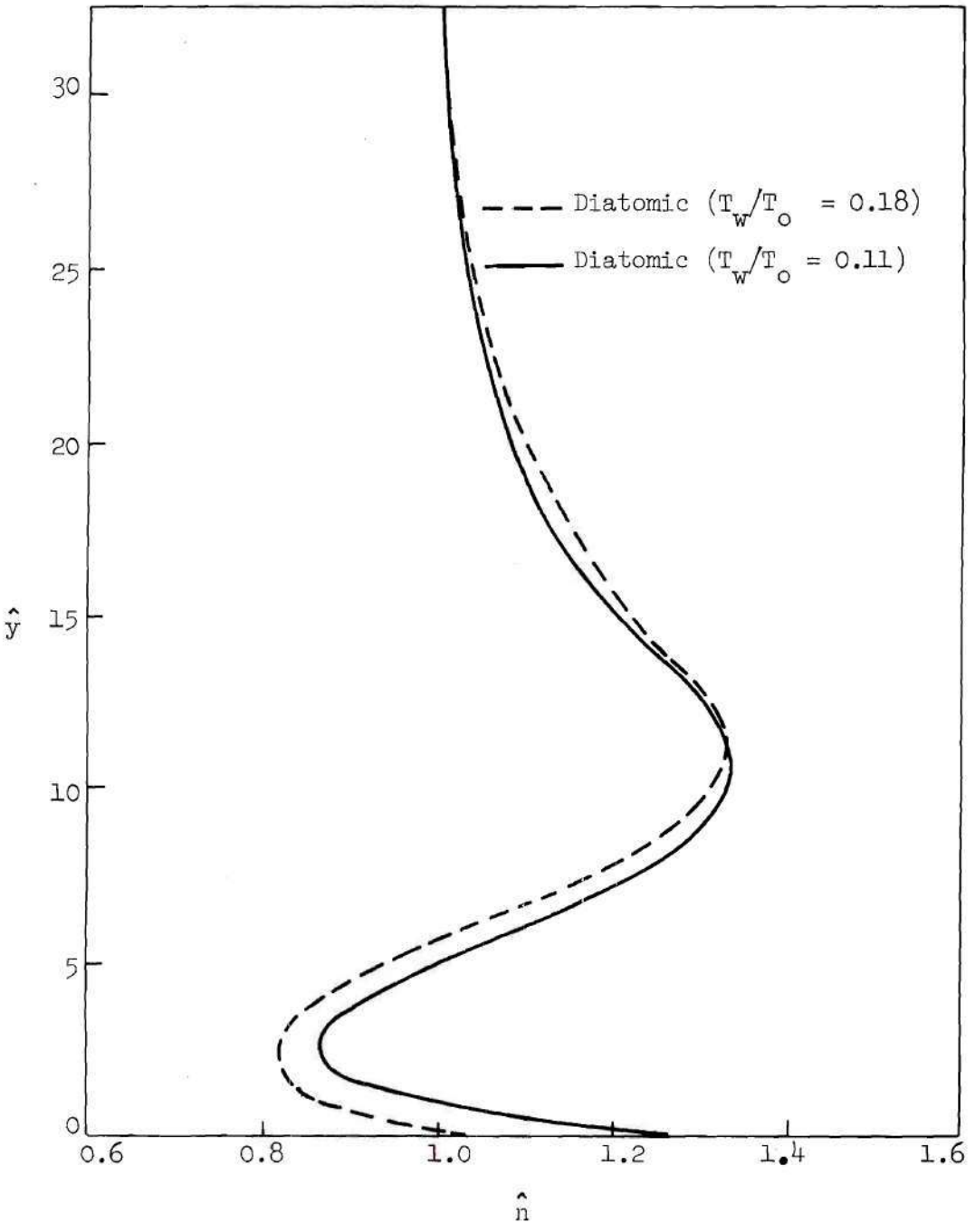

Figure 46. Flat Plate Density Profiles for the Different Wall Temperatures at $\hat{x}$ = 36.

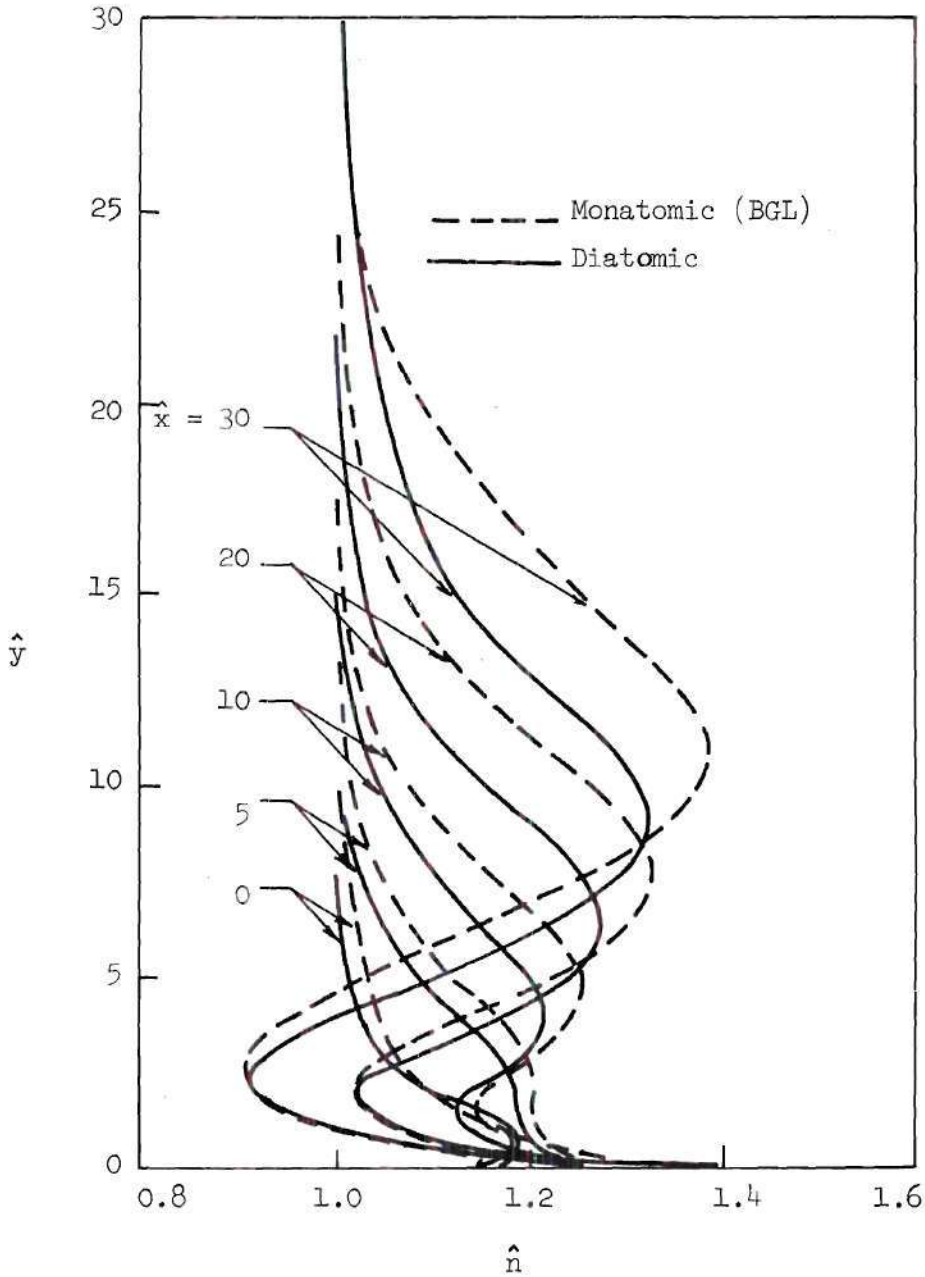

Figure 47. Flat Plate Density Profiles at Various $\hat{x}$ Station.

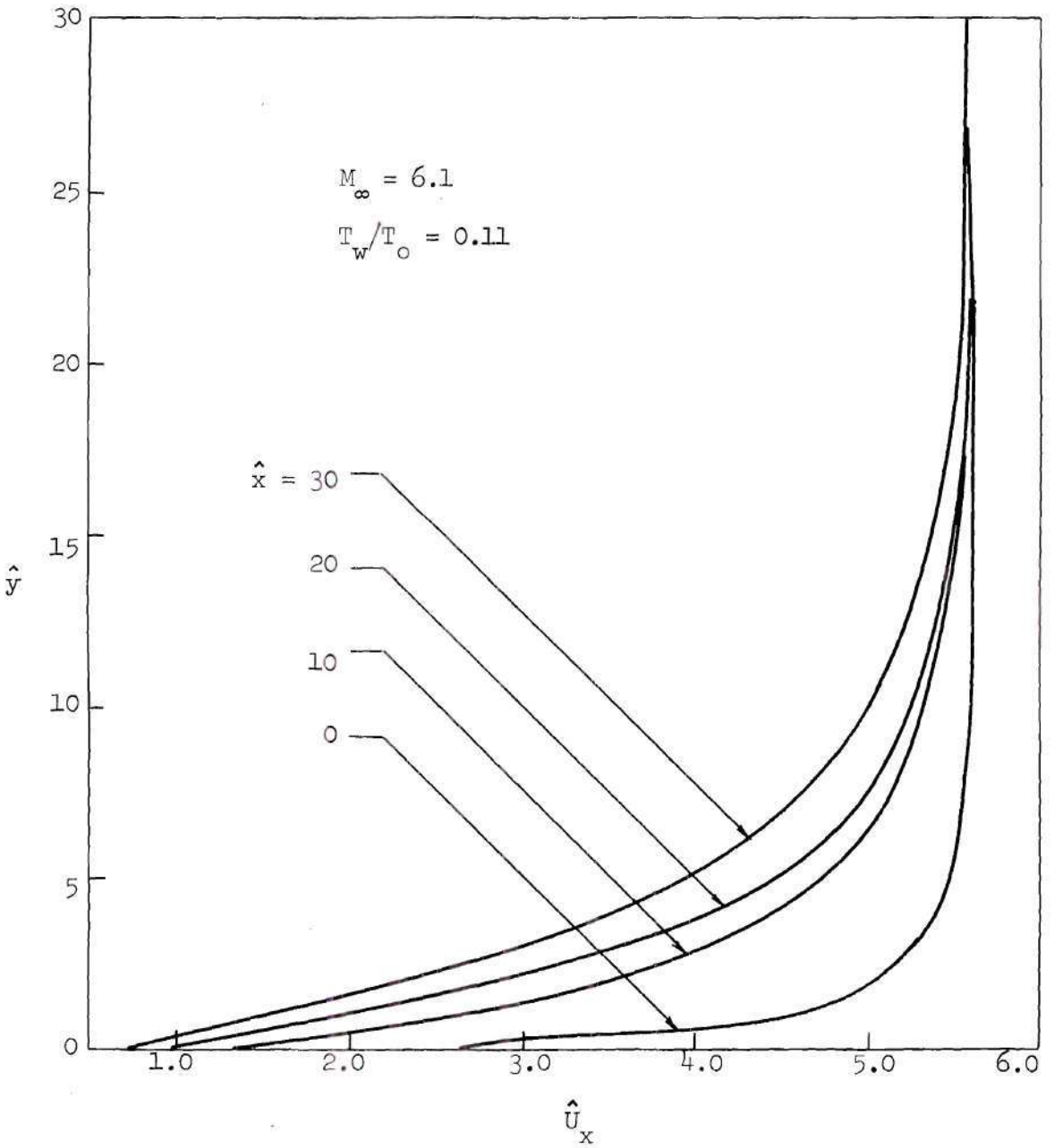

Figure 48. Flat Plate Tangential Velocity Profiles for a Monatomic Gas.

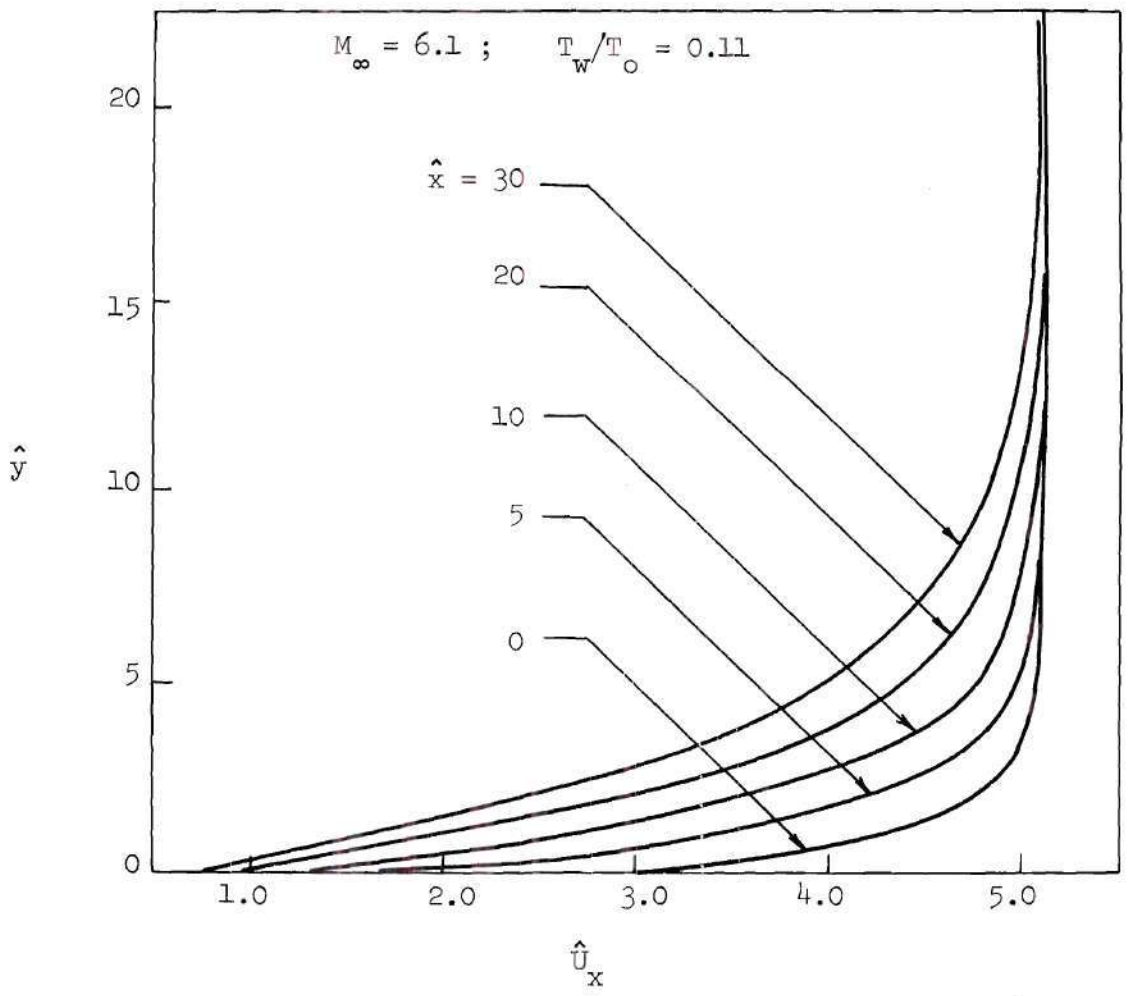

Figure 49. Flat Plate Tangential Velocity Profiles for a Diatomic Gas.

respectively. For both gases the slip velocity at the surface decreases as one moves away from the leading edge. It is found that at the trailing edge slip velocity is higher than the value just upstream due to the gas expansion.

Normal Velocity Profiles

Figure 50 illustrates variation of the normal velocity profiles along the plate. These profiles demonstrate the formation of shock waves as do the density profiles in Figure 47. The strength of the shock wave is seen to grow from the leading edge. However, the influence of the trailing edge can be seen to be present even at $\hat{x} = 20$. It is seen that the shock wave for a monatomic gas is stronger than for a diatomic gas due to the absence of internal degrees of freedom. The influence of the trailing edge is felt farther upstream for the monatomic gas than the diatomic gas.

Temperature Profiles

The temperature profiles for monatomic and diatomic gases at various $\hat{x}$ stations are given in Figure 51. The temperatures for the diatomic gas are significantly lower than those of the monatomic gas since the internal degrees of freedom of diatomic molecules soak up energy. The temperature gradients for the monatomic gas are higher than those for the diatomic gas.

Surface Pressure Distribution

Experimental measurements of surface pressure are made within cavities inside the surface. The measurements are usually made

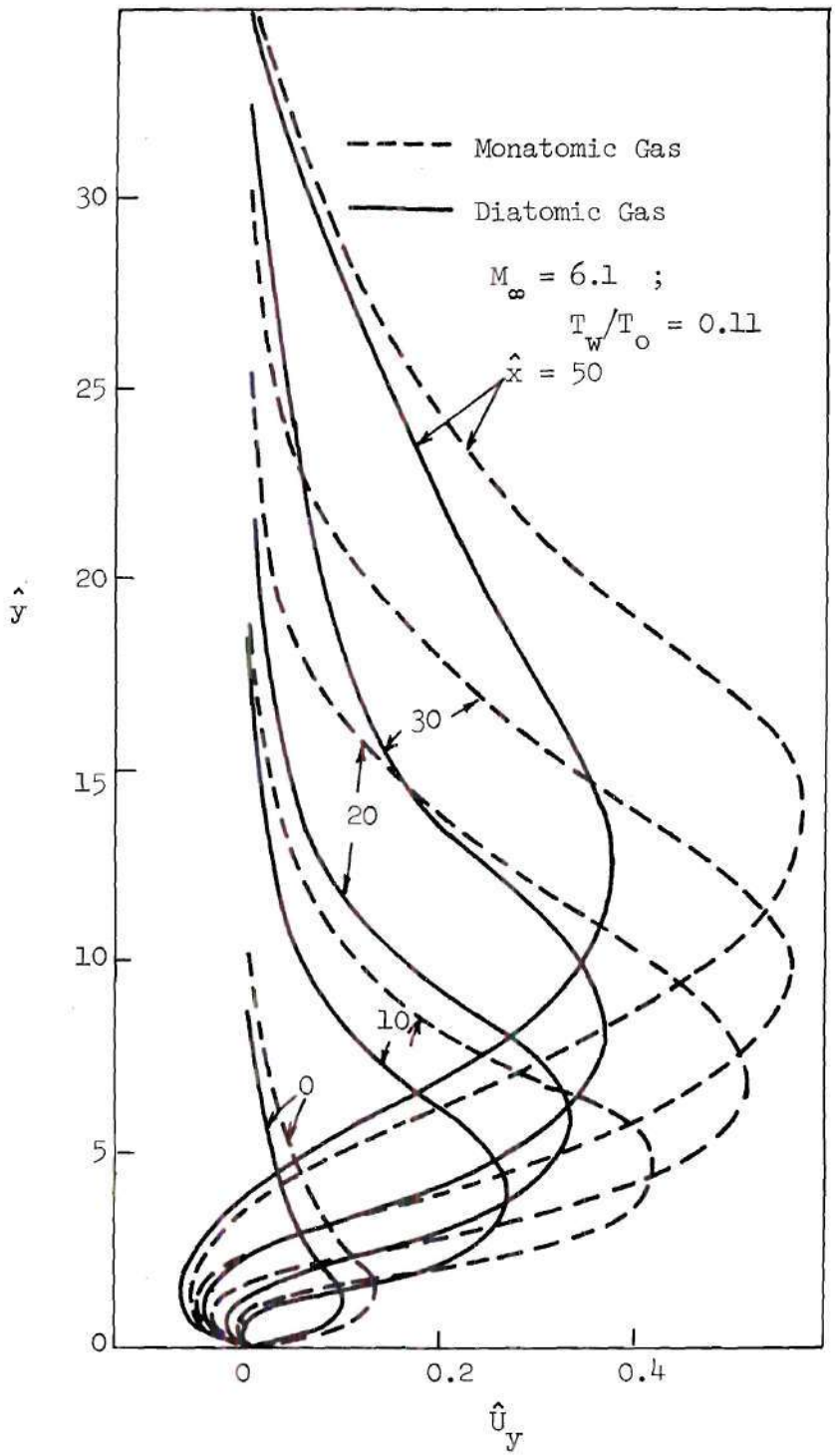

Figure 50. Flat Plate Normal Velocity Profiles.

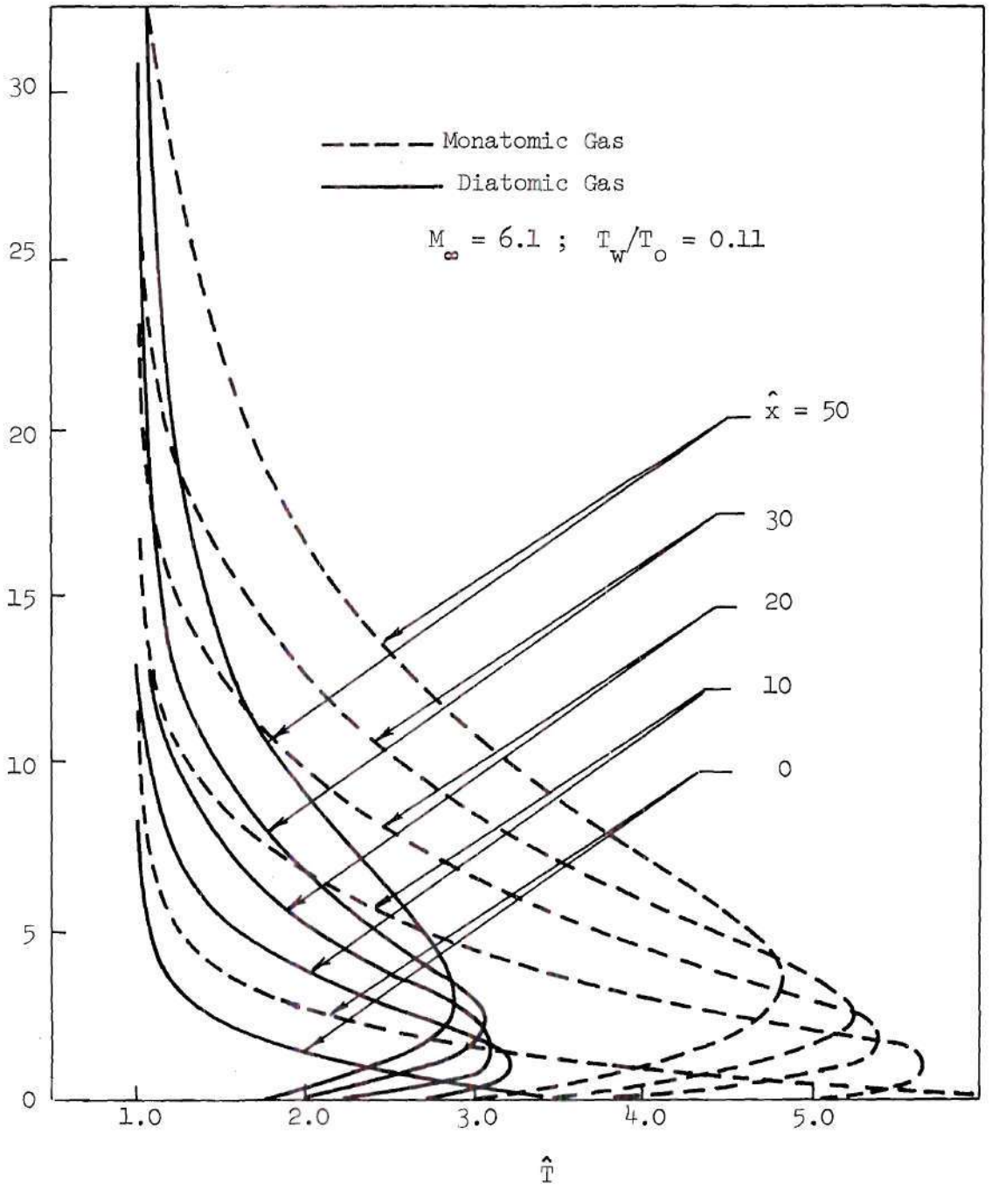

Figure 51. Flat Plate Temperature Profile.

using pressure transducers [71, 78] kept at the exit end of the orifice tubes. These pressure transducers are extremely temperature sensitive. The pressure just inside the orifice cavity is generally assumed to equal that existing at the pressure transducer, based on the assumption that no temperature gradients exist between them. Since these pressure measurements are made within cavities in the surface, they estimate only the net normal momentum transferred to the surface, p_{yy}, and not the equilibrium pressure which is given by the equation,

$$p = \frac{1}{3}\left(p_{xx} + p_{yy} + p_{zz}\right) = nkT$$

It has been observed by many experimentalists that the configuration of the orifice affected the pressure measurements substantially. This is basically due to the slip velocity at the surface. When there is no slip at the surface, each one of the components of pressure, namely, p_{xx}, p_{yy}, and p_{zz} are all of the same order and so the configuration of the orifice will not affect the surface pressure measurements as long as the orifice diameter is small compared to the local mean free path. In regions where slip velocity is present, none of the three components are equal. Depending on the configuration of the orifice, different components of the three pressure terms may be measured.

Figure 52 shows the normal pressure (p_{yy}) distribution along the plate for both monatomic and diatomic gases. The experimental data obtained by Moulic [75] are for the monatomic gas and those obtained by Metcalf, et al. [67] are for the diatomic gas. The p_{yy} distribution of the diatomic gas agrees quite well with the experimental data of Ref. 67. Note that

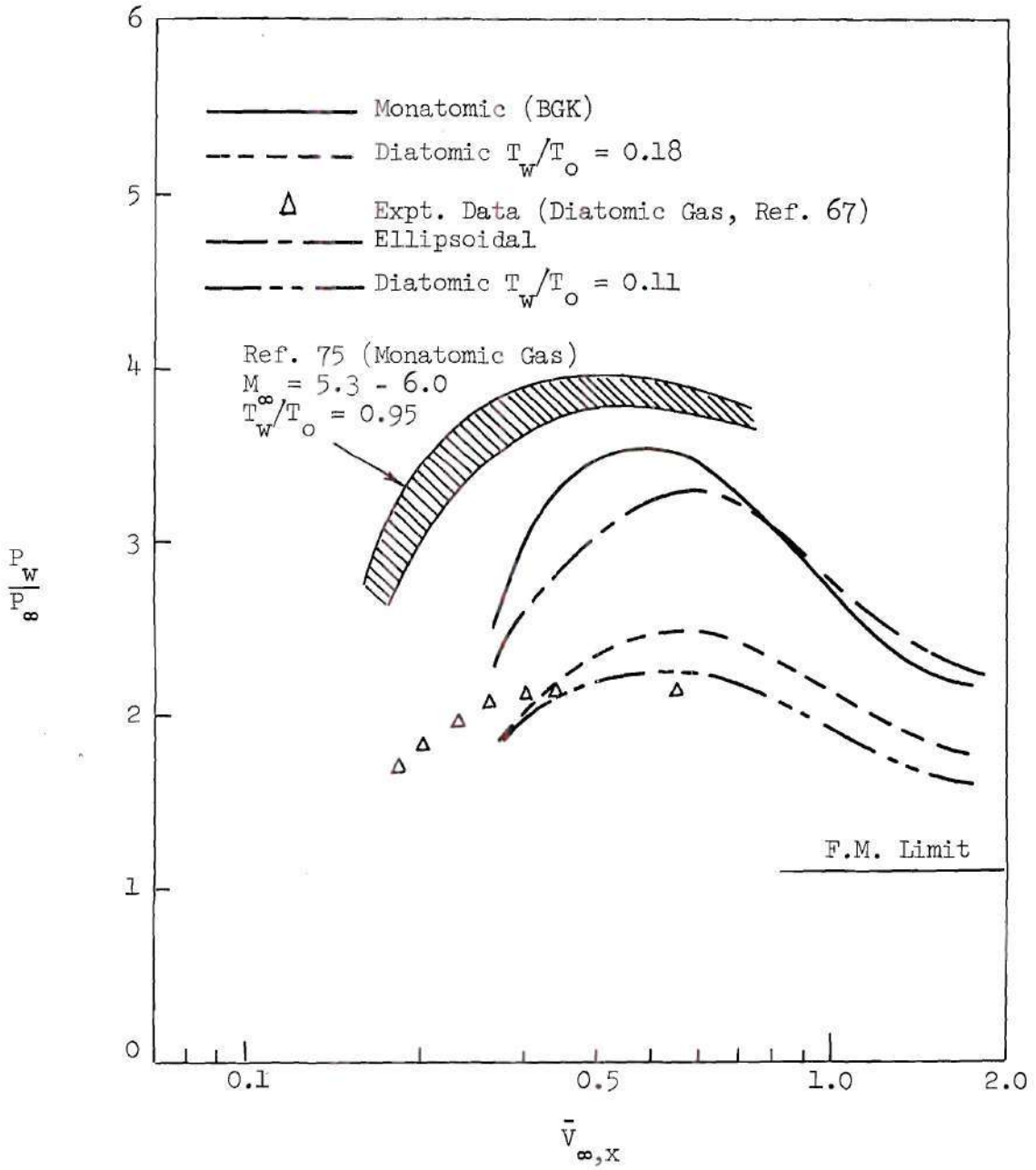

Figure 52. Normal Pressure

the effect of wall temperature on p_{yy} is large in the kinetic and transition regions and becomes small in the continuum end. In the transition region the p_{yy} distribution for the monatomic gas has a sharper peak than for the diatomic gas. A similar trend is also seen in the results of Becker [80]. It is found that an increase in Mach number will increase the surface pressure and a similar trend is seen in Figure 52 for an increase in surface temperature. The present results are in good qualitative agreement with the data given in Ref. 75. Another interesting feature in the present results is that the pressure at the leading edge does not reach the free molecular limit and is in agreement with the predictions by many investigators. It is important to note that the length of the plate in the present study is shorter than the length in experimental conditions of Ref. 67, and that theoretical results for $\bar{V}_{\infty,x} < 0.3$ should not be considered accurate due to the effect of the trailing edge.

Skin Friction

The variation of skin friction coefficient along the plate is shown in Figure 53. The skin friction distribution also has a plateau. The skin friction for the monatomic gas is constantly larger than that for the diatomic gas due to the higher velocity gradient. The effect of wall temperature on the skin friction is negligible.

Heat Transfer

The variation of heat transfer coefficient along the plate is shown in Figure 54. The trend is as expected. The temperature distribution along the plate also has a plateau and so one expects the heat

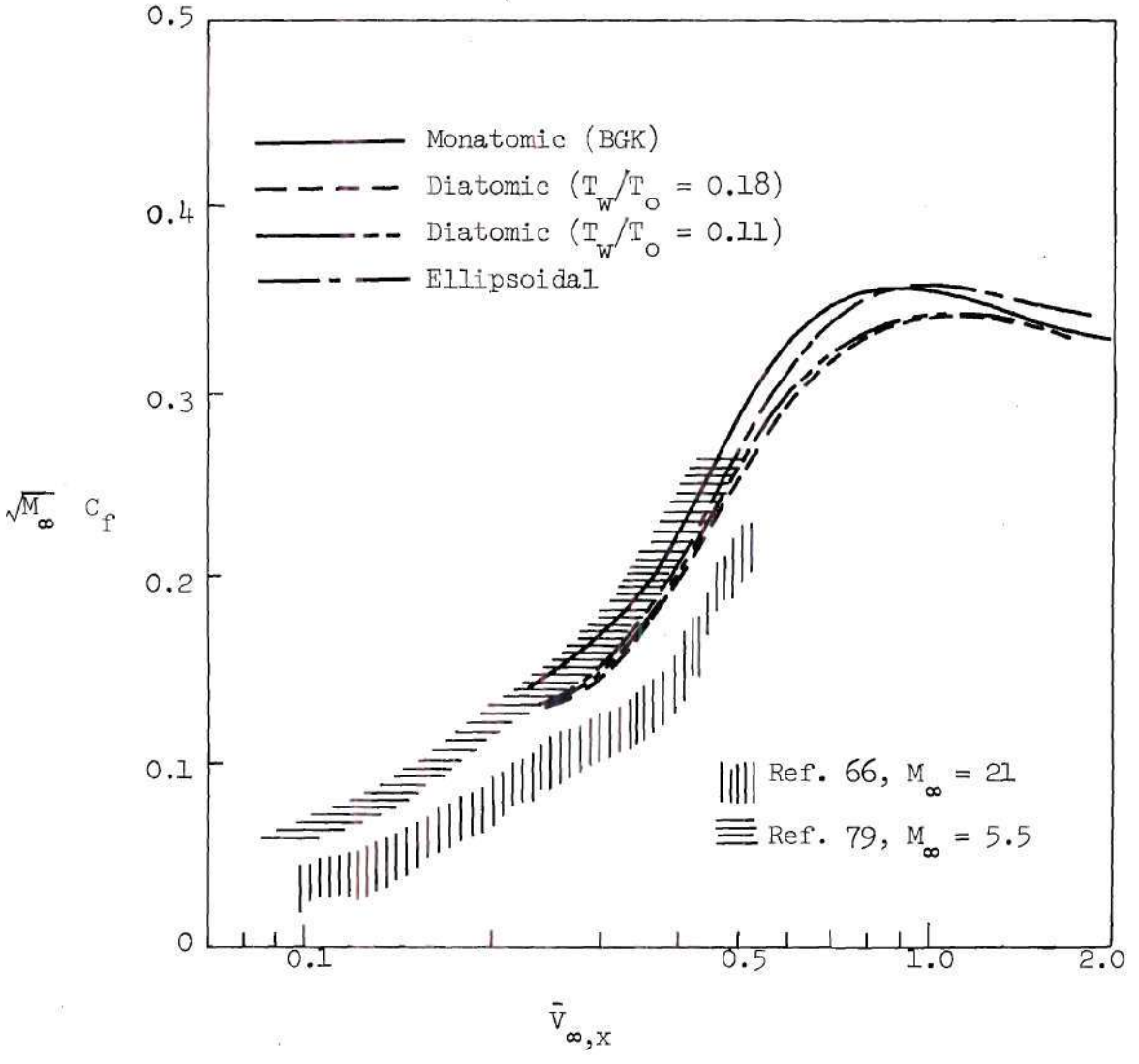

Figure 53. Skin Friction Coefficient.

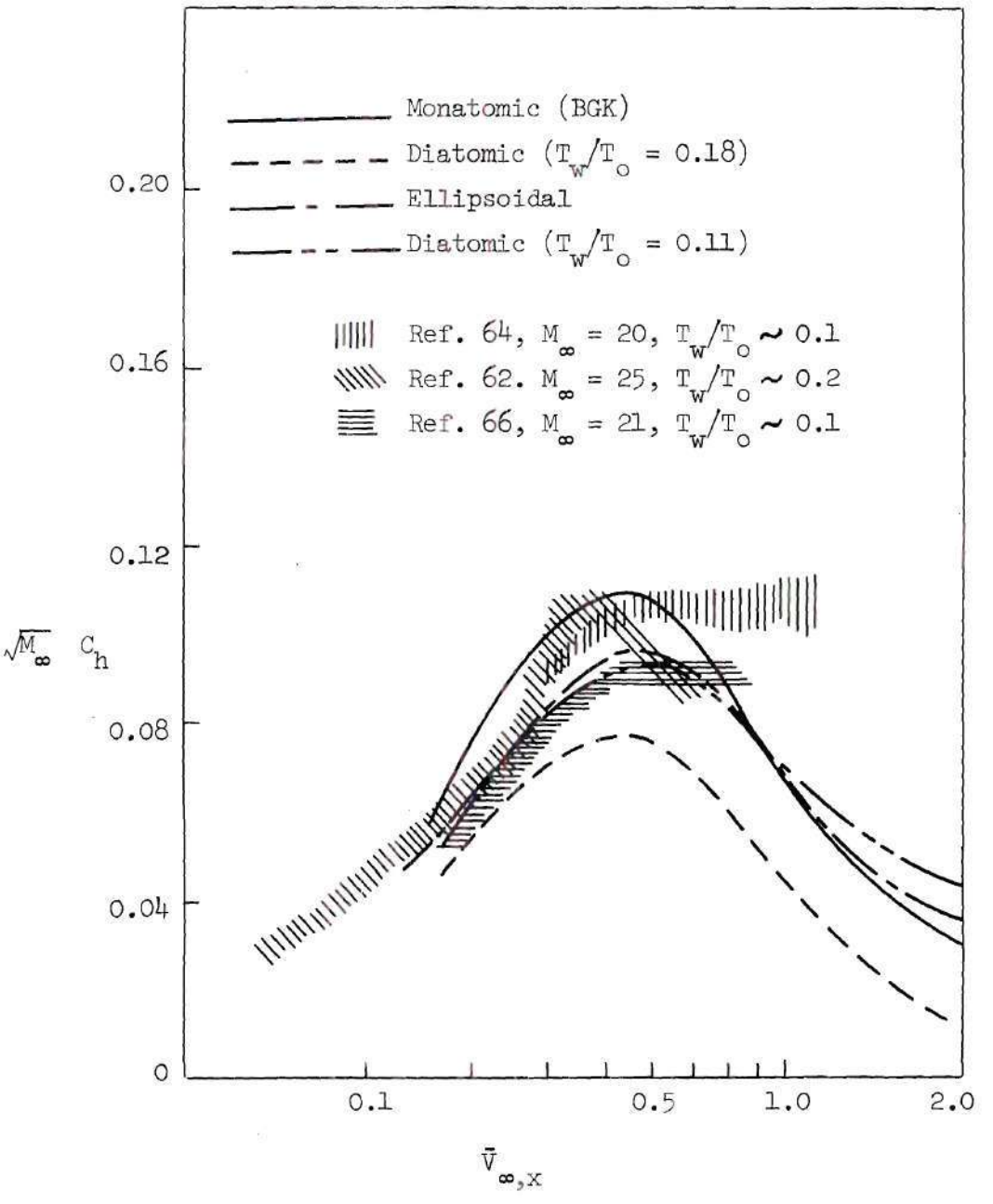

Figure 54. Heat Transfer Coefficient.

transfer to be higher downstream of the leading edge. The heat transfer should be zero far away from the plate. The effect of wall temperature on the heat transfer in the kinetic and transition regions is large and is as expected.

In the present study, only four discrete energy levels were considered. The values of number density in the fourth energy level are quite small which shows that it is enough to consider just four energy levels.

Concluding Remarks

The discrete ordinate method has been applied to the leading edge problem in a monatomic gas as well as a diatomic gas. The finite difference scheme used in the numerical calculation is that of a closed-boundary value approach, and thus the upstream influence can be taken into account. The only assumptions made in the analysis are that the BGK model is used for the collision integral and that the diffuse reflection from the plate is assumed. The results of the present investigation can be summarized in the following concluding remarks.

The entire flow field obtained from the present study is in fairly good agreement with experimental data. Surface pressures are measured within cavities in the surface, and so these measurements of pressure correspond to the net normal momentum transferred to the surface. Depending on the configuration of the orifice various components of momentum flux are measured. In regions where slip velocity is large, this is extremely critical. The surface pressure measurements do not correspond to the equilibrium pressure value. This is clearly shown by the fact that

the normal pressure (p_{yy}) distribution in the present study agrees very well with the experimental data.

The gradients in density, velocity and temperature for the diatomic gas are smaller than those for the monatomic gas. As a consequence the heat transfer coefficient and skin friction coefficient are larger for the monatomic gas than those for the diatomic gas. No attempt has been made to classify the flow field into different regimes.

CHAPTER VI

DISCUSSION AND CONCLUSIONS

Rarefied gasdynamic problems have been studied by many investigators in recent years. However most of the studies have been made by considering the fluid as a monatomic gas [4-8, 17-30]. In practical gasdynamic problems, air must be considered as a mixture of diatomic gases which have fully excited rotational energy at ordinary temperature. Therefore, it is the purpose of this investigation to solve several nonlinear rarefied gasdynamic problems for a diatomic gas. The problems under consideration are the nonlinear Couette problem with heat transfer, the nonlinear Rayleigh problem, and the two-dimensional leading edge flow problem. The Boltzmann equation with the Bhatnagar-Gross-Krook-Morse model [10] is used as a governing equation and the method of discrete ordinates [26] is used as a tool. This method has been successfully applied to solve both the linearized [17-25] and nonlinear [4-8, 26-29] Boltzmann equations with the BGK model for a monatomic gas. The usefulness and accuracy of the method have been established in the solutions of one-dimensional nonlinear rarefied gasdynamic problems (the Couette flow [5] and the shock structure problem [27]). In Reference 5 the results obtained by the method were compared with Anderson's accurate numerical results [30] and were found to be in very good agreement. The method is then applied to solve several nonlinear gasdynamic problems for a rarefied diatomic gas in the present study.

Most theoretical treatment of viscous gasdynamic problems used simplifying assumptions to make the equations tractable for analyses. In contrast, the solutions achieved by the present technique utilized only the assumption of the BGK type model. The approximation to the Boltzmann equation involved in the present study is made only in the sense of numerical truncations. Based on the success of the application of the present method to the solution of the leading edge problem for a rarefied diatomic gas, it appears that the method of discrete ordinates has suitable flexibility for adaptation to many practical situations which may arise in physical problems. For sufficiently higher Mach numbers, however, a large computer storage requirement is necessary.

The results of the present investigation may be summarized in the following conclusions:

1. For the linear Couette flow case the density results obtained by the present method are seen to be in reasonably good agreement with experimental data of Teagan and Springer [33] for all flow regimes except possibly $1/K_n = 2.58$ where a rather low value of accommodation coefficient is needed to fit with the experimental data. The density results obtained for the nonlinear heat transfer case are in excellent agreement with experimental data of Alofs, et al. [34]. It is thus concluded that the accuracy and applicability of the BGKM model is reasonably good for this one-dimensional problem.
2. The nonlinear Rayleigh problem in a diatomic gas has been solved. There are no experimental data available for comparing with the calculated results. However, the trend and the shape of the

profiles are consistent with those of the monatomic gas case. It is observed that at each instant of time, the diatomic gas gives smaller slip velocities at the plate than does the monatomic gas.

3. The flow field calculated for the leading edge problem presents a reasonable picture of macroscopic properties and their spacial variations. The results are found to be more reasonable than those based on the initial value approach [4, 6, 8] in which the up-stream effect was not considered. The comparison between the calculated density profiles at $\hat{x} = 18$ and 36 with the most recent experimental data of Lillicrap and Berry [68] reveals that the thickness of the shock layer agrees fairly well with the experimental data, although the calculated shock wave is slightly weaker than that of experimental data. The results also indicate that the thickness of the shock layer for the monatomic gas is always larger than that of the diatomic gas.

4. The normal velocity profiles generated for the leading edge problem demonstrate the formation of shock waves as do the density profiles. The results indicate that the shock wave of a monatomic gas is stronger than for a diatomic gas due to the absence of internal degrees of freedom. The influence of the trailing edge is felt farther upstream for the monatomic gas than the diatomic gas.

5. The temperature profiles generated for the leading edge problem indicate that the temperatures for the diatomic gas are significantly lower than those of the monatomic gas since the internal

degrees of freedom of diatomic molecules soak up energy.

6. In existing experimental literature [71, 75, 78] the surface pressures generated for the leading edge problem are measured within cavities in the surface, and so the measurements of pressure correspond to the net normal momentum transferred to the surface (p_{yy}). The calculated normal pressure (p_{yy}) distribution in the present study agrees well with experimental data [67].

7. In the leading edge problem the gradients in density, velocity, and temperature for the diatomic gas are smaller than those for the monatomic gas. As a consequence the heat transfer coefficient and skin friction coefficient are larger for the monatomic gas than those for the diatomic gas. Since existing experimental data for the heat transfer and skin friction coefficients scatter rather widely, no firm conclusion can be drawn as to the accuracy of the present results for these two coefficients.

APPENDICES

APPENDIX A

THE NEW "ODD" EQUALLY SPACED QUADRATURE

The weighting coefficients of the new "odd" equally spaced quadrature can be obtained in the same way as that of the old "odd" equally spaced quadrature [26]. The following integration formula is thus considered:

$$\int_0^1 f(v) \cong \sum_{i=1}^{n} k_i f(\alpha_i)$$

where the weighting coefficients $k_i (i = 1, \ldots, n)$ are determined in the same way as before and are presented below. The arguments α_i are taken to be $\frac{1}{2n}$, $\frac{3}{2n}$, ..., $1 - \frac{1}{2n}$.

The weighting coefficients, k_i, for $(n = 3, \ldots, 8)$, are presented in the following:

$n = 3$, $k_1 = k_3 = 0.375$

$k_2 = 0.25$

$n = 4$, $k_1 = k_4 = 0.270833333$

$k_2 = k_3 = 0.229166666$

$n = 5$, $k_1 = k_5 = 0.238715277$

$k_2 = k_4 = 0.086805555$

$k_3 = 0.348958333$

$n = 6$, $k_1 = k_6 = 0.19296875$

$k_2 = k_5 = 0.10859375$

$k_3 = k_4 = 0.19843750$

$n = 7,\ k_1 = k_7 = 0.1790002$

$k_2 = k_6 = 0.0063802$

$k_3 = k_5 = 0.4051432$

$k_4 = -\ 0.1810474$

$n = 8,\ k_1 = k_8 = 0.1527503$

$k_2 = k_7 = 0.0368556$

$k_3 = k_6 = 0.2437639$

$k_4 = k_5 = 0.0666299$

APPENDIX B

APPROXIMATE ENERGY LEVELS FOR ROTATION

Consider the quantum mechanical expression for the equilibrium distribution of number density in a given ℓ^{th} quantum state

$$\bar{n}_{\ell eq} = \bar{n} \frac{e^{-\bar{E}_\ell/\bar{T}}}{\sum_\ell e^{-\bar{E}_\ell/\bar{T}}} \tag{1}$$

If the quantum levels are spaced close together and there are many such levels, then the states may be approximated by a continuous variable and the summation in Equation (1) becomes an integral as follows

$$\theta \sum_\ell e^{-\bar{E}_\ell/\bar{T}} = \int_0^\infty e^{-\bar{E}/\bar{T}} \, d\bar{E} \tag{2}$$

where θ is the spacing between adjacent quantum states, assuming spacing is constant. For the rigid rotator this is precisely the case and $\theta = h\nu = \frac{h}{8\pi^2 kI}$. Now suppose we are interested in rediscretizing the energy levels, where the new ficticous levels do not correspond one to one with the actual quantum states. Denote such a discretized level by the subscript s. First, consider the case where we want to use a constant spacing between the new levels, call it $\Delta \bar{E}$. Then

$$\bar{n}_{s eq} = \sum_{\ell=m}^{n} \bar{n}_{\ell eq} \tag{3}$$

where $\sum_{\ell=m}^{n}$ is a sum over the (n - m) quantum states contained within $\Delta\bar{E}$. Substitute Equation (1) and (2) into Equation (3), we have

$$\bar{n}_{s\,eq} = \bar{n}\,\frac{\sum_{\ell=m}^{n} e^{-\bar{E}_\ell/\bar{T}}}{\sum_{\ell} e^{-\bar{E}_\ell/\bar{T}}}$$

$$= \bar{n}\,\frac{\theta \sum_{\ell=m}^{n} e^{-\bar{E}_\ell/\bar{T}}}{\int_0^\infty e^{-\bar{E}/\bar{T}}\, d\bar{E}}$$

$$= \bar{n}\,\frac{\theta\,(n-m)\, e^{-\bar{E}_s/\bar{T}}}{\Delta\bar{E} \sum_{s} e^{-\bar{E}_s/\bar{T}}}$$

$$= \bar{n}\,\frac{e^{-\bar{E}_s/\bar{T}}}{\sum_{s} e^{-\bar{E}_s/\bar{T}}} \qquad (4)$$

The above equation is the approximate evergy levels for rotation with equal spaced energy levels.

Next, we want to optimize the $\bar{E}_s$ in such a way that the error in

$$\sum_{s} \Delta\bar{E}_s\, e^{-\bar{E}_s/\bar{T}} = \int_0^\infty e^{-\bar{E}/\bar{T}}\, d\bar{E}$$

is a minimum.

Equation (4) can be rewritten as

$$\bar{n}_{seq} = \bar{n}\,\frac{\Delta\bar{E}_s}{\bar{T}}\,e^{-\bar{E}_s/\bar{T}} \tag{5}$$

Since

$$\sum_s \Delta\bar{E}_s\, e^{-\bar{E}_s/\bar{T}} = \int_0^\infty e^{-\bar{E}/\bar{T}}\, d\bar{E} = \bar{T} \tag{6}$$

but

$$\int_0^\infty e^{-\bar{E}/\bar{T}}\, d\bar{E} = \int_0^\infty e^{-\bar{E}/\bar{T}}\, e^{\bar{E}}\cdot e^{-\bar{E}}\, d\bar{E} \tag{7}$$

Now use a Gauss-Laguerre Quadrature, we have from Equation (7)

$$\int_0^\infty e^{-\bar{E}/\bar{T}}\, d\bar{E} \cong \sum_{s=1}^{N} R_s\, e^{\bar{E}_s}\, e^{-\bar{E}_s/\bar{T}} \tag{8}$$

comparing this with Equation (6), we see that may let

$$\Delta\bar{E}_s = R_s\, e^{\bar{E}_s}$$

where R_s is the Gauss-Laguerre weighting coefficient corresponding to the $\bar{E}_s$ roots of the Laguerre polynomial of degree N. Therefore Equation (5) becomes

$$\bar{n}_{seq} = \bar{n}\,\frac{R_s\, e^{\bar{E}_s\left(1-\frac{1}{\bar{T}}\right)}}{\bar{T}} \tag{9}$$

BIBLIOGRAPHY

1. P. L. Bhatnagar, E. P. Gross, and M. Krook, "A Model for Collision Processes in Gases," Physical Review, 94, 511 (1954).
2. L. H. Holway, "New Statistical Models for Kinetic Theory: Method of Construction," Physics of Fluids, 9, 1658 (1966).
3. C. Cercignani and Tironi, Nuovo Cimento, 43, 64 (1966).
4. A. B. Huang and D. L. Hartley, "Kinetic Theory of the Sharp Leading Edge Problem in Supersonic Flow," presented at the 18th International Astronautical Congress, Belgrade, Yugoslavia, Sept. 24-29 (1967). Also, Physics of Fluids, 12, 96-108 (1969).
5. A. B. Huang and D. L. Hartley, "Nonlinear Couette Flow with Heat Transfer," Physics of Fluids, 11, 1321 (1968).
6. A. B. Huang and P. F. Hwang, "Kinetic Theory of the Sharp Leading Edge Problem II, Hypersonic Flow," presented at the 19th International Astronautical Congress, New York, N. Y. October 13-19 (1968). Also, Proceedings, p. 521-545 (1970).
7. A. B. Huang and D. P. Giddens, "Some Analytic Solutions to the Linearized Boltzmann Equation with the Ellipsoidal Model," Physics of Fluids (to be published).
8. A. B. Huang and P. F. Hwang, "The Supersonic Leading Edge Problem According to the Ellipsoidal Model," Physics of Fluids, 13, 309-317 (1970).
9. C. S. Wang Chang and G. E. Uhlenbeck, University of Michigan Engineering Research Report No. CM-681 (1951).

10. T. F. Morse, "Kinetic Model for Gases with Internal Degree of Freedom," Physics of Fluids, 7, 159 (1964).

11. F. B. Hanson and T. F. Morse, "Kinetic Models for a Gas with Internal Structure," Physics of Fluids, 10, 345 (1967).

12. C. A. Brau, "Kinetic Theory of Polyatomic Gases: Models for the Collision Processes," Physics of Fluids, 10, 48 (1967).

13. S. K. Hsu and T. F. Morse, "Kinetic Theory of Heat Transfer for a Gas with Internal Degrees of Freedom," Rarefied Gasdynamics, Edited by C. L. Brundin, p. 419.

14. J. W. Cipolla, Jr., and T. F. Morse, "Kinetic Description of Cylindrical Heat Conduction in a Polyatomic Gas," Physics of Fluids, 11, 1291 (1968).

15. R. Venkataraman and T. F. Morse, "Kinetic Theory of Shock Structure in a Gas with Internal Degrees of Freedom," in Rarefied Gas Dynamics, Ed. by L. Trilling and H. Wachman, p. 353 (1969).

16. D. P. Giddens, H. F. Barbarika, and A. B. Huang, "Shock Structure in a Diatomic Gas," presented at the 7th International Symposium on Rarefied Gas Dynamics, Pisa, Italy. June 29 - July 3 (1970)(to be published in the Proceedings).

17. A. B. Huang and D. P. Giddens, "The Discrete Ordinate Method for the Linearized Value Problems in Kinetic Theory of Gases," in Rarefied Gas Dynamics, ed. by C. L. Brundin, 481 (Academic Press, New York, 1967).

18. A. B. Huang and D. P. Giddens, "The Discrete Ordinate Method for Unsteady Linearized Boltzmann-Bhatnagar-Gross-Krook Equation,"

Physics of Fluids, 10, 232 (1967).

19. A. B. Huang, D. P. Giddens, and C. W. Bagnel, "Rarefied Gas Flow Between Parallel Plates Based on the Discrete Ordinate Method," Physics of Fluids, 10, 498 (1967).

20. A. B. Huang and D. P. Giddens, "Rayleigh's Problem at Low Mach Numbers Based on Kinetic Theory," J. AIAA, 5, 1354 (1967).

21. A. B. Huang, "Slip Coefficient of a Gas," Physics of Fluids, 11, 61 (1968).

22. A. B. Huang and D. P. Giddens, "Kinetic Theory of the Transient Development of Couette Flow Between Parallel Plates," Physics of Fluids, 11, 446 (1968).

23. A. B. Huang, "Evaluation of the $\int_0^\infty u^m \exp(-u^2 - x/u)\,du$ by the Discrete Ordinate Method," J. of Math. and Phys., 46, 107 (1967).

24. A. B. Huang and D. P. Giddens, "A New Table for a Modified (Half-Range) Gauss-Hermite Quadrature with an Evaluation of the Integral $\int_0^\infty e^{-u^2-(x/u)}\,du$," J. of Math. and Phys., 47, 213 (1968).

25. D. P. Giddens, "Study of Rarefied Gas Flows by the Discrete Ordinate Method," Georgia Institute of Technology, Ph.D. Thesis (1966).

26. A. B. Huang, "A General Discrete Ordinate Method for the Dynamics of Rarefied Gases," Georgia Institute of Technology, School of Aerospace Engineering, Rarefied Gas Dynamics and Plasma Laboratory, Report No. 4 (1967).

27. D. P. Giddens, A. B. Huang, and Y. C. Young, "Evaluation of Two Statistical Models Using the Shock Structure Problem," Physics of Fluids (to be published).

28. A. B. Huang and D. L. Hartley, "Nonlinear Rarefied Rayleigh's Problem," J. AIAA, 6, 2023 (1968).

29. D. L. Hartley, "A Study of Non-Linear Rarefied Gas Flow Problems," Georgia Institute of Technology, Ph.D. Thesis (1967).

30. D. Anderson, "Numerical Solution of the Krook Kinetic Equation," J. of Fluid Mechanics, 25, 271 (1966).

31. Z. Kopal, Numerical Analysis, Wiley and Sons, New York (1961).

32. A. B. Huang, "Kinetic Theory of the Rarefied Supersonic Flow Over a Finite Plate," in Rarefied Gas Dynamics, ed. by L. Trilling and H. Wachman, p. 529 (1969).

33. W. P. Teagan and G. S. Springer, "Heat-Transfer and Density Distribution Measurements Between Parallel Plates in the Transition Regime," Physics of Fluids, 11, 497 (1968).

34. D. J. Alofs, R. O. Flagan, and G. S. Springer, "Density Distribution Measurements in Rarefied Gases Contained Between Parallel Plates at High Temperature Differences," presented at 7th Rarefied Gas Symposium, June, 1970, at DiPisa, Italy.

35. S. Chapman and T. G. Cowling, The Mathematical Theory of Non-Uniform Gases, Cambridge University Press, London (1958).

36. H. Schlichting, Boundary Layer Theory, McGraw-Hill Book Company, Inc., New York, 4th Edition (1962).

37. D. R. Willis, "New Interpolation Scheme for Predicting Heat Transfer in Rarefied Gases," Paper No. 69-WA/HT-30, ASME Winter Meeting, Nov. 16-20, 1969.

38. P. Bassanini, C. Cercignani, and C. D. Pagani, "Comparison of Kinetic Theory Analyses of Linearized Heat Transfer Between

Parallel Plates," International Journal of Heat and Mass Transfer, 10, 447 (1967).

39. Private communication between G. S. Springer and A. B. Huang.

40. L. Rayleigh, "On the Motion of Solid Bodies Through Viscous Liquid," Philosophical Magazine, Vol. 21, p. 697-711 (1911).

41. L. Howarth, "Some Aspects of Rayleigh's Problem for a Compress ible Fluid," Quarterly Journal of Mechanics and Applied Mathematics, Vol. 4, p. 157-169 (1951).

42. C. R. Illingworth, "Unsteady Laminer Flow of Gas Near an Infinite Flat Plate," Proc. of the Cambridge Philosophical Society, Vol. 46, p. 603-613 (1950).

43. K. Stewartson, "On the Motion of a Flat Plate at High Speed in a Viscous Compressible Fluid. I. Impulsive Motion," Proc. of the Cambridge Philosophical Society, Vol. 51, p. 209-219 (1955).

44. F. H. Harlow and B. D. Meixver, "Motion of a Viscous Compressible Gas Adjacent to a Sliding Plate," Physics of Fluids, 4, p. 1202-1206 (1961).

45. M. D. Van Dyke, "Impulsive Motion of an Infinite Plate in a Viscous Compressible Fluid," Z. Augew Math. Phys., Vol. 3, p. 343-353 (1952).

46. M. Hanin, "On Rayleigh's Problem for Compressible Fluids," Quarterly Journal of Mechanics and Applied Mathematics, Vol. 13, p. 184-198 (1960).

47. E. P. Gross and E. A. Jackson, "Kinetic Theory of the Impulsive Motion of an Infinite Plane," Physics of Fluids, 1, 318-328 (1958).

48. H. Yang and L. Lees, "Rayleigh's Problem at Low Mach Number

According to the Kinetic Theory of Gases," Journal of Mathematics and Physics, Vol. 35, p. 195-235 (1956).

49. C. Cercignani and F. Sernagiotto, "Rayleigh's Problem at Low Mach Numbers According to Kinetic Theory," in Rarefied Gas Dynamics, ed. by J. H. deLeeuw, (Academic Press, Inc., New York) p. 332-353 (1965).

50. Y. Sone, "Kinetic Theory Analysis of the Linearized Rayleigh Problem," Physics of Fluids, 7, 470-471 (1964).

51. A. B. Huang and D. P. Giddens, "Rayleigh's Problem at Low Mach Numbers Based on Kinetic Theory," J. AIAA, 5, 1354-1356 (1967).

52. C. K. Chu, "The High Mach Number Rayleigh Problem According to the Krook Equation," in Rarefied Gas Dynamics, ed. by C. L. Brundin (Academic Press, Inc., New York) p. 589-607 (1967).

53. A. B. Huang and D. L. Hartley, "Nonlinear Rarefied Rayleigh's Problem," J. AIAA, 6, 2023 (1968).

54. Becker, J. V., J. Appl. Phys., 21, 619 (1950).

55. Oguchi, H., Rarefied Gasdynamics, Supplement 2, II, 181 (1963).

56. Jain, A. C., and T. Y. Li, Research Foundation, University of Cincinatti Tech. Report, A.E. 6401 (1964).

57. Pan, Y. S. and Ronald F. Probstein, M.I.T. Fluid Mechanics Laboratory Pub. No. 64-8 (1964).

58. Charwat, A. F., Rarefied Gasdynamics, Supplement 1, 553 (1961).

59. Kogan, M. N., Astronautica ACTA, 11, 1 (1965).

60. Bird, G. A., AIAA Journal, 4, 1(1966).

61. Schaaf, S. A., F. C. Hurlbut, L. Talbot and J. Aroesty, ARS J., 29, 597 (1959).

62. Nagamatsu, H. T., J. A. Weil and R. C. Sheer, High Temperature Aspects of Hypersonic Flow, Pergamon Press, New York, p. 717 (1963).

63. Nagamatsu, H. T., J. A. Weil and R. C. Sheer, ARS J., 32, 533 (1962).

64. Vidal, R. J. and C. E. Wittliff, Rarefied Gasdynamics, J. Laurmann, Vol. II, 343 (1963).

65. Burke, A. F., W. C. Smith, E. D. Dowling and D. R. Carlson, CAL Rept. AA-1596-y-1 (1962).

66. Wallace, J. E. and A. F. Burke, Rarefied Gasdynamics, ed. by J. H. deLeeuw, 487 (1965).

67. Metcalf, S. C., D. C. Lillicrap and C. J. Berry, "A Study of the Effect of Surface Conditions on the Shock Layer Development Over the Sharp Edged Shapes in Low Reynolds Number High Speed Flow," Rarefied Gasdynamics, Suppl. 5, Vol. I, ed. by L. Trilling and H. Wachman, Academic Press, New York, p. 593 (1969).

68. Lillicrap, D. C. and C. J. Berry, "Experimental Model for High Speed Rarefied Flow Over a Sharp Flat Plate," Physics of Fluids, 13, No. 5, May, 1970.

69. Vogenitz, F. W., J. E. Broadwell and G. A. Bird, "Leading Edge Flow by Monte Carlo Direct Simulation Technique", AIAA Journal, 8, (3), 504 (1970).

70. Potter, J. L. M. Kinslow, D. E. Boylan, Rarefied Gasdynamics, Supplement 3, 2, (1965).

71. Kinslow, Max and G. D. Arney, Jr., AGARDograph, 119, August, 1967.

72. Kinslow, Max and G. D. Arney, Jr., 6th Symposium on Rarefied Gasdynamics, Vol. 1, Academic Press, New York, 691-698 (1969).

73. Hortsman, C. C., "Number Flux Measurements on Sharp Plates and Wedges in the Kinetic Flow Regime," presented at the Seventh Rarefied Gasdynamics Symposium (to be published).

74. Kinslow, Max and J. Leith Potter, "Re-evaluation of Parameters Relative to the Orifice Effect," presented at the 7th Rarefied Gasdynamics Symposium (to be published).

75. Moulic, E. S., and G. J. Maslach, 5th Symposium on Rarefied Gasdynamics, ed. by Brundin, 971 (1966).

76. Becker, M. and D. F. Boylan, Rarefied Gasdynamics, ed. by Brundin, 993 (1966).

77. Deskins, H. E. and D. E. Boylan, AIAA J., Vol. 3, No. 5, May, 1965, p. 950-957.

78. Berry, C. J., J. Sci. Instrum., 83 (1967).

79. Moulic, E. S., Jr., "Local Skin Friction and Induced Pressure Measurements on a Sharp-edged Insulated Flat Plate in Low Density Hypersonic Flow," U. of Calif. (Berkeley) Tech. Report on NSF Grant GP-2520, Series 7, No. 3, (1966).

80. Becker, M., "Flat Plate Flow Field and Surface Measurements from Merged Layer into Transition Regime", Sixth Rarefied Gasdynamics (1969).

VITA

Pang-feng Hwang was born in Hsinchu, Taiwan, on October 14, 1936. His parents are Yin-tze and Wan-jin Hwang. He completed his high school education at Hsinchu High School, Hsinchu, Taiwan, in June, 1956.

In September of 1956, he entered the National Taiwan University, and in June of 1960, was graduated with honor as a Bachelor of Agricultural Engineering.

He has served in National China's Air Force as a Second Lieutenant from July of 1960 to October of 1961. In November of 1961 he was employed by the Bureau of Water Conservancy at Taipei, Taiwan.

He attended North Carolina State University in September of 1962 as a graduate student. The degree of Master of Science in Agriculture Engineering was awarded him in June of 1964. Then he stayed two months in the Department of Agriculture Engineering of North Carolina State University as a research associate.

In September of 1964 he was employed by Morehouse College at Atlanta, Georgia as an instructor. In March of 1965, he was admitted to the Georgia Institute of Technology as a part-time graduate student in the Department of Civil Engineering. In September of 1965, he transferred to the Department of Aerospace Engineering. In July of 1966, he continued his graduate study as a research assistant. He has been elected to the memberships of Sigma Gamma Tau and Sigma Xi.

In September 1970, he was employed by the Metropolitan Junior College District.

On june 22, 1964, he married the former Li-hwa Chen of Hwalien, Taiwan; they have one child, Charles Hwang.